ISTC Project No. 3380-P

Advanced singlet oxygen generator

Final Project Technical Report

on the work performed from 0.2 01, 2006 to 01 31, 2009

Lebedev Physical Institute Rassian Academy of Sciences, Samara Branch

Project Manager	**V.D.Nikolaev** **Ph.D**	
Director	**Petrov A.L.** **Ph.D**	

January 2009

Report Documentation Page

1. REPORT DATE **02 FEB 2009**	2. REPORT TYPE	3. DATES COVERED

4. TITLE AND SUBTITLE **An advanced singlet oxygen generator**	5a. CONTRACT NUMBER **ISTC Registration No. 3380**
	5b. GRANT NUMBER
	5c. PROGRAM ELEMENT NUMBER
6. AUTHOR(S) **Valery Dmitrievich Nikolaev**	5d. PROJECT NUMBER
	5e. TASK NUMBER
	5f. WORK UNIT NUMBER
7. PERFORMING ORGANIZATION NAME(S) AND ADDRESS(ES) **P.N. Lebedev Physical Institute,Nova-Safovaya Str. 221,Samara 443011, Russia, , ,**	8. PERFORMING ORGANIZATION REPORT NUMBER
9. SPONSORING/MONITORING AGENCY NAME(S) AND ADDRESS(ES)	10. SPONSOR/MONITOR'S ACRONYM(S)
	11. SPONSOR/MONITOR'S REPORT NUMBER(S)

12. DISTRIBUTION/AVAILABILITY STATEMENT
Approved for public release; distribution unlimited.

13. SUPPLEMENTARY NOTES
The original document contains color images.

14. ABSTRACT

This report results from a contract tasking P. N. Lebedev Physical Institute as follows: The singlet oxygen O2(1Delta), O2(1Sigma) can be used for medical treatment, sterilization, the deactivation of biological and chemical agents, as source of the energy for gas lasers. The most efficient singlet oxygen generators (SOG) are based on the reaction of chlorine with the basic hydrogen peroxide (BHP). In the frame of the proposed project the bubble SOG with BHP layer under centrifugal acceleration will be developed and studied. This type SOG has not been studied in up to now. The efficiency of the chlorine absorption and O2(Delta) generation in the BHP under centrifugal acceleration is one of the task of the proposed project. Three versions of the SOGs with the BHP layer under centrifugal acceleration will be developed and studied. Finally it is proposed to develop an efficient source of singlet oxygen for applications in science and technology. The results of this project will be discussed with representatives of Partner and will be published in common report on conferences and articles. The personnel of the participant have 20 years experience in study and development of different types SOG. The laboratory of the participant is equipped with devices, facilities and methods for investigations of SOG. The personnel of participant successfully executed projects in development of SOG including in the frame of ISTC projects 1826P, 2230P. Meeting the goals of this project helps Russian scientists to integrate into international scientific cooperation, supports basic and applied research and design for peaceful purposes.

15. SUBJECT TERMS

16. SECURITY CLASSIFICATION OF:			17. LIMITATION OF ABSTRACT	18. NUMBER OF PAGES	19a. NAME OF RESPONSIBLE PERSON
a. REPORT **unclassified**	b. ABSTRACT **unclassified**	c. THIS PAGE **unclassified**		**94**	

Title of the Project: Advanced singlet oxygen generator

Commencement Date: 02 01, 2006

Duration: 36 months

Project Manager Nikolaev V.D.

phone number: 846-335-66-54

fax number: 846-335-56-00

e-mail address: Nikolaev@fian.smr.ru

Leading Institute: Lebedev Physical Institute, Samara Branch
Novosadovaya 221, Samara, Russia, 443011
846-3356654
laser@fian.smr.ru
www.fian.smr.ru

Keywords: singlet oxygen, centrifugal, bubbling, gas-generator, absorption

Objectives of the project

The objective of this project according to Technical Task the bubble SOG with basic hydrogen peroxide (BHP) layer under high centrifugal acceleration will be developed and studied. The efficiency of the chlorine absorption and $O_2(^1\Delta)$ generation in the BHP under centrifugal acceleration is one of the task of the proposed project. Three versions of the SOGs with the BHP layer under centrifugal acceleration will be developed and studied. Finally it is proposed to develop an efficient source of singlet oxygen for applications in science and technology.

The information will be obtained about

- influence of the BHP layer height on chlorine utilization and $O_2(^1\Delta)$ production

- influence of the centrifugal acceleration on chlorine utilization and $O_2(^1\Delta)$ production

- influence of the BHP molarity on chlorine utilization and $O_2(^1\Delta)$ production

- influence of BHP/chlorine ration on chlorine utilization and $O_2(^1\Delta)$ production

- influence of buffer gas dilution on chlorine utilization and $O_2(^1\Delta)$ production

- upper limit of oxygen pressure with high $O_2(^1\Delta)$ yield

- upper limit of oxygen flux from BHP surface

- droplet separation efficiency in the rotary bubble SOG

- water vapor fraction in the oxygen flow

- SOG parameters to achieve high Cl_2 utilization and high $O_2(^1\Delta)$ yield

- opportunity of using bubble SOG with BHP layer under high centrifugal acceleration as an efficient source of $O_2(^1\Delta)$.

Scope of Work and Technical Approach

The following is planned:

1) to study the hydrodynamics of the gas dispersion into liquid under high centrifugal acceleration

2) to develop the physical-chemical model of the chlorine absorption and $O_2(^1\Delta)$ generation in bubbles, float to the surface under high artificial gravity

3) to develop the rotary bubble type oxygen generator with nominal oxygen flow rate of 30 mmole/s

4) to develop oxygen generator with rotary bubble layer with nominal oxygen flow rate of 30 and 50 mmole/s with minimal transport losses of $O_2(^1\Delta)$

5) to study chlorine absorption and singlet oxygen production in reactors with rotary bubble BHP layer in a wide range of parameters

6) to study droplet production and separation in reactors with rotary bubble layer

7) to define the range of parameters of rotary bubble generator for achievement of high chlorine utilization and high $O_2(^1\Delta)$ yield

8) to define the maximum partial oxygen pressure and highest specific oxygen productivity in reactors with rotary bubble layer

9) to test efficiency of reactors with rotary bubble layer at COIL performance

1. Introduction.

It is known that the specific productivity of the bubble type mass transfer apparatus substantially increases when the liquid phase is under high centrifugal acceleration. The increase of the centrifugal acceleration results in the decrease of the size of the generated bubbles and the increase of the bubble velocity. The centrifugal acceleration in the bubble layer can be produced by rotation of the liquid phase on the internal surface of the perforated cylinder or cone. The absorbed gas is blow in the liquid through the nozzles of the perforated surface. The size and the velocity of the bubbles depend on liquid properties, the nozzle size, gas velocity in nozzles, centrifugal acceleration and number of nozzles per cm^2. The decrease of the generated bubbles size and increase of their velocity substantially increase the rate of mass transfer inside bubble. A high bubble velocity and short gas residence time in the bubble layer allow to keep high $O_2(^1\Delta)$ fraction at high pressures. A high convective mass transfer rate permits to increase the liquid residence time in the reactor without substantial decrease of the absorption rate in the bubble. Therefore the ratio of (Cl_2 molar rate / BHP volumetric rate) can be substantially increased in the single pass BHP flow mode.

The proposed advanced SOG is based on the centrifugal bubbling mass and heat transfer apparatus. Some designs of the centrifugal bubbling mass and heat transfer apparatus are described in several patents and scientific papers [for example, **1-16**].

In the present project a two centrifugal bubbling SOG concepts are investigated. In the first one the BHP is supplied on the inner surface of the rotating cylinder or cone and a viscosity force or special blades force to rotate BHP layer. The gas is injected through cylindrical orifices normally to the surface of the rotary bubbler. In the second one the additional rotation of the BHP layer is provided by injection of the gas angularly to the bubble surface in the direction of the rotation of the bubbler.

2.   Theoretical analysis of the centrifugal bubbling singlet oxygen generator.

Chlorine absorption efficiency strongly depends on the gas-liquid specific contact surface, rate of renewal of this surface and gas-liquid contact time. $O_2(^1\Delta)$ yield in the outflow gas depends on the detachment yield, pressure and gas-liquid contact time. So the size of the generated bubbles and their velocity are the most important characteristics of centrifugal bubbling SOG.

2.1.   Bubble velocity.

The review of the periodical literature and monographs showed that a very small works devoted to the theoretical analysis of hydrodynamics and mass-heat transfer processes in the centrifugal bubbling apparatus. For the estimations we will use very simplified, qualified and intuitive speculations.

First of all let's consider motion of a single bubble in liquid being under high centrifugal acceleration. The centrifugal bubbling apparatus works at the conditions of a high gas molar flow rate through the nozzle and a high centrifugal acceleration. The observation showed that at these conditions the shape of the produced bubbles is close to the sphere [1, 2, 3]. For bubble of radius $r_b>1$ mm and velocity $U_b>200$ cm/s the Reynolds number $Re_B>400$. The balance of drag force and buoyancy force results in equation

$$\pi r_b^2 \frac{\rho_\ell U_b^2}{2} c_b = \frac{4}{3}\pi r_b^3(\rho_\ell - \rho_g)G \approx \frac{4}{3}\pi r_b^3 \rho_\ell G \qquad (1)$$

At high Re_b number c_b slowly depends on Re_b. For example in the case of solid sphere $c_b \approx 0.4$ for $500<Re_b<10^4$ [17]. But it was found that for spherical gas bubble in the field of a high centrifugal acceleration $c_b \approx 1 \div 2$ [3]. Therefore the bubble velocity in the field of high centrifugal acceleration is [3] (when $c_b=1.86$)

$$U_b = 1.43\sqrt{r_b G} \qquad \textbf{(2)}$$
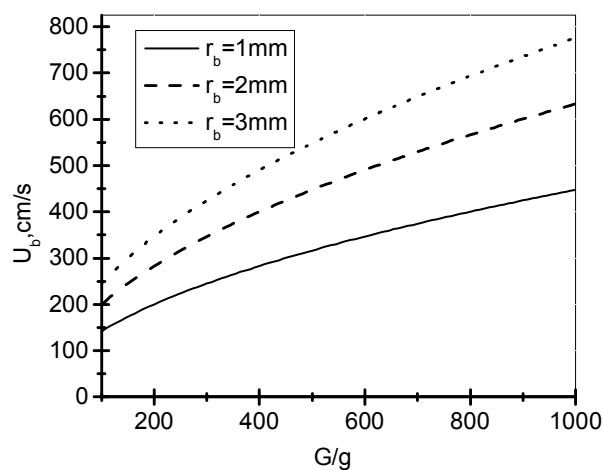
Fig. 1. The velocity of a single bubble ($g=980 cm/s^2$).

2.2. Detachment size of the single bubble for the cylindrical nozzles.

Bubbling-jetting transition. Bubbling or jetting regimes can occur when gas is injected into liquid through the cylindrical nozzle. In the bubbling regime, the dispersed gas moves in liquid as bubbles. In the jetting regime the gas moves from the nozzle to the liquid surface as continuous jet. Some correlations have been proposed for the bubbling to jetting mode transition. We will use the simplest correlation obtained for conditions when surface tension force is negligible in comparison with buoyancy force and gas momentum force. For the single nozzle the bubbling regimes occurs when

$$\frac{H}{d_n} > 1.5 \left(\frac{U_g^2 \rho_g}{d_n G \rho_\ell} \right)^{0.5} \quad [18] \qquad (3)$$

This criterion follows from the balance of the gas momentum force and hydrostatic force.

When the distance between nozzles is comparable with the size of bubblers the bubbling occurs when

$$\frac{H}{d_n} > \frac{1.1}{F} \left(\frac{U_g^2 \rho_g}{\rho_\ell H G} \right)^{0.5} \quad [19] \qquad (4)$$

For reverse inequality the jetting of gas takes place. If the gas pressure over liquid column $P_g \ll P_l = \rho_l G H (1-H/D)$ then $\rho_g = \mu P_l/(RT_l)$ and one obtains from (3)

$$\frac{H}{d_n} > 2.25 k \left(\frac{U_g}{U_s} \right)^2 \approx 3.4 \left(\frac{U_g}{U_s} \right)^2 \qquad (3A)$$

So, at subsonic gas velocity from the nozzle and $H/d_n > 3.4$ the bubbling regime is expected. Analogously from (4) one obtains criteria

$$\frac{H}{d_n} > \frac{1.6}{F} \frac{U_g}{U_s} \quad (4A)$$

The bubbling regime is expected when $H/d_n > 3.2$ for $F < 0.5$ and subsonic gas velocity.

When $U_g \approx U_s$ and $\rho_g > (P_l/RT)$ the criteria (3A), (4A) are not valid and the jetting regime is expected.

It is expected that the efficiency of chlorine utilization will be higher and BHP aerosols generation will be minimal in the case of the bubbling regime than for the jetting regime.

Single bubble generation. Let's assume that the BHP column rotates together with the bubbler or the velocity U_l of the liquid relative to the bubbler small so that we can neglect the **knife effect**. The axial BHP velocity relatively gas nozzle occurs only because of necessity to remove the depleted BHP from the bubbler surface. Estimation of the time needed for the bubble formation and frequency of the bubble generation in a high centrifugal field was made in papers [**4**,**5**]. Breaking the balance of forces affecting on the bubble induces detachment of the bubble from the nozzle. Processing of experimental data [**4**] resulted in next correlations for the detachment bubble size, time of the bubble growth, frequency of generation. For zero liquid cross velocity $U_l=0$ and $U_g<U_s$ the detachment radius of the single bubble is given by [**4**]

$$r_b = \frac{d_n}{2} \times 0.68 \frac{\left(\rho_\ell / \rho_g \right)^{0.14}}{1 + \left(\eta_g / \eta_\ell \right)^{0.32}} \left(\frac{U_g^2}{d_n G} \right)^{0.16} \qquad \textbf{(5)}$$

Time of the bubble formation is given by

$$\tau = \frac{\sqrt{0.12 \times 10^{-6} C^2 + 1.05 \times 10^{-3} C + 0.21} - 0.35 \times 10^{-3}}{C} \qquad \textbf{(6)}$$

and the frequency of the bubble generation is given by

$$f = \sqrt{0.25 \times C^2 + 0.71 \times C + 0.19 \times 10^6} - 0.44 \times 10^3 \qquad \textbf{(7)}$$

where $C = \sqrt{\dfrac{G}{d_n} \left(\dfrac{\rho_g d_n G}{\rho_\ell U_g^2} \right)^{0.1}} \operatorname{Re}_g^{0.06}$.

If $U_l \neq 0$ the detachment bubble radius is equal to $r_b \left(1 - 1.12 \times 10^{-4} \operatorname{Re}_w \right)$ and frequency of the bubble generation increases in $\left(1 + 3.1 \times 10^{-4} \operatorname{Re}_w \right)$ times [6], here r_b is defined by formula (5). We will assume that output gas temperature is equal to the temperature of the bubbler ($T_g \approx T_l$) (because rather isothermal than adiabatic regime of the gas flow in the nozzle).

In the case of the subsonic gas velocity one obtains at the exit of the nozzle:

$$\rho_g = \mu(P_l + P_g)/RT_l, \qquad U_g = \frac{4(m_c + m_H)\mu}{\rho_g \pi d_n^2} \qquad (8)$$

In the case of the sonic gas velocity at the exit of the nozzle one obtains

$$U_g = U_s = (kRT_l/\mu)^{0.5}, \quad \rho_g = \frac{4(m_c + m_H)\mu}{U_s \pi d_n^2} \qquad (9)$$

The transition from (8) to (9) occurs when calculated $U_g \geq U_s$. In the case of the sonic gas velocity $\rho_g > \mu(P_l + P_g)/RT_l$ and the expansion of the gas inside bubble results in increase of the bubble size in $(RT_l \rho_g / \mu(P_l + P_g))^{1/3}$ times.

In the approximation when $P_g \ll P_l$ (low gas pressure over BHP), $U_g < U_s$, $\eta_g \ll \eta_l$ one can obtain

$$r_b = \frac{d_n^{0.2}}{2} \times 0.68 \frac{(RT_\ell)^{0.46}}{H^{0.46} \mu^{0.14} \rho_\ell^{0.32}} \left(\frac{4(m_c + m_H)}{\pi} \right)^{0.32} \left(\frac{1}{G} \right)^{0.62} \qquad \textbf{(10)}$$

$$\text{Or } r_b = \frac{d_n^{0.84}}{2} \times 0.68 \frac{(RT_\ell / \mu)^{0.14}}{H^{0.14}} (U_g)^{0.32} \left(\frac{1}{G} \right)^{0.3} \qquad (10A)$$

The viscosity of the BHP has been measured (Fig. 2). The density of BHP-1 was $\rho_l = 1.31$ g/cm^3, BHP-2 $\rho_l = 1.2$ g/cm^3. The freezing temperature of the BHP-2 is less than -30C and freezing temperature of the BHP-1 is near -15C. The KCl solubility is a very low in the BHP-2. For example at [KCl]=1.6M a solid salt fragments were observed at temperature -10C. The KCl is much better soluble in the BHP-1. For example the solid KCl was not observed up to [KCl]=3.2M at the BHP temperature -15C. Therefore BHP-1 is a good solution for the SOG with the single BHP liquid burn down pass.
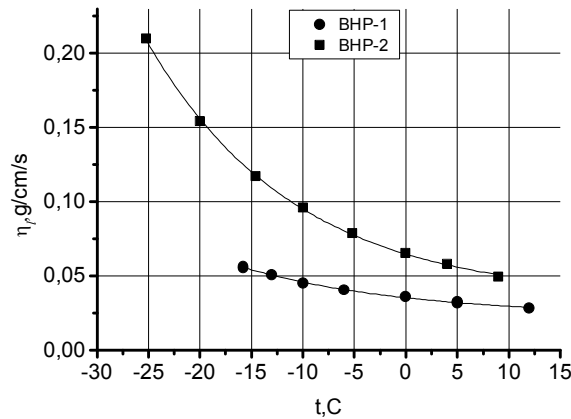
Fig. 2. The viscosity of the BHP. BHP-1(2M of KOH, 11 M of H_2O_2), BHP-2(6.5M of KOH, 7.5M of H_2O_2)

The dependence of the viscosity can be fit by the first exponential decay:

For BHP-1 by
$$\eta_\ell = 0.023 + 0.011228 \exp\left(-\frac{t_\ell}{16.2}\right), \quad (t_l=-15C \div +12C) \tag{11}$$

For BHP-2 by
$$\eta_\ell = 0.0348 + 0.03 \exp\left(-\frac{t_\ell}{14.34}\right) \quad (t_l=-25C \div +10C) \tag{12}$$

Estimations of the detachment bubble radius when BHP velocity relative to the bubbler surface $U_l=0$ are presented in Fig. 3.
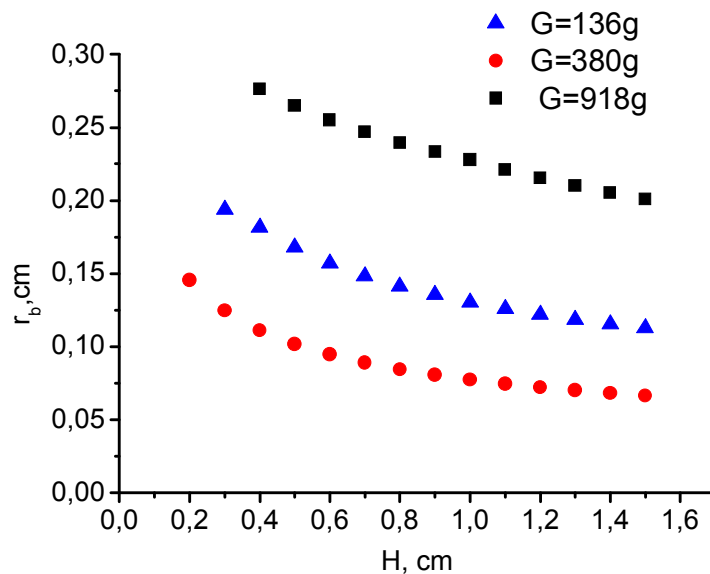
Fig. 3. Bubble radius. d_n=0.3 mm, m_c=62μmole/s, m_H=160μmole/s, t_l=-20C. Physical-chemical data from Table 1, viscosity data for BHP-2. The calculations are reasonable only when $2r_b>H$.

For d_n=0.3 mm, H~10 mm, G=380g the diameter of the generated bubbles is ~3mm. It is seen from (10A) the increase of the nozzle diameter results in increase of the generated bubble size as $d_n^{0.84}$ at the constant gas velocity. As seen from (10) the increase of the acceleration and BHP column height result in the decrease of the detachment bubble size at constant gas molar flow rate through the nozzle.

It is expected that for tangential injection of gas into BHP column when the axis of the nozzles or slits is turned on the angle to the bubbler surface the size of the bubbles will be less than for the normal injection.

This consideration is not valid when the distance between nozzles is less that the size of bubble. Also it is not valid when gas is injected through slit nozzles. When SOGs operated at high density of cylindrical nozzles per $1 cm^2$ or relatively high cross section area of slit nozzles per $1 cm^2$ and high specific gas loading per nozzle the coalescence of the generated bubbles occur. In this case the gas "cushion" is formed near bubbler surface. This gas cushion is quite unstable and destroys into bubbles. The size of bubbles rather depends on physical properties of BHP and centrifugal acceleration. The bubbles size reduction continues until they become stable against momentum head of the liquid. It occurs when tension pressure $2\sigma_\ell / r_b$ equals to the pressure $c_b \rho_\ell U_b^2/2$ of the liquid momentum head. On the other hand liquid momentum head $\pi r_b^2 c_b \rho_\ell U_b^2/2$ should be equals

to the buoyancy force $\dfrac{4\pi r_b^3}{3} G\rho_\ell$. So the stable size of bubble is proportional to the capillary size:

$r_b \sim L_c = \sqrt{\sigma_\ell / (\rho_\ell G)}$, where σ_ℓ is surface tension, G is the centrifugal acceleration, ρ_ℓ is liquid density.

2.3.   Observation of the bubble generation in the centrifugal field.

The dispersion of the air through the single nozzle into glycerin (60%) water solution has been studied. This water-glycerin solution has η_l=0.11 g/cm/s, ρ_l=1.15 that is close to the properties of the BHP-2. The scheme for the observation how gas interacts with liquid is presented in **Fig. 4**. The diameter of the rotating bubbler was of D=9 cm. The time of the photo camera exposition was of $\sim 2\times 10^{-5}$c. The observed shape of the gas phase is presented in **Fig. 5**-**Fig. 8**.
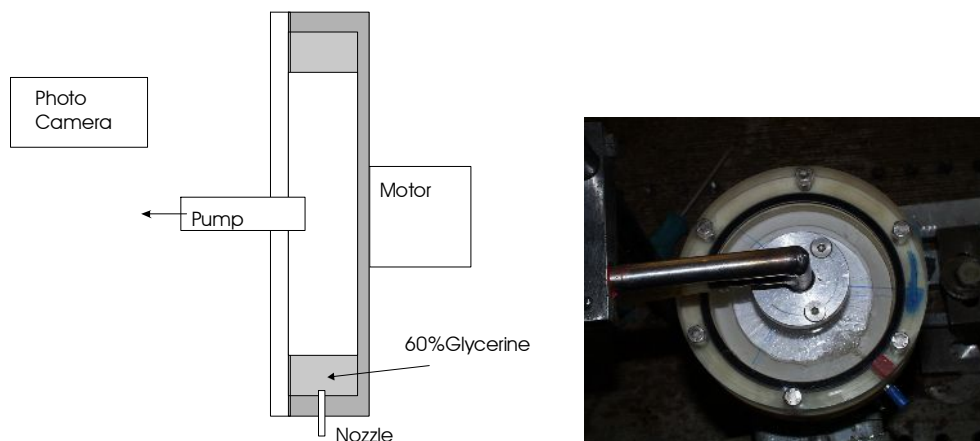
Fig. 4. Rotating bubbler with single nozzle.

A   *B*   *C*

Fig. 5. The gas-liquid structure. $d_n=0.03$ cm, D=9 cm, $m_{air}=0.29$ mmole/s, $P_g=50$ torr, H≈9 mm (the width of the black rubber is 5 mm). A - n=27s^{-1}, B - n=45s^{-1}, C - n=56s^{-1}.

The mass flow rate of the air through the nozzle is equal to the mass flow rate of the helium-chlorine mixture (m_c≈107 μmole/s, m_H=162 μmole/s). At low n=27c^{-1} no bubbling but only jetting regime was observed. In condition for photo A the sonic air velocity at the nozzle exit is expected. At n=45c^{-1} and n=56c^{-1} only bubbling was observed. The observed bubbles have the spherical shape. The estimated bubble radius according to formula (5) is in a good agreement with observed. For higher G the size of the bubble is less (compare B and C pictures in Fig. 5). Let's estimate the bubble velocity in the picture B. The diameter of the bubble $2r_b$≈0.3cm, the centrifugal acceleration G=3.6×10^{5}cm/c^2 (~367g), the liquid column pressure P_l=296 torr (H≈1 cm), gas density near nozzle ρ_g=μ(P_g+P_l)/RT$_l$=5.5×10^{-4}g/cm^3. The time of the bubble formation is τ≈ ρ_g($4\pi r_b^3$/3)/(μm_{air})≈10^{-3}c (in a good agreement with calculated 8.5×10^{-4}s according to (6)). One can see in the Fig. 5B that the previous bubble just now left the liquid column. So the rough estimation of the bubble velocity is U_b=(H/2/τ)=500 cm/s. This value of the bubble velocity is slightly higher than estimated according to the formula (2).

Fig. 6 shows the generated gas structure for the single nozzle 0.5mm in diameter.

The jetting of the gas
d_n=0.55mm, n=30c^{-1},
m_{air}=1mmole/s
P_g=50 torr, H≈8mm

The bubbling of the gas
d_n=0.55mm, n=50s^{-1}, m_{air}=1mmole/s
P_g=50 torr, H≈8mm
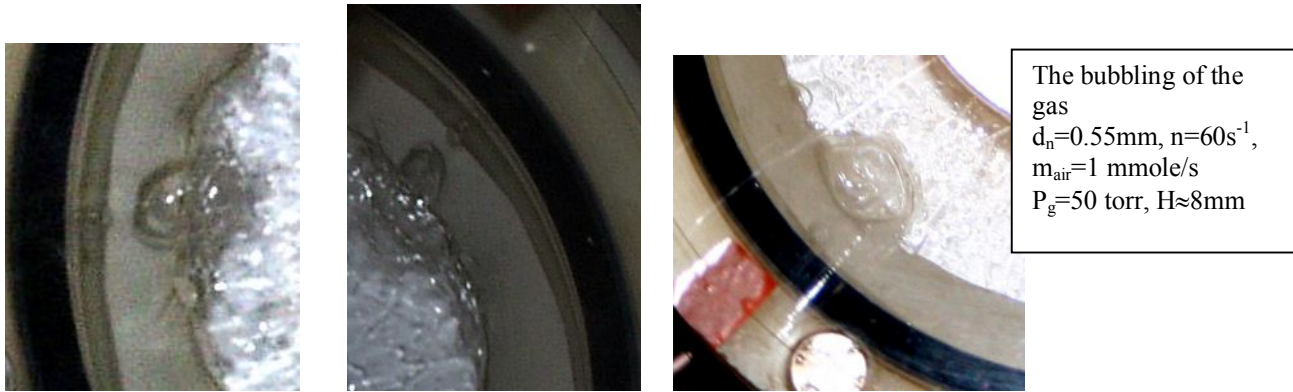
Fig. 6. The gas-liquid structure when the air is injected through the nozzle d_n=0.55mm into the 60% glycerin.

It is seen that the diameter of the bubble is of ~5 mm for the nozzle with d_n=0.55mm. This value is correlated with estimated from formula (5).

Fig. **7** shows the gas-liquid structure with single 0.95mm nozzle.
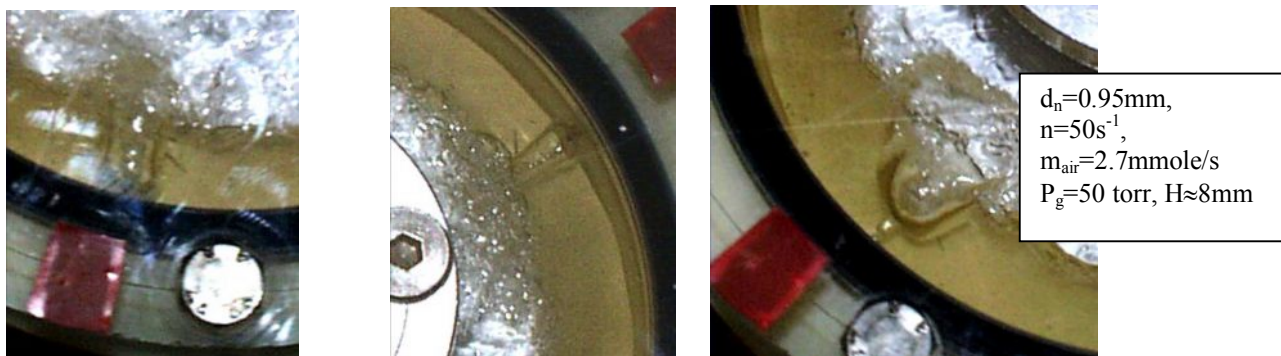
It seen that bubble size is compared with liquid column height and sometimes the jetting of the gas is observed even at high G= 453g.

Fig. 7. The gas-liquid structure for d_n=0.95 mm.

It seen that the increase of the centrifugal acceleration (887g) resulted in gas bubbling even at low H and big d_n (right photo).

Fig. 8 shows the gas-liquid structure with single 0.95mm nozzle turned on the angle ~ 90° to the normal. The tangential injection of the gas stream into liquid through many nozzles can induce additional rotation of liquid column and increasing of the centrifugal acceleration.

d_n=0.95mm, n=40s^{-1}, m_{air}=2mmole/s P_g=50 torr, H≈10mm

d_n=0.95mm, n=50s^{-1}, m_{air}=2mmole/s P_g=50 torr, H≈10mm

d_n=0.95mm, n=60s^{-1}, m_{air}=2mmole/s, P_g=50 torr, H≈10mm
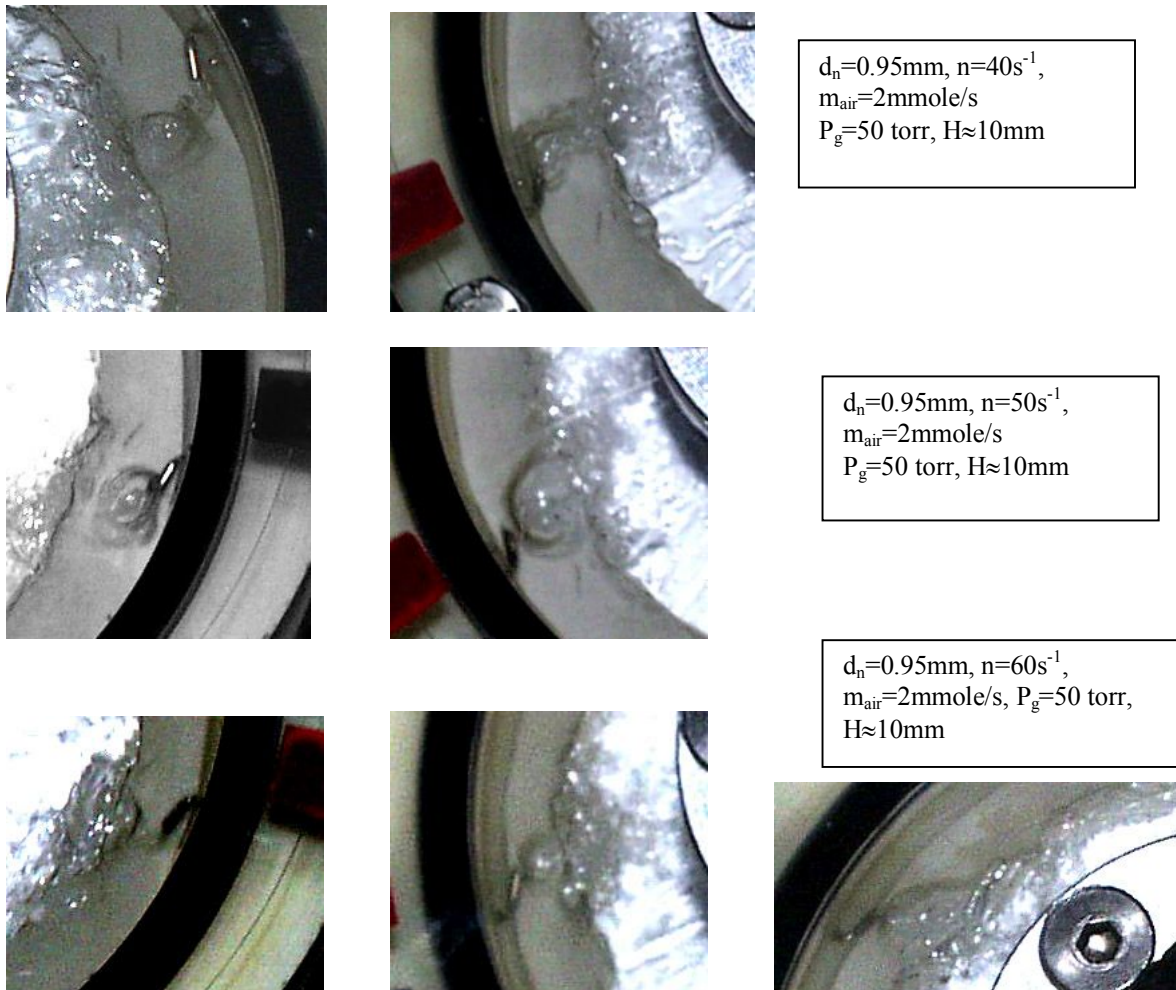
Fig. 8. The gas-liquid structure with single 0.95mm nozzle turned on the angle ~90° to the normal.

It is seen that at the tangential gas injection the length of the gas jet penetration into liquid is small and bubble grows in normal direction.

When the distance between is comparable with diameter of the bubble generated by single nozzle the picture of gas dispersion is a quite differ (Fig.10). The distance between nozzles is equal to 5mm, air molar flow rate equals to 1 mmole/s. The injection of air through the slit nozzles also generates "caviar" above liquid column (Fig.9). Looking on these figures it is quite difficult to say anything about size of gas impurities in liquid. It seem to us that picture in Fig.9 is more close to the situation when the size of the gas impurities is determined by capillary instability as described in page 8.
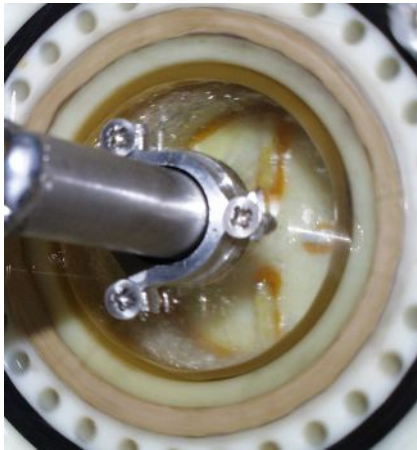
Fig. 9. Injection of 120 mmole/s of air through 92 slits 0.2mm×8mm of size.

Fig. 10. Injection of air into 60% glycerin through 4 nozzles 0.55mm in diameter.

2.4.   Estimation of the chlorine utilization and $O_2(^1\Delta)$ yield.

Before starting CBSOG design it is quite important preliminary to find the dependence of the chlorine utilization and $O_2(^1\Delta)$ yield versus working parameters. The estimations will be made in the approximation of the generation of sequences of the bubbles from the cylindrical nozzle. The chlorine absorption kinetics is different on the stage of the bubble growth and on the stage of the bubble rising. We will assume that the gas velocity in the gas nozzle is a several hundred meters per second or sonic. A high rate of the hydrodynamic renewal of the growing surface of the bubble is expected and the chlorine absorption can be described in the approximation of the first order reaction or when HO_2^- concentration N_B=const. In the simplest approximation the chlorine and helium molar flow rates through the nozzle are assumed constant. In this case the radius of the growing bubble is described by formula

$$r(t) = r_b\left(\frac{t}{\tau}\right)^{1/3} \tag{13}$$

The amount of chlorine Q_c inside the bubble is described by formula

$$\frac{dQ_c}{dt} = m_c - \frac{3\beta}{r(t)}Q_c \tag{14}$$

The solution of (14) gives the chlorine utilization when the bubble detaches from the nozzle ($t=\tau$)

$$U1 = 1 - \frac{Q_c(\tau)}{\tau\,m_c} = 1 - \frac{1}{\tau}\exp(-4.5\tau\beta/r_b)\int_0^\tau \exp\left(4.5\tau^{1/3}y^{2/3}\beta/r_b\right)dy \tag{15}$$

or

$$U1 = 1 - \frac{1.5}{q}\left(1 - \exp(-q)\int_0^1 \exp(qy^2)dy\right), \text{ where } q = \frac{4.5\tau\beta}{r_b} \tag{15a}$$

Approximately U1=1-exp(-0.341q).

We also assume that at the stage of the bubble raising the Hill vortex is generated inside the bubble. This vortex dramatically enhances the mass transfer rate in the gas phase. So we will assume that the gas diffusion resistance is negligible and the rate of chlorine absorption is defined only by the liquid resistance or by mass transfer rate β. We will assume that hydrodynamic renewal of the bubble surface is too fast to compensate the depletion of chemicals near the bubble surface. In this case the mass transfer rate β is defined by the rate constant of the reaction and chlorine diffusivity. At the stage of the bubble raising the chlorine content in bubble is described by equation

$$U_b(x)\frac{dQ_c}{dx} = -\beta\frac{3}{r}Q_c, \qquad \mathbf{Q_c(x=0)=(1-U1)m_c\tau} \qquad \textbf{(16)}$$

As bubble rise the hydrostatic pressure decreases, bubble radius increases and bubble velocity increases as

$$r = r_b\left(\frac{P_\ell + P_g}{P_\ell + P_g - \rho_\ell xG}\right)^{1/3}, \quad U_b(x) = U_b\left(\frac{P_\ell + P_g}{P_\ell + P_g - \rho_\ell xG}\right)^{1/6} \qquad \textbf{(17)}$$

Because we assume that H<<D/2 the value of G is approximately independent on x. The solution of (14) gives the chlorine utilization when the bubble leaves the BHP column (x=H-r_b):

$$U = 1 - \frac{Q_c(x=H-r_b)}{m_c\tau} = 1-(1-U1)\times\exp\left(-\frac{2(H-r_b)\beta}{r_bU_b}\frac{P_\ell + P_g}{P_\ell}\left(1-\left(\frac{P_g}{P_\ell + P_g}\right)^{3/2}\right)\right) \qquad \textbf{(18)}$$

For the estimation of the $O_2(^1\Delta)$ yield we will assume that detachment yield Y_d is constant because we assume that no strong depletion of HO_2 takes place. All $O_2(^1\Delta)$ losses inside the bubble is due to homogeneous quenching and $O_2(^1\Delta)$ yield depends only pτ parameter. Roughly this parameter is equal to

$$\chi(torr\times s)=m_c/(m_c+m_H)(2P_g+P_l)/2*H/U_b \qquad (19)$$

The homogeneous quenching is due to the reactions

$O_2(^1\Delta) + O_2(^1\Delta) \rightarrow O_2(^1\Sigma) + O_2(^3\Sigma)$, 2.7×10^{-17} cm^3/s
$O_2(^1\Sigma) + H_2O \rightarrow O_2(^1\Delta) + H_2O$, 6.7×10^{-12} cm^3/s
$O_2(^1\Delta) + O_2(^1\Delta) \rightarrow O_2(^3\Sigma)+ O_2(^3\Sigma)$, 1.7×10^{-17} cm^3/s
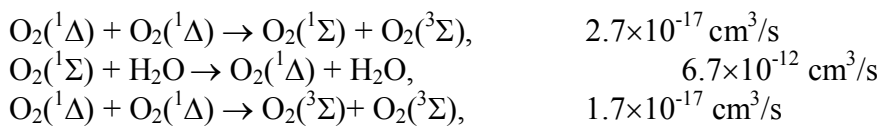
The singlet oxygen yield approximately is equal to

$$\mathbf{Y = \frac{Y_d}{1+2Y_d\chi f(U)}} \qquad \textbf{(20)}$$

Where $2(torr\times s)^{-1}$ in (20) is the $O_2(^1\Delta)$ quenching rate constant and

$$f(U) = -\frac{\ln(1-U)+U(1+0.5U)}{U^2} \qquad \textbf{[20]}.$$

The physical-chemical data used for the estimations of the chlorine utilization and $O_2(^1\Delta)$ yield are shown in **Ошибка! Неверная ссылка закладки.**.

Table 1. Physical-chemical data for the estimation of $O_2(^1\Delta)$ yield.

$D_c = 3 \times 10^{-10} T_l / \eta_l$
$D_H = 6 \times 10^{-10} T_l / \eta_l$
$\eta_g \approx 1.8 \times 10^{-4}$ g/cm/s $(O_2 + He + Cl_2$ mixture)
viscosity BHP-1: $\eta_\ell (g/cm/s) = 0.019 + 0.01\exp(-t_\ell/16.2)$, BHP-2: $\eta_\ell (g/cm/s) = 0.02657 + 0.0229\exp(-t_\ell/14.34)$
$H_c \approx 1$
$K = 5 \times 10^8 M^{-1} s^{-1}$ [7]
$Y_d = 0.8$

For the calculation of U_b, τ, r_b formulas (2), (5-6) have been used. The examples of the estimation of the chlorine utilization and $O_2(^1\Delta)$ yield are presented in Fig. 11 and Fig. 12. According to these calculations the chlorine utilization and $O_2(^1\Delta)$ yield are approximately the same for BHP-2 and for BHP-1. Indeed the KOH molarity in BHP-2 is higher than in BHP-1 in 3 times, but the viscosity of BHP-2 in three time higher than viscosity of BHP-2. Therefore the mass transfer rate β for BHP-1 is approximately the same as for BHP-2. The estimations showed that for this example more than 30% of chlorine is absorbed at the stage of the bubble growth. The $O_2(^1\Delta)$ yield substantially decreases with the increase of the acceleration and BHP column height. For the nozzle diameter $d_n=0.5$mm the chlorine utilization is less than for $d_n=0.3$mm but $O_2(^1\Delta)$ yield is higher.

A

B
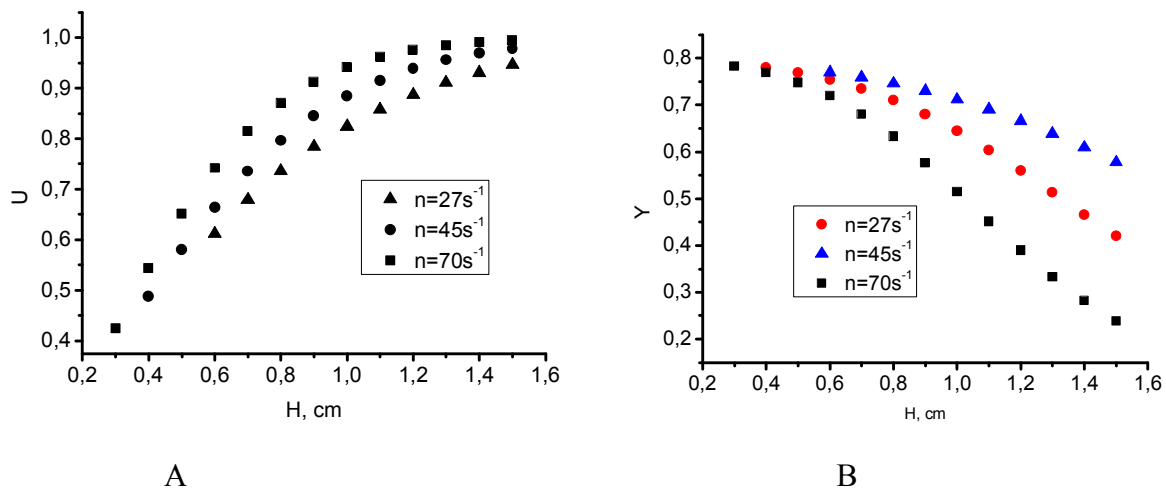
Fig. 11. Chlorine utilization (A) and $O_2(^1\Delta)$ yield (B). $d_n=0.3$ mm, $m_c=62$μmole/s, $m_H=160$μmole/s, $D=9.3$ cm, $t_i=-15$C, $P_g=35$ torr. Physical-chemical data from Table 1, viscosity data for BHP-1.

A   B
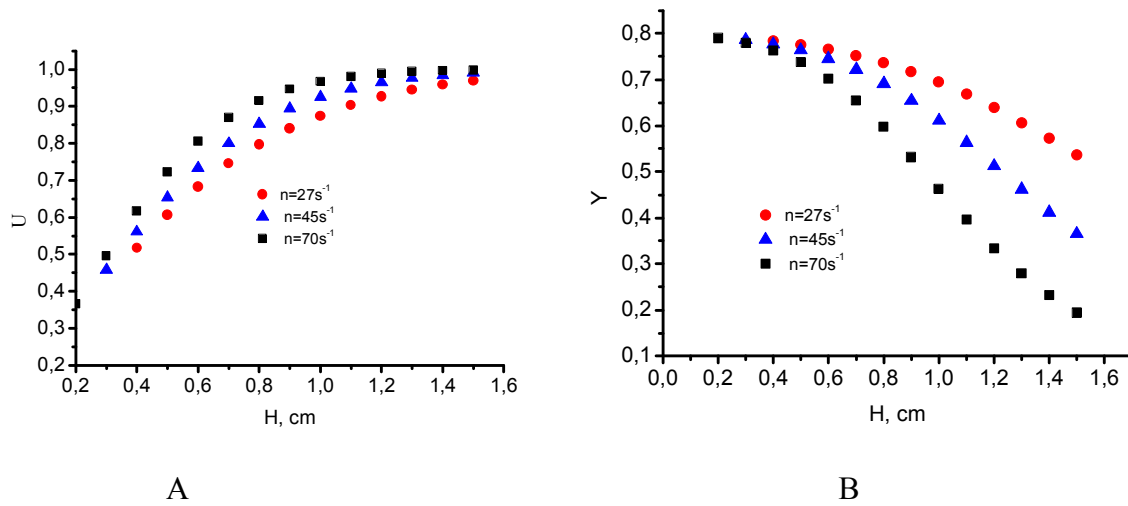
Fig. 12. Chlorine utilization (A) and $O_2(^1\Delta)$ yield (B). d_n=0.3 mm, m_c=62μmole/s, m_H=160μmole/s, D=9.3 cm, t_i=-20C, P_g=35 torr. Physical-chemical data from Table 1, viscosity data for BHP-2.

Let's now estimate the requirements to achieve "good" chlorine utilization and $O_2(^1\Delta)$ yield when **P_g=400 torr, m_c:m_H=1:3** and P_g>>P_l (thin BHP column height). The bubble rise time is $\dfrac{H}{1.43\sqrt{r_b G}}$.

To achieve "good" utilization the inequality should be valid

$$\beta \frac{3H}{r_b 1.43\sqrt{r_b G}} \geq 3 \quad \text{or} \quad \beta \frac{H}{r_b^{1.5} G^{0.5}} \geq 1. \qquad \textbf{(21)}$$

To achieve "good" $O_2(^1\Delta)$ yield one needs

$$\frac{Y_d m_c P_g H}{(m_c + m_H)1.43\sqrt{r_b G}} < 0.1 \qquad \textbf{(22)}$$

For $\beta \approx 50$ cm/s, P_g=400 torr, m_c:m_H=1:3, Y_d=0.8 one obtains

$$\frac{H}{r_b^{1.5} G^{0.5}} \geq 0.02 \text{ s/cm} \quad \textbf{and} \quad \frac{H}{\sqrt{r_b G}} < \textbf{0.0018 s} \qquad \textbf{(23)}$$

From (23) one obtains the maximum bubble radius r_b<0.1 cm. But simultaneously the inequality $\dfrac{H}{\sqrt{r_b G}} < 0.0018$ s should be valid.

In **Ошибка! Неверная ссылка закладки.** the parameters of the centrifugal bubble SOG are presented to achieve a "good" utilization and $O_2(^1\Delta)$ yield at the exit of the gas from the BHP column.

Table 2. Parameters of the centrifugal SOG to achieve "good" utilization and $O_2(^1\Delta)$ yield for the output oxygen pressure ~100 torr.

r_b, mm	H, mm	G, cm/s^2 (g)	P_l, torr
1	4	5×10^5 (510g)	177
0.5	3	5.5×10^5 (560g)	148
0.25	2	5×10^5 (510g)	88

How to generate such small bubbles? The most evident solution for the generation of small bubbles is to decrease the nozzle diameter and the gas velocity in the nozzle. But in this case the oxygen flux from the bubbler surface and superficial gas velocity will decrease. On the other hand using the "big diameter" nozzles is better to avoid clogging of nozzles by KCl particles or by extraneous particles. The external force is needed for the destruction of the bubbles generated by "big diameter" nozzles.

2.5.   Estimation of final BHP temperature and water vapor fraction.

In the single burn down CBSOG the output water vapor fraction should be low enough and the consumption of the BHP high. Let's consider the BHP layer moving with velocity U_l along perforated wall (**Fig. 13**).
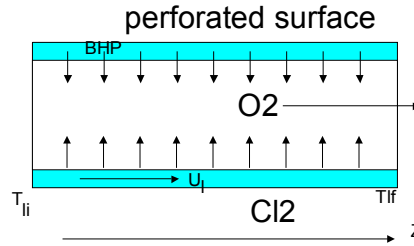
Fig. 13.

The BHP temperature increases because of the heat release in the process of $O_2(^1\Delta)$ generation. The evaporation of the water vapor dumps the BHP temperature rise. We assume that water vapor partial pressure in the bursting bubble is close to the saturated value and much less than oxygen+chlorine gas pressure over BHP column($P_{sw} \ll m_c P_g(m_c+m_H)$). We ignore also gas heat capacity and reverse water vapor condensation into BHP. Hence the local water vapor flux from the BHP is $m_w=\eta_w m_c=(1+A)P_{sw}/P_g$ and the BHP temperature increases along z as

$$\frac{dt_\ell}{dz} = \frac{Um_c \times (Q_r + (1-Y)\times Q_\Delta) - m_c\eta_w(z)Q_w}{U_\ell \times H \times C_\ell} = \frac{M_c}{LV_\ell}\frac{U\times(Q_r+(1-Y)\times Q_\Delta)-\eta_w(z)Q_w}{C_\ell} \qquad \textbf{(24)}$$

In the case of the low water vapor fraction $U\times(Q_r+(1-Y)\times Q_\Delta) \gg \eta_w(z)Q_w$ we can neglect by heat of water vapor evaporation. In this approximation the BHP temperature t_l lineally depends on z and at the exit of the SOG the BHP temperature is
.

$$t_{\ell f} = t_{\ell i} + \frac{UM_c \times (Q_r + (1-Y)\times Q_\Delta)}{V_\ell C_\ell} \qquad \textbf{(25)}$$

The saturated vapor pressure over BHP was measured (Fig. 14). The water vapor fraction substantially higher than H_2O_2 vapor fraction (especially for BHP-2). So approximately it will be assumed that measured total vapor pressure is almost water vapor pressure.
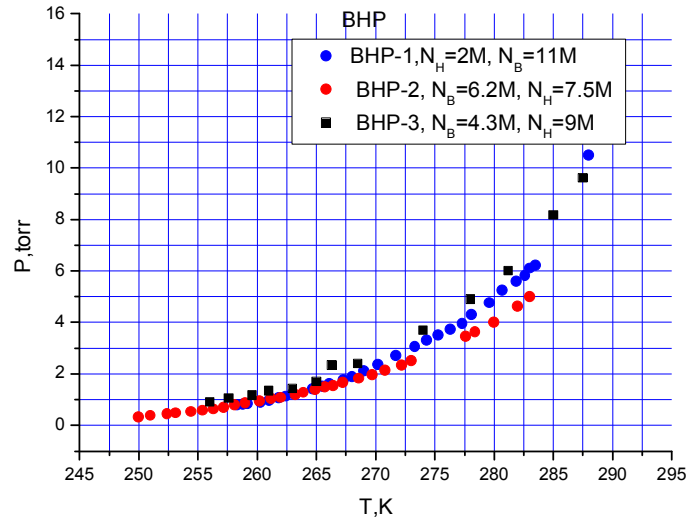
Fig. 14. *Saturated vapor pressure over the BHP.*

The water vapor pressure in the range of temperatures t_l=-25C÷+15C can be described by formulas:

For BHP-1: $P_{sw}(torr) = \exp(22.50 - 5856.47/T_\ell)$ **(26)**

Or $P_{ws}(torr) = 2.82\exp(0.07784t_\ell)$ **(26a)**

For BHP-2: $P_{sw}(torr) = \exp(20.518 - 5352.79/T_\ell)$ **(27)**

or $P_{ws}(torr) = 2.43\exp(0.073t_\ell)$ **(27a)**

For BHP-3 $P_{ws}(torr)=\exp(21.46-5523.45/T)$.

The local fraction of the water vapor to the oxygen+chlorine mixture in the bursting bubble is

$$\eta_w(z) = (1+A)P_{ws}(z)/P_g. \tag{28}$$

The integration of (24) gives the water vapor fraction at exit of the SOG

$$\eta_w = \frac{1}{L}\int_0^L \eta_w(z)dz = \frac{(1+A)}{P_g L}\int_0^L P_{ws}(z)dz = \frac{(1+A)}{P_g}\frac{P_{wsf} - P_{wsi}}{\ln\left(\dfrac{P_{wsf}}{P_{wsi}}\right)} \tag{29}$$

Where P_{wsi} and P_{wsf} are the water vapor saturated pressures for BHP temperatures t_{li} and t_{lf} accordingly. The efficiency of the BHP consumption is $\eta_{BHP}=2UM_c/N_B/V_l$.

The results of the calculations are presented in Fig. 15 and Fig.16 (C_l=3.7 J/cm^3/K, U=100%, Y=0.7, Q_r=113 kJ/mole, Q_Δ=94 kJ/mole). The real exit BHP temperature and water vapor fraction is expected to be less because we neglected by heat of water evaporation.

a)   b)
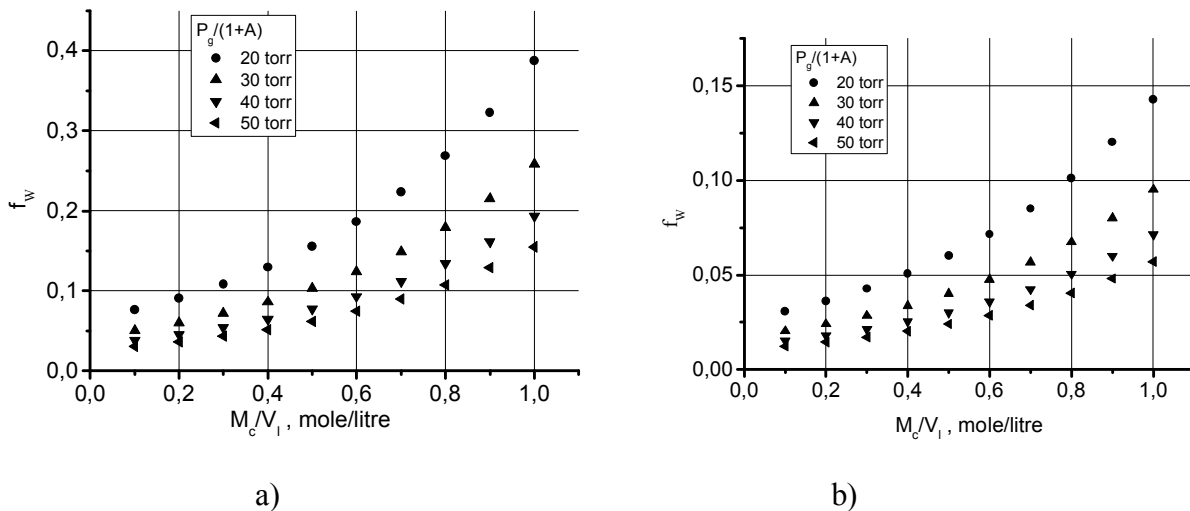
Fig. 15. Water vapor fraction at different partial oxygen pressure over BHP. a) BHP-1, t_{li}=-15C, b) BHP-2, t_{li}=-20C.

The efficiency of the BHP consumption in single burn down and final BHP temperature are shown in Fig.16.

a   **b**
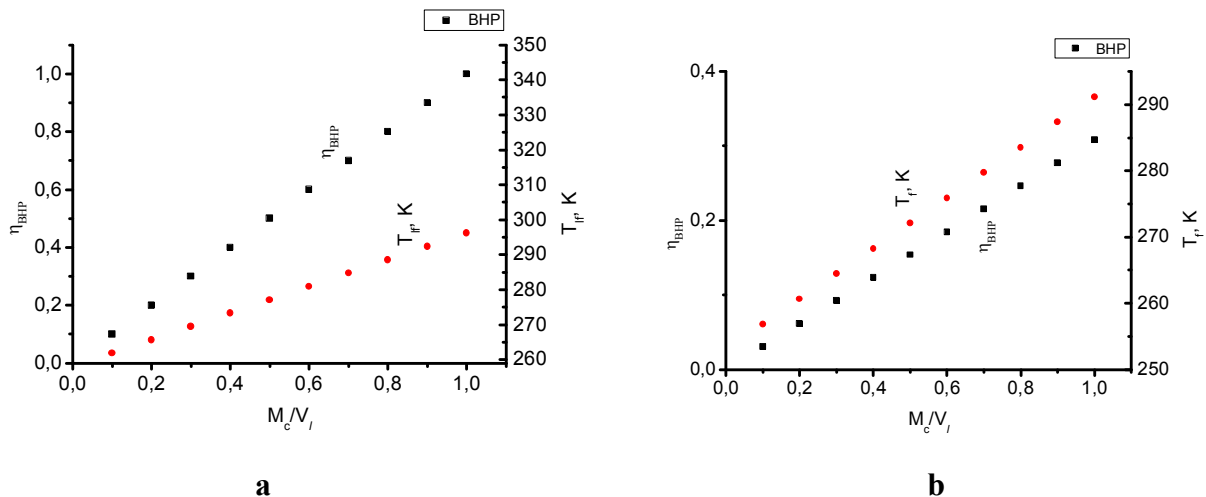
Fig. 16. The efficiency of the BHP consumption in single burn down and final BHP temperature. a) BHP-1, t_{li}=-15C, b) BHP-2, t_{li}=-20C.

For the BHP-1 the water vapor fraction is less than 20% at BHP consumption 50%, ratio M_c/V_l=0.6 mole/liter and active gas (chlorine + oxygen) pressure more than 20 torr. The water vapor fraction is less than 10% at BHP consumption 50%, ratio M_c/V_l=0.6 mole/liter and active gas (chlorine + oxygen) pressure more than 40 torr. The outlet BHP temperature is ~280K for both cases.

For the BHP-2 the water vapor fraction is less than 15% at BHP consumption 30%, ratio M_c/V_l=1 mole/liter and active gas (chlorine, oxygen) pressure more than 20 torr. The water vapor fraction is less than 10% at BHP consumption 30%, ratio M_c/V_l=1 mole/litre and active gas (chlorine, oxygen) pressure more than 30 torr. The outlet BHP temperature is ~290K for both cases.

It is quite important to emphasize that output water vapor pressure more than in $\ln\left(\dfrac{P_{wsf}}{P_{wsi}}\right)$ times

less than saturated water vapor pressure for the output BHP temperature.

2.6.   Estimation of size and velocity of the produced droplets.

The droplet (aerosol) fraction at the exit of the SOG is a very important parameter. A big fraction of the liquid phase at the exit of the SOG results in the increasing of the water-hydrogen peroxide vapor fraction, clogging of the gas transport duct by solid particles and light scattering. Let's estimate the maximum permissible liquid fraction at the exit of SOG.

Roughly it is assumed that 10% of the water vapor molar fraction relative to Cl_2+O_2 doesn't effect on the gain medium quality. We will assume $Cl_2:O_2:He=0.1:0.9:3$ gas composition at the exit of the SOG. 10% of the molar fraction relative to the $Cl_2:O_2$ mixture corresponds to the 4% of water mass fraction to the total mass of the gas phase. The mass water fraction in the BHP is presented in

Table 3.

Table 3. Mass fraction of the BHP components.

	Fraction of the free H_2O_2	Fraction of the free H_2O	Fraction of the KHO_2
BHP-1 (2M of KOH+11 M H_2O_2, ρ_l=1.2 g/cm^3)	28.3%	59.5%	12.2%
BHP-2 (6.5M of KOH+7.5M H_2O_2, ρ_l=1.3 g/cm^3)	2.6%	60.9%	36.5%

Influence on water vapor fraction. The 4% mass water fraction corresponds to the 6.7% of the BHP mass fraction. The droplet realizes the water as vapor and residue consists of $KHO_2\bullet H_2O_2\bullet H_2O$ complex. So no all molecules leave the droplet. The evaporation of the droplets has negligible effect on the total water vapor fraction if BHP mass fraction f_d will be substantially less than 6.7%.

Influence on the gas-transport duct clogging. Let's now estimate maximum aerosol fraction for the minimal clogging of the gas-transport duct. We assume that total gas molar flux in the transport duct ~40 mmole/cm^2/s or gas mass flux ~0.12 g/cm^2/s. During 60 s of SOG operation 7.2 g/cm^2 of the gas mass pass through 1cm^2 of the gas transport duct. Let's assume that gas transport duct is a slit of 1 cm in width and all droplets deposit on the short length ~1 cm in this slit. The clogging of the slit will be substantial when dry deposit will have the thickness ~0.1 cm. The dry deposit consists of $KHO_2\bullet H_2O_2\bullet H_2O$ complex. Let's suppose that ~50% of the water molecules leave the droplet and density of the deposit ~1 g/cm^3. Hence the clogging of the gas-transport duct will be negligible when f_d will be less than 10%.

Influence on the light scattering. Let's assume that the size of the particles $KHO_2\bullet H_2O_2\bullet H_2O$ is more that several microns and separation of the particles doesn't occur in the gas transport duct. In this case the extinction coefficient is approximately $2\pi r_d^2 n_d$. The $Cl_2:O_2:He=0.1:0.9:3$ mixture at 10 torr and temperature of 200K has the density $\rho_{g1}=9\times10^{-6}$ g/cm^3. The extinction coefficient should be substantially less than gain (equals to ~0.01cm^{-1}) or $2\pi r_d^2 n_d<10^{-4}$cm^{-1} to achieve good chemical efficiency. The mass fraction of the liquid (solid) particles of the $KHO_2\bullet H_2O_2\bullet H_2O$ is $4\rho_l\pi r_d^3 n_d/3/\rho_{g1}$. Hence the mass fraction of the droplets should be less than 10(cm^{-1})×r_d. If $r_d\approx10^{-2}$cm (100μm) the mass fraction f_d should be less than 10%. But in the case of $r_d=10^{-3}$cm (10μm) one obtains requirement $f_d<1\%$.

Hence the droplet evaporation, gas-transport clogging and light scattering give approximately equivalent requirements on the aerosol fraction in the gas outflow from SOG in the case of big droplets ($r_d>100$μm). But low light scattering limitation plays much more important role in the case of the small size droplets ($r_d<10$μm).

2.7.   Mechanism of the aerosol/droplet generation in the bubble SOG.

The burst of the bubble is a very quite complex hydrodynamic problem. Some estimations of the size and velocities of the droplet generated during the burst of the bubble and liquid entrainment by gas stream were studied, for example, in papers [21-26]. All reviewed works were devoted to droplet generation at conditions of the earth gravity and atmospheric pressure. But we didn't find any articles about discussion of the mechanism of the droplet generation at bubble burst in the conditions of a high centrifugal acceleration, high bubble rise velocity and gas pressure lower that 1 atmosphere.

The mechanism of the droplet generation during the burst of the single bubble is presented in Fig. 17. (figure from reference [24]). In a low gas flux regime (ideal bubble flow, earth gravity conditions, standard atmospheric pressure and low superficial gas velocity) uniformly sized bubbles steadily rise. Let's consider bubbling conditions (Fig. 17, a). When the bubble reaches the liquid surface it stops and forms the liquid film dome (t_0). The rapture of the dome film (t_1) occurs when the eigenfrequency of the dome membrane equals to the eigenfrequency of the bubble. These droplets are called film droplets. At t_2 the liquid jet is formatted and at some conditions it disintegrates into droplets (at t_3). This droplet is called jet droplets. The churn turbulent condition (Fig. 17b) occurs at a high gas fluxes and droplet generation is the result of direct momentum exchange mechanisms between the gas flow and the liquid.
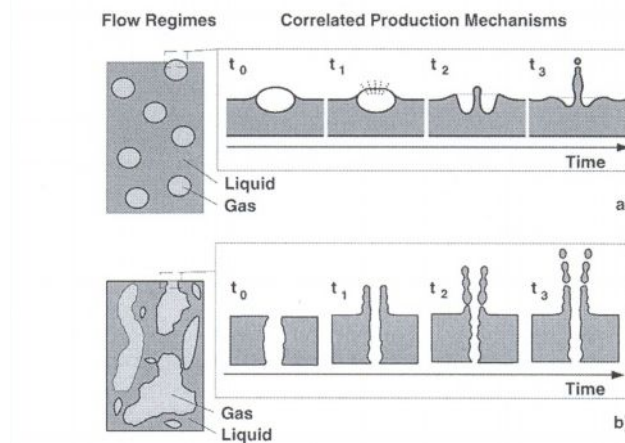
Fig. 17. Mechanism of droplet generation. a) Bubbling conditions, b) churn turbulent conditions.

Film droplets. The amount of the liquid that carries away by released gas is equal to the mass of this film. The volume of the film dome is defined as product of the dome area A_f and the thickness δ_f of the film. A number of droplets can be up to several hundred. Let's introduce the capillary length:

$$\ell_c = \sqrt{\frac{2\sigma}{\rho_\ell G}} \ .$$

It was found [24] that the thickness of the film δ_f, its area A_f and volume of the film V_f are equal to

$$\delta_f = 1.83 \frac{\sigma}{U_s^2 \rho_\ell} \times \left(d^*\right)^{2(-0.805 + 0.115\ln d^* + 0.0217(\ln d^*)^2 + 0.00126(\ln d^*)^3)} \tag{30}$$

$$A_f = \ell_c^2 0.317 \times \left(d^*\right)^{3.524 - 0.24\ln d^* - 0.00194(\ln d^*)^2}$$

$V_f = \delta_f \times A_f$

Here $d^* = 2r_b/l_c$ is a reduced diameter of the rising bubble. The equivalent droplet diameter is

$$d_d = \sqrt[3]{\frac{6V_f}{n_d}} \qquad (31)$$

The mass fraction of the generated droplets is

$$f_d = 6V_f \rho_\ell /(\pi d_b^3 \rho_g)$$

The calculated mass fraction of the film droplets are presented in Fig. 18.
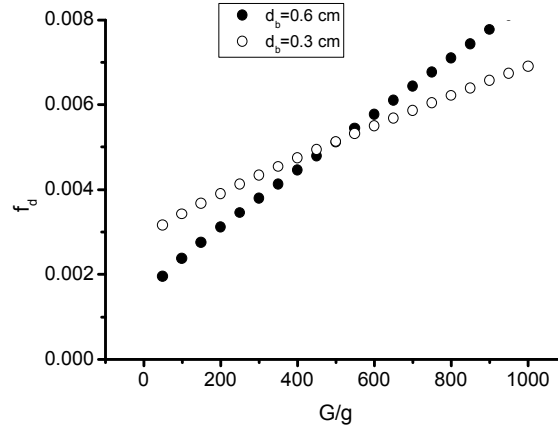
Fig. 18. Droplet mass fraction in the case of the film droplets conditions. σ_l=50 din/cm, P_g=35 torr.

The film thickness is of the order of several molecular diameters. Because of a very small size of film droplet it initial velocity is of the order of superficial velocity U_{sf}:

$$U_{sf} = f\frac{\pi d_n^3}{6}N_n$$

Jet droplets. After bursting of the bubble film, a jet (so-called "sultan") may be formed by the liquid flowing back into the cavity (Fig. 17.1a, instant t_2) [20-25]. This jet may disintegrate into droplets, called jet droplets. In contrast to film droplets the number of jet droplets is smaller and their size larger. The main force that induces generation of the jet is the surface tension. The limitation of the maximum bubble radius at which the jet bubbles can be generated is due to the next mechanism [21]. The film rupture occurs when the top of the bubble is located at the height h_c (Fig. 19). The h_c is higher for the bigger bubbles because velocity of the bigger bubble is higher and opposite surface tension force is relatively low. So at some critical bubble size the height h_c is comparable with bubble radius and the liquid jet is not generated after the film rapture. The maximum size of the bubble that can generate jet droplet is defined from limitation of the Eotvos criteria [21]:

$$Eo = \frac{4\rho_\ell Gr_b^2}{\sigma_\ell} < 6 \qquad (32)$$

For water and G=9.8 m/c^2 the maximum bubble radius 0.34 cm. If 2.5mm<d_b<6.8 mm only one droplet is generated. The diameter of this droplet is

$$d_d(cm) = 0.3341(d_b(cm))^{1.5}$$

The initial velocity of this droplet in this case can be estimated from the conservation law of energy. The excess of the surface energy equaled approximately to $\pi\sigma d_b^2/4$ is

transformed into kinetic energy of the droplet $\dfrac{\pi\rho_\ell d_d^3 U_d^2}{12}$. Results of the estimations are presented in

Table 4. For larger bubble size the droplet velocity is less and it's diameter is higher.

Table 4. *The size and velocity of the jet droplet.* $\sigma_l=50$ *din/cm²*, $\rho_l=1.3$ *g/cm³*.

d_b(cm)	0.3	0.5	0.6
d_d(cm)	0.055	0.12	0.15
U_d(cm/s)	285	150	120

The estimation presented in

Table 4 is in a good agreement with exact solution in paper [21]. For the conditions of a high centrifugal acceleration G=400g formula (32) gives maximal bubble radius r_b=0.017 cm=0.17mm at which the jet droplet can be generated. We plan to generate bigger bubbles. So it is expected that at high G the jet droplets will not be generated.

444   J. M. Boulton-Stone and J. R. Blake

Fig. 19
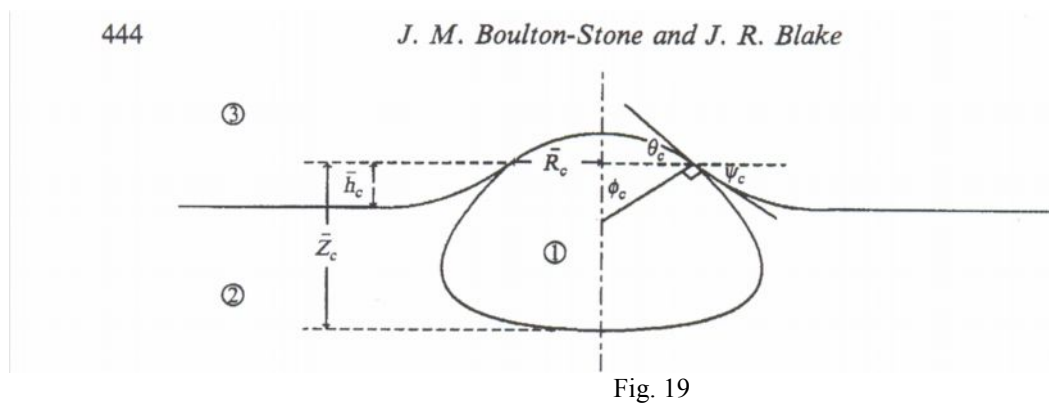
Droplets at churn turbulent conditions. It is the most complex regime of droplet generation especially in the centrifugal bubbling SOG. In the centrifugal SOG the gas velocity in the nozzle is a very high and times of the bubble formation and detachment are very short. As the bubble starts to grow, the pressure inside bubble is higher than the liquid pressure P_l+P_g (Fig. 20, bubble position A). The pressure inside bubble at instant of the detachment can be defined if one knows the time of the bubble growth (for example from reference [27]), ambient pressure and gas flow rate in the nozzle. The bubble rises and grows after detachment from the nozzle. The bubble velocity in the centrifugal SOG is very high and the ambient liquid pressure near the bubble changes too quickly. In the centrifugal SOG the pressure gradient in liquid is a very high ~400 torr/cm. Hence for the bubbles of the radius of several mm the liquid pressure in the neighborhood of the bubble is substantially anisotropic (Fig. 20, position B). Because the gas pressure in bubble is uniform the resultant force acting on the top of the bubble is stronger than force acting on the sides and bottom of the bubble (position B). Possibly this effect prevents to flatten of the bubble by momentum head

of the ambient liquid and bubble saves the shape close to the sphere. When the bubble approaches to the liquid surface where the liquid pressure is close to the P_g, the gas pressure in the bubble can be substantially higher than the gas pressure P_g over BHP. At this position the associated local mass of the liquid on the top of the bubble is much less than at the lower part of the bubble. This overpressure expands the bubble to the form of the ellipse (or mushroom), pushes the head of the bubble to the gas-liquid surface and forms the fast expanded liquid film dome over liquid surface (position C). This film dome can be fast destroyed (position D). The gas releases from the bubble at high velocity and generates droplets due to the high overpressure in the bubble relative to pressure over BHP (position C). This situation differs greatly from the bubble rupture at earth gravity condition when gas pressure inside bubbles practically equals to the pressure of ambient liquid.
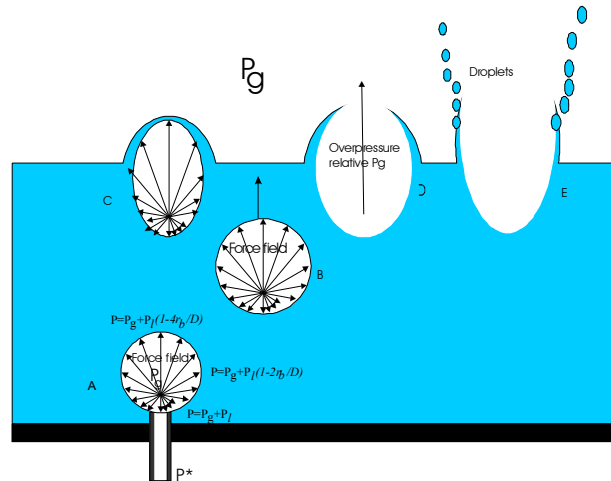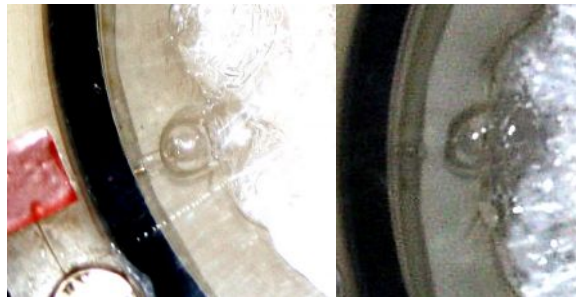
position C   Position E   Position D

Fig. 20. The shape of the bubble at different positions from the nozzle.

For simplicity we assume that the nozzle diameter is much less than detachment bubble diameter, the upper end of the nozzle is located slightly upper than bubbler surface and the height of the liquid column is substantially thicker than bubble diameter. Let's assume that the liquid pressure neighborhood of the bubble doesn't depend on azimuth and polar angle in spite of mentioned above high pressure gradient. The rate of the bubble expansion and pressure in the bubble can be estimated from the well know Reyleigh-Plesset equation:

$$r\frac{d^2 r}{dt^2} + \frac{3}{2}\left(\frac{dr}{dt}\right)^2 = \frac{1}{\rho_\ell}\left(p_g(t) - p_\ell - \eta_\ell \frac{dr}{rdt}\right) \qquad \textbf{(33)}$$

Here we neglect by surface tension, $p_g(t)$-pressure inside the bubble, p_l is the liquid pressure in the neighborhood of the bubble. The additional equations are different for the stage of the bubble growth and stage of the bubble rising.

The stage of bubble growth. The gas molar flow rate through the nozzle is determined by pressure difference between nozzle input and output. We assume that the drag force in the gas nozzle is negligible and gas velocity in the nozzle is subsonic. In this case the gas molar flow rate through the nozzle is given by well known formula:

$$m = m_0 \sqrt{\frac{1 - \left(\dfrac{p_g(t)}{P^*}\right)^{k/(k-1)}}{1 - \left(\dfrac{P_g + P_\ell}{P^*}\right)^{k/(k-1)}}} \left(\frac{p_g(t)}{P_g + P_\ell}\right)^{1/k}$$

where $m = m_c + m_H$ is the current total molar flow rate, m_0 is the maximum total molar rate, when $p_g = P_g + P_l$, P^* is the gas pressure at the nozzle inlet, $P_g + P_l$ is the total pressure at the outlet of the nozzle. The pressure inside the bubble and it radius at the stage of the bubble growth are connected via ratio

$$\frac{d}{dt}\left(\frac{4\pi r^3 p_g}{3}\right) = mRT$$

Equation (33) is integrated from t=0 to t=τ, where τ is the time of the bubble growth.

The rising bubble stage. Assuming isothermal conditions for the gas inside the bubble the additional equation $r^3 p_g$=const is valid at the stage of the bubble rising. The current time in equation (33) is $t = x/U_b$, where x is the distance from the nozzle. The instant at which bubble escapes from the liquid surface is $t_{es} \approx H/U_b$.

We will make estimations of the bubble gas overpressure near the liquid surface for the next input data: m_0=1.2 mmole/s, G= 400g, P_l=357 torr, P_g=35 torr, P*=550 torr, H=1 cm, ρ_l=1.3 g/cm^3, η=0.1 g/cm/s, time of the bubble growth τ=10^{-3}c, T=258K.

For these conditions and the instant of the bubble detachment the calculation gives values for its radius r_b=0.21 cm and for the pressure inside the bubble 378 torr (**Fig. 21**).
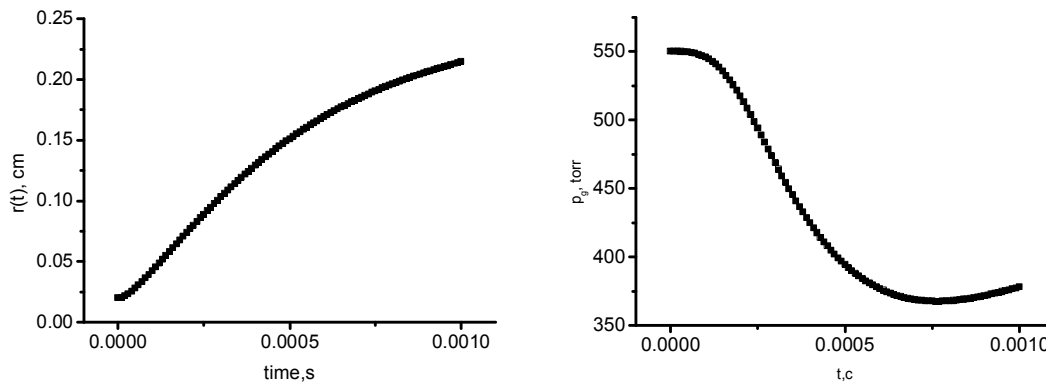
Fig. 21. Radius of the growing bubble and pressure inside the bubble at the stage of the growth.

The average gas molar flow rate $\overline{m}$ =1 mmole/s. The bubble parameters at the instant of the detachment were put like input data for the stage of the bubble rising. The dependencies of the bubble radius and inside gas pressure are presented in Fig. 22.
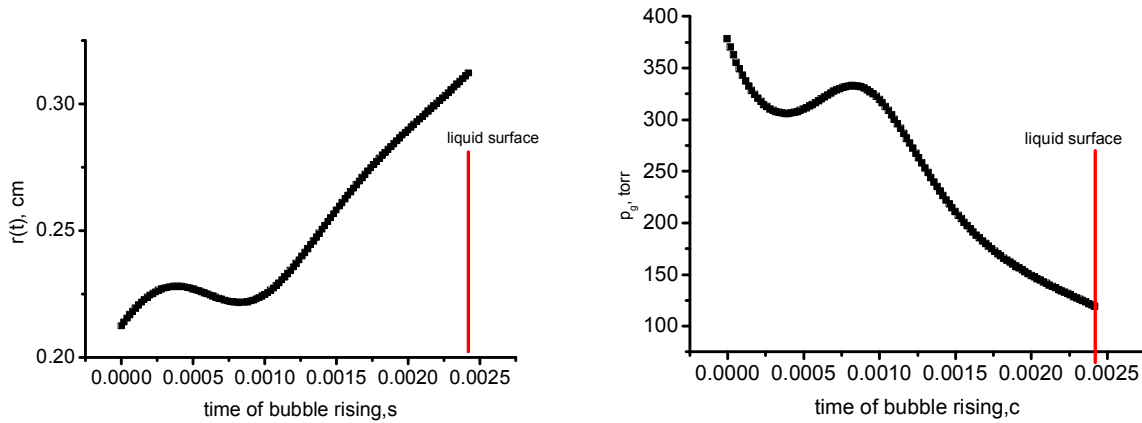
Fig. 22. Radius of the bubble and pressure inside the bubble at the stage of the rising.

It is seen from Fig. 21 that the pressure p_g inside the bubble in 3 times higher than the gas pressure over liquid P_g=35 torr when bubble is near the liquid surface. The further calculations showed that with the increase of the pressure over liquid P_g the pressure inside bubble approaches to P_g. For example, at P_g=100 torr the pressure inside the bubble located near liquid surface is 136 torr. Hence increase of the ratio P_g/P_l results in a lower gas velocity and lower liquid entrainment effect is expected. The observed size of the generated droplet of order of several hundred microns or more (Fig. 23)

Fig. 23. Ensemble of the droplets (caviar) generated by 4 nozzles (0.55 mm in diameter) at the centrifugal acceleration G=652g. The molar flow rate of the air through the each nozzle is 0.8mmole/s.

2.8. Estimation of the droplet separation efficiency.

Let's consider the trajectory of the droplets flying out from the liquid surface. In the laboratory coordinate system the motion of the droplets is described by equations **(Fig. 24)**:

$$\frac{4\pi r_d^3 \rho_\ell}{3}\frac{d\vec{v}_d}{dt} = -c_d \pi r_d^2 \frac{|\vec{v}_d - \vec{v}_g|(\vec{v}_d - \vec{v}_g)\rho_g}{2}, \quad \frac{d\vec{R}_d}{dt} = \vec{v}_d$$

The drag coefficient depends on the droplet Reynolds number Re_d. For the droplets with d_d=10÷100μm, $|\vec{v}_d - \vec{v}_g|$=1÷10 m/s, v_g=0.1÷10 cm^2/s (or P_g=10÷1000 torr) Re_d=10^{-2}÷100. In the range of Re_d=10^{-2}÷500 the drag coefficient is c_d=18.5/$Re_d^{0.6}$ [35] with a good approximation. It is necessary to know the distribution of the gas velocity in the cavity of the centrifugal BSOG. We assume that gas rotates with the same angular velocity as a bubbler and gas moves radially to the center of the cavity into the gas collector **(Fig. 24)**.. The axial gas velocity between bubbler and gas collector equals to zero. Hence $(v_g)_x$=2πny-U_{sf}×(D/2)×x/(x^2+y^2)$^{0.5}$, $(v_g)_y$=-2πnx-

$U_{sf} \times (D/2) \times y/(x^2+y^2)^{0.5}$. It is assumed that droplet fly out in the point (-D/2, 0). The initial droplet velocity is $v_{dx}=-2\pi ny+U_d \times \sin(\varphi)$, $v_{dy}=U_d \times \cos(\varphi)$, where U_d is the initial absolute droplet velocity. The separation is assumed successful if during flight time $R_d^2<R_c^2$ and at any instant $|\bar{R}_d(t)|=D/2$ or all droplets are captured by liquid surface again. The calculations of the minimal droplet radius at which separation will be successful are presented in Table 5.
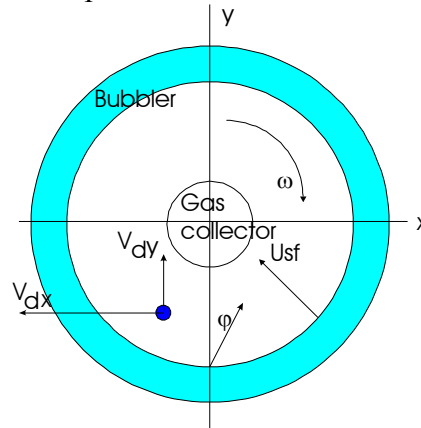
Fig. 24. Geometry of the centrifugal bubbler SOG. The gas collector locates in the centre. The gas moves from the bubbler to the collector.

These calculation examples of the separation efficiency demonstrated that

1) $(r_d)_{min}$ depends only on G but not separately on n and D.

2) The increase of the P_g at constant gas flux from the bubbler decreases $(r_d)_{min}$

3) The initial droplet velocity influences on $(r_d)_{min}$ slowly

4) The droplets with $r_d<10 \div 25$ μm at G>500g, $U_{sf}=10$ m/s can be efficiently separated without special additional separator. Only small droplets can penetrate to the exit of SOG.

A big droplets dropped back on the liquid surface approximately with velocity U_d relative to the liquid surface and can generate new droplets (secondary emission) having less size and lower velocity. It is quite complex to estimate size and velocity of the secondary generated droplets.

Table 5. Minimal radius of the separated droplets. ρ_l=1.3 g/cm^3, ν_g(cm^2/s)$\approx$100/P$_g$(torr)

a) Influence of the angle φ of the droplet launching.

n, s^{-1}	P$_g$, Torr	U$_{sf}$, m/s	U$_d$, m/s	D, cm	R$_c$,cm	φ, degree	(r$_d$)$_{min}$, μm
45	50	10	4	5	1	0	19
45	50	10	4	5	1	30	25
45	50	10	4	5	1	45	25
45	50	10	4	5	1	60	25

a) Influence of the rotation velocity at D=5cm.

n, s^{-1}	P$_g$, Torr	U$_{sf}$, m/s	U$_d$, m/s	D, cm	R$_c$, cm	φ, degree	(r$_d$)$_{min}$, μm
45	50	10	4	5	1	0	19
70	50	10	4	5	1	0	10
100	50	10	4	5	1	0	7

c) Influence of the rotation velocity at D=8 cm

n, s^{-1}	P$_g$, Torr	U$_{sf}$, m/s	U$_d$, m/s	D, cm	R$_c$, cm	φ, degree	(r$_d$)$_{min}$, μm
45	50	10	4	8	2	0	14
70	50	10	4	8	2	0	9
100	50	10	4	8	2	0	6

d) Influence of the bubbler radius (n^{2}D =constant or constant centrifugal acceleration G=500g)

n, s^{-1}	P$_g$, Torr	U$_{sf}$, m/s	U$_d$, m/s	D, cm	R$_c$,cm	φ, degree	(r$_d$)$_{min}$, μm
55.7	50	10	4	8	2	0	11
35	50	10	4	20	5	0	11
28.6	50	10	4	30	5	0	11

e) Influence of the gas pressure P$_g$ at constant gas flux or U$_{sf}$P$_g$=const. Calculations were made for gas molar flux from the bubbler surface N$_n$m=10 mmole/cm^2/s.

n, c^{-1}	P$_g$, Torr	U$_{sf}$, m/s	U$_d$, m/s	D, cm	R$_c$,cm	φ, degree	(r$_d$)$_{min}$, μm
50	50	36	4	10	2	0	34
50	100	18	4	10	2	0	22
50	150	12	4	10	2	0	18
50	200	9	4	10	2	0	15

g) Influence of the initial droplet velocity.

n, s^{-1}	P$_g$, Torr	U$_{sf}$, m/s	U$_d$, m/s	D, cm	R$_c$, cm	φ, degree	(r$_d$)$_{min}$, μm
50	100	18	0.5	10	2	0	20
50	100	18	1	5	2	0	21
50	100	18	2	5	2	0	21
50	100	18	4	5	2	0	22
50	100	18	10	5	2	0	24
50	100	18	15	5	2	0	25

2.9.   Estimation of the optimal SOG parameters for generation of 50 mmole/s of oxygen.

We will assume that CBSOG is designed optimally if

a) $O_2(^1\Delta)$ yield is higher 50%

b) Utilization is higher 90%

c) Low water vapor fraction relative $O_2 \leq 10\%$

d) No big droplets at the exit CBSOG

e) Mass fraction of micron and submicron aerosol of BHP $\leq 1\%$

f) No catastrophic liquid entrainment or good adhesion of BHP layer to the bubbler surface

g) Maximum oxygen flux at which a)-e) are valid

h) Minimum BHP volumetric rate at which a)-h) are valid.

For the first design of the CBSOG the next initial hardware parameters have been selected: bubbler radius D=93 mm, nozzle diameter of d_n=0.27 mm, nozzle length of 9 mm and the total number of the nozzles 561. This choice has to ensure the Cl_2:He=50:90 mixture pressure in front of the nozzles less than 1 atm and to ensure total chlorine molar flow rate up to 50 mmole/s.

The main task was to find **maximum nozzle density** for the maximization of the input chlorine flux $m_c N_n$ and simultaneously to avoid bubble coalescence at the stage of their growth for providing the good BHP layer adhesion with the bubbler surface.

According to the model of chlorine absorption and $O_2(^1\Delta)$ producing in the CBSOG for such hardware the rotation velocity was limited by $n\approx45c^{-1}$ and the height of the BHP column was limited by $h\approx0.8$ cm to achieve U>90% and Y>60% simultaneously (**Fig. 25**). At maximum $n=45c^{-1}$ and h=10 mm the hydrostatic BHP pressure on the bubble surface is $P_l=300\ torr$. At P_g=100torr the total pressure in front of the nozzles has to be ~496 torr to ensure the chlorine molar flow rate 50 mmole/s. P_g=100 torr is the maximum gas pressure over BHP to ensure Y>60%. Superficial gas velocities of ~2.5 m/s ensure efficient droplet separation with size bigger 10µm.
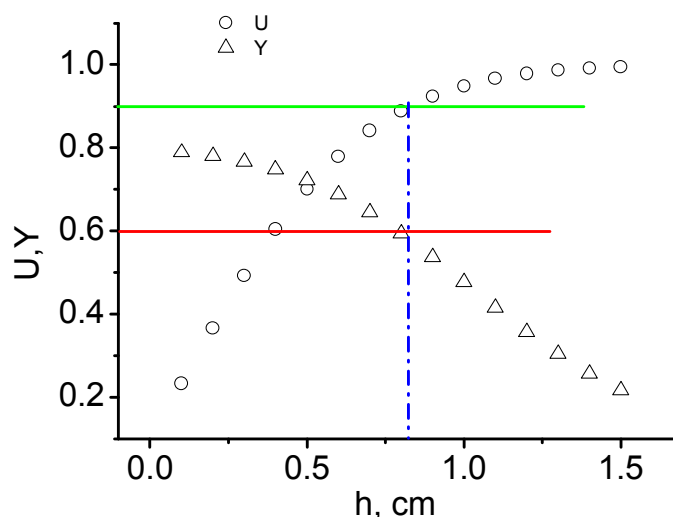
Fig. 25. The chlorine utilization and $O_2(^1\Delta)$ yield vs BHP column height.

The expected diameter of the generated bubbles is equaled to ~2.5 mm. The coalescence of the generated bubbles will be avoided if the distance between nozzles will be more that 2.5 mm or the

density of nozzles N_n will not exceed 16 nozzles/cm^2. In this case the oxygen flux will be $Um_C N_n$=1.28 mmole/cm^2/s. Hence the working bubbler area should be less than 36 cm^2.

The maximum oxygen partial pressure over BHP is limited by $100\times50/(140)$=35 torr. In this case according to the thermal CBSOG model the minimal BHP volumetric rate has to be at least 100 cm^3/s at initial BHP temperature -15C and chlorine molar flow rate M_c=50 mmole/s to keep water vapor fraction less than 10% relative to the oxygen.

The final designed CBSOG parameters are presented in Table 6.

Table 6. The optimal parameters CBSOG.

D	9.3 cm
d_n	0.3 mm
n	$<45s^{-1}$
P_g	<100 torr
Chlorine molar flow rate	50 mmole/s
Number of nozzles	561
Minimal distance between nozzles	2.5mm
Maximum oxygen flux	1.28 mmole/cm^2/s
BHP volumetric rate	>100 cm^3/s

3. A first version of centrifugal bubbling SOG (CBSOG-1).

The results of the preliminary simulation of the chlorine absorption and $O_2(^1\Delta)$ generation were the basis for the first design of the centrifugal bubble SOG. The principle design of the centrifugal bubble SOG is presented in Fig.26. The outer non-rotating cylindrical housing contains the rotary bubbler (black marked). The BHP is fed to the BSOG through a channel made in the rotary motion feedthrough and covers the internal surface of the rotary bubbler. The spent BHP drains through orifices into the duct between the rotary bubbler and the non-rotating housing and is pumped out to the dump tank. The chlorine-helium mixture enters through the channel made in the rotary motion feedthrough to the rotary bubbler. From this cavity plenum, the chlorine-helium mixture bubbles into the BHP layer through small cylindrical nozzles made in the rotary bubbler. The gas bubbles burst at the surface of the BHP layer and the realized gas containing $O_2(^1\Delta)$ flows out through the holes made in the internal perforated cylinder. The gas pressure over the BHP layer was controlled by the total area of the holes in the internal perforated cylinder. It was possible to remove this perforated cylinder and install a Teflon body and separator inside bubbler to reduce duct volume.
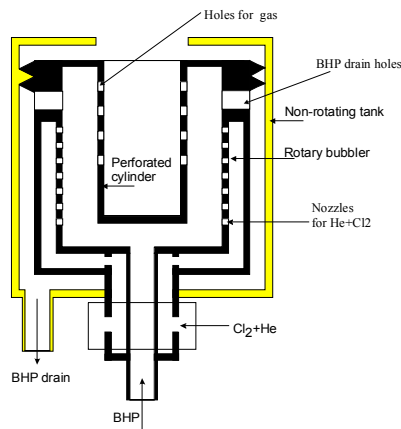
Fig. 27 The design of CBSOG
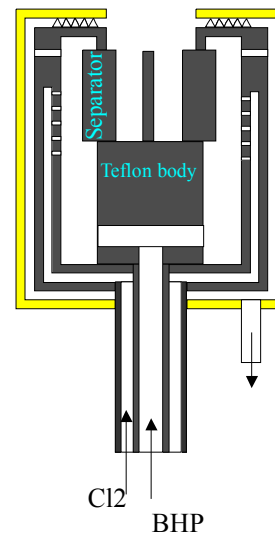
Fig. 26. The design of CBSOG with central Teflon body

The main design parameters of the CBSOG are presented in Table 7.

Table 7.

Designation	Function
D	Determines the centrifugal acceleration
H_b	Determines the time of the stabilization of BHP column height
d_n	Determines the size and velocity of the bubbles, gas pressure in front of the gas nozzles
N	Determines the gas pressure in front of gas nozzles. The product $\pi N d_n^2/4$ is the total gas nozzle area.
N_n, $N_n=1/a^2$	Determines bubble or jetting regime, bubble coalescence.
$S_b=N/N_n$	Determines the superficial gas velocity over BHP surface
$F_n=\pi N_n d_n^2$	Determines bubble or jetting regime, bubble coalescence, superficial gas velocity over BHP surface
l_n	Determines hydraulic resistance for the gas, total gas pressure in front of gas nozzles and the gas velocity in nozzles
S_g	Determines the gas pressure over BHP, superficial gas velocity over BHP surface, gas residences time, $O_2(^1\Delta)$ transport losses, water vapor fraction, efficiency of droplet separation
R_c	The product $H_b(R^2-R_c^2)\pi$ determines the gas transport volume in high pressure duct, gas residence time, $O_2(^1\Delta)$ losses, efficiency of droplet separation. In some versions of CBSOG the perforated cylinder was not installed.
S_l	Determines the BHP column height H and axial velocity U_l for the fixed BHP volumetric rate V_l and centrifugal acceleration G

The first versions of CBSOG-1 have the geometrical parameters of bubblers listed in Table 8. All versions of CBSOG had identical D, H_b. The CBSOG-1 was designed so that it was quit easy to change all another parameters (d_n, N_n, N, a etc).

Table 8. Geometrical parameters of bubblers for CBSOG-1.

Parameter	CBSOG-1 modifications								
	a	b	c	d	e	f	g	h	i**
D , mm	93	93	93	93	93	93	93	93	93
H_b, mm	100	100	100	100	100	100	100	100	100
d_n, mm	0.3	0.3	0.3	0.3	0.3	0.3	0.55	0.55	0.95
N	561	561	561	561	561	561	165	165	55
N_n, cm^{-2} a, mm	3.43 , 5.4	3.43, 5.4	3.43 5.4	3.43 5.4	11.1 3	11.1 3	3.78 5.4	7.71 3.6	5.16 4.4
S_b, cm^2	163	163	163	163	50	50	43.6	21.4	10.6
F_n, 10^{-3}	2.4	2.4	2.4	2.4	7.8	7.8	9	18	36.5
l_n	9	9	9	9	9	9	5	5	9
S_g, cm^2	7.5	1.33	1.33	1.1	6	6	6	TB*	TB*
R_c, cm	1.5	1.5	1.5	1.5	1.5	1.5	1.5	SP***	SP***
S_l, cm^2	0.64	0.64	0.32	0.32	0.64	0.32	0.38	0.64	0.64

* Teflon body was installed inside bubbler instead of the perforated cylinder.

** Axis of nozzles directed on angle 30° to the bubbler surface.

*** separator

 It is necessary to describe the gas nozzle arrangement in bubblers of CBSOG-1 modifications.

a, b, c, d- 561 nozzles ∅0.3mm were uniformly arranged on the side surface of the bubbler, 11 rows (the working height in vertical direction ~60 mm) , with 51 nozzles over the entire circuit (**Fig. 28**). The axis of the nozzles is normal to the bubbler surface.
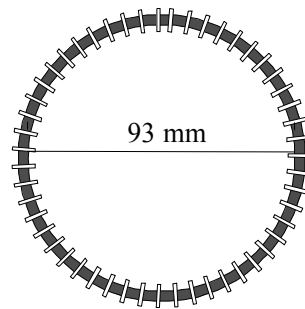
Fig. 28. Gas nozzle arrangement in CBSOG-1 (a-d).

e, f -561 nozzles ∅0.3mm were uniformly arranged on the side surface of the bubble, 5.5 rows (the working height in vertical direction ~12 mm), with 102 nozzles over the entire circuit (

Fig. 29). The axis of the nozzles is normal to the bubbler surface.
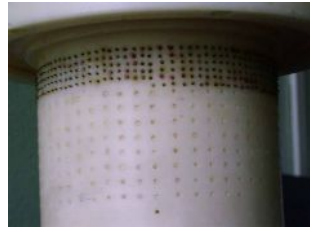
Fig. 29. Gas nozzle arrangement in CBSOG-1, e, f.

g- 165 nozzles ∅0.55mm were uniformly arranged on the side surface of the bubble, 3 rows (the working height in vertical direction ~15 mm), with 55 nozzles over the entire circuit (**Fig. 30**). The axis of the nozzles is normal to the bubbler surface.
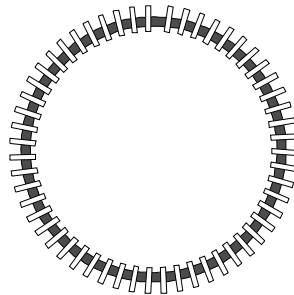
Fig. 30. Gas nozzle arrangement in CBSOG-1, g.

h- 165 nozzles ∅0.55mm were arranged only in the opposite quadrants of the circuit (**Fig. 31**), 6 rows (the working height ~15 mm). The axis of the nozzles is normal to the bubbler surface.
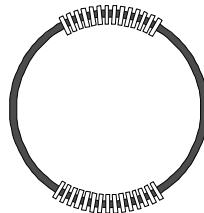
Fig. 31. Gas nozzle arrangement in CBSOG-1h.

i- ∅0.95mm were arranged only in the four parts of the circuit (Fig. 32), 3 rows (the working height ~10 mm). The axis of the nozzles is on the angle 30° to bubbler surface.

Fig. 32. Gas nozzle arrangement in CBSOG-1i.

Some views of the designed CBSOG-1 are presented in **Fig. 33**,**Fig. 34**

Fig. 33.The outer view of CBSOG-1.
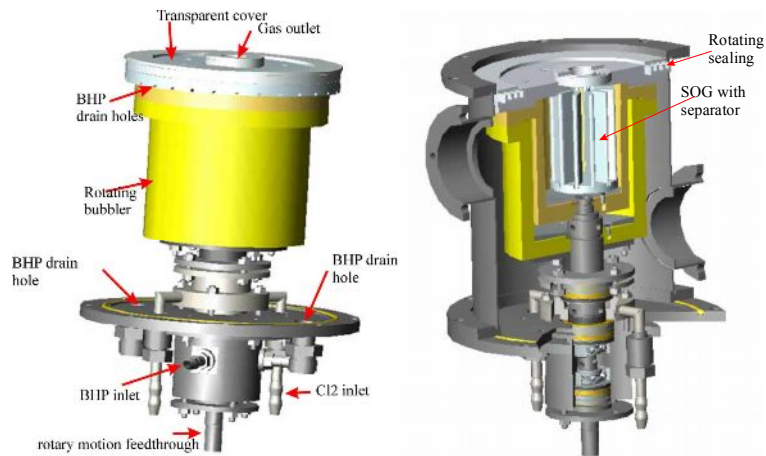
Fig. 34. The internal parts of CBSOG-1 (rotating parts are marked yellow).

The Photo of the manufactured parts of CBSOG-1 are presented below.
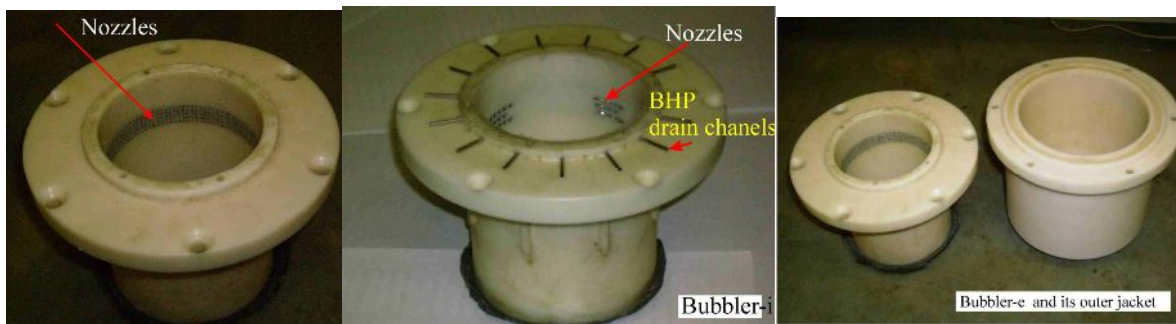
Bubbler for CBSOG-1e Bubbler for CBSOG-1i   Bubbler-e and jacket separately

Bubbler-e inserted into jacket   Cover of the bubbler   Rotary bubbler CBSOG-1e with cover

Rotary motion feedthough   Cl2 gas input

Assembling of rotary motion feedthrough and inlet of chlorine.
Assembling of rotary bubbler with motion feedthrough and the inlet of chlorine system.

4. Diagnostic system.

A special chamber was installed downstream CBSOG to measure $O_2(^1\Delta)$ yield, chlorine utilization and water vapor concentration. $O_2(^1\Delta)$ emission of 1.27 μm was registered by Ge-photo detector, of 0.762μm from $O_2(^1\Sigma)$ by Si-photo detector. Both photo detectors were equipped with filters to cut other spectral bands. At the first stage of project (CBSOG-1) the gas temperature T_g was measured by 0.15 mm thermocouple covered by glass. The concentration and partial pressure of water vapor in chamber were determined from ratio

$$N_w = C_1 \frac{I_{1.27}^2}{I_{0.762}}, \quad P_w = N_w R T_g$$

and concentration of $O_2(^1\Delta)$ from the ratio

$$N_\Delta = C_2 I_{1.27}$$

where $I_{1.27}$ and $I_{0.762}$ are the signals of 1.27 μm and 0.762 μm photo-detectors respectively, C_1, C_2 are the coefficients to be determined. C_1 and C_2 later were recalibrated from the calibration procedure using multi channel optical registration of oxygen emission spectrum described below (this procedure also described in 7th Quarter Report).

Advanced diagnostic of CBSOG. Singlet oxygen emits light in 1268 nm, 762 nm, dimol emission in 632nm and 703 nm bands corresponding to the processes:

Spontaneous emission of $O_2(^1\Delta)$

$$O_2(^1\Delta, v=0) \rightarrow O_2(^3\Sigma, v=0) + h\nu(\lambda=1268 \text{ нм}), \tag{34}$$

Spontaneous emission of $O_2(^1\Sigma)$

$$O_2(^1\Sigma, v=0) \rightarrow O_2(^3\Sigma, v=0) + h\nu(\lambda=762 \text{нм}), \tag{35}$$

Dimole emission

$$O_2(^1\Delta, v=0) + O_2(^1\Delta, v=0) \rightarrow O_2(^3\Sigma, v=0) + O_2(^3\Sigma, v=0) + h\nu(\lambda=634 \text{нм}) \tag{36}$$

$$O_2(^1\Delta, v=0) + O_2(^1\Delta, v=0) \rightarrow O_2(^3\Sigma, v=0) + O_2(^3\Sigma, v=1) + h\nu(\lambda=703 \text{нм}) \tag{37}$$
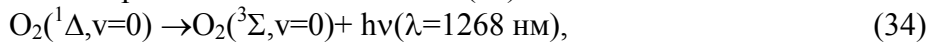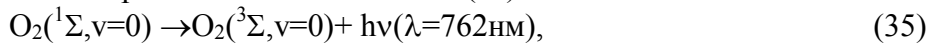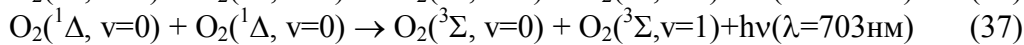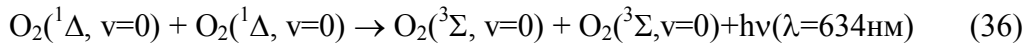
$O_2(^1\Sigma)$ is generated in pooling process

$$O_2(^1\Delta) + O_2(^1\Delta) \rightarrow O_2(^1\Sigma) + O_2(^3\Sigma), \tag{38}$$
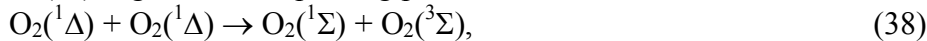
$O_2(^1\Sigma)$ mainly is quenched by water molecules in the process

$$O_2(^1\Sigma) + H_2O \rightarrow O_2(^1\Delta) + H_2O, \tag{39}$$

We have used a multi channel spectra analyzers (MSA) for the advanced SOG diagnostics. The spectrum of light emitted by the gas that outflow from SOG was analyzed by two spectrometers. A first spectra analyzer M266 was equipped with two CCD cameras, one for visible range (Hamamatsu S5931-1024S) and another for the IR range (Hamamatsu G9212-512S). The second analyzer AvaSpec-3648 was used to detect spectra range 600-800 nm.

A number of counts detected by MSA in each spectral range are equal to

$$F_{1268}(\lambda) = S(\lambda) V q_{1268}(\lambda) A_\Delta N_\Delta.$$

$$F_{762}(\lambda) = S(\lambda) q_{762}(\lambda) V A_\Sigma k_{38} N_\Delta^2 / (k_{39} N_W)$$

$$F_{634}(\lambda) = S(\lambda) V q_{634}(\lambda) k_{36} N_\Delta^2,$$

$$F_{703}(\lambda) = S(\lambda) V q_{703}(\lambda) k_{37} N_\Delta^2,$$

where $S(\lambda)$ is the spectral sensitivity, V is a volume factor, $q(\lambda)$ is the line shape convoluted with MSA spectral shape, A is Einstein coefficient, k_i is rate constant, N_W - water vapor concentration, N_Δ - $O_2(^1\Delta)$ concentration.

Einstein coefficients A and rate constants of the processes (36), (37) were calculated taking into account the strength of bands (Table 9) by formula $8\pi S \dfrac{g_1}{g_2} \dfrac{c}{\lambda^2}$, g_1, g_2 are the degeneracy of levels.

Table 9. Band strength and rate constants.

process	band strength, S	g_1/g_2	rate constant
34	$(32,5\pm0,8)\times10^{-25}$см [30]	3/2	$A_\Delta=(2.24\pm0,06)\times10^{-4}$с$^{-1}$
	$(31\pm1)\times10^{-25}$см [31]		$A_\Delta=(2.18\pm0,07)\times10^{-4}$с$^{-1}$
35	$(1.92\pm2)\times10^{-22}$см [30]	3/1	$A_\Sigma=(7,48\pm0,09)\times10^{-2}$с$^{-1}$
36	$(3.19\pm0.03)\times10^{-43}$см^2 (T=294K) [28]	1	$k_{36}=(6.06\pm0.06)\times10^{-23}$см^3/с
	$(3.26\pm0.14)\times10^{-43}$см^2 (T=298K) [29]		$k_{36}=(6.2\pm0.3)\times10^{-23}$см^3/с
37			$k_{37}=1.06k_{36}$ [this work]
38			$k_{38}=(2.7\pm0.4)\times10^{-17}$см^3/с [32]
39			$k_{39}=(6.71\pm0.53)\times10^{-12}$см^3/с [33]

The scheme of measurements is presented in Fig. 35. A rectangular chamber with cross section 50x15 mm was installed downstream CBSOG. The emission from this chamber was collected by optical fibers and delivered to the input slit of MSA. The volume factor V for M-266 differs from factor V for AvaSpec-3648. But volume factor V for M-266+ Hamamatsu S5931-1024S is the same as for M-266+(Hamamatsu G9212-512S).
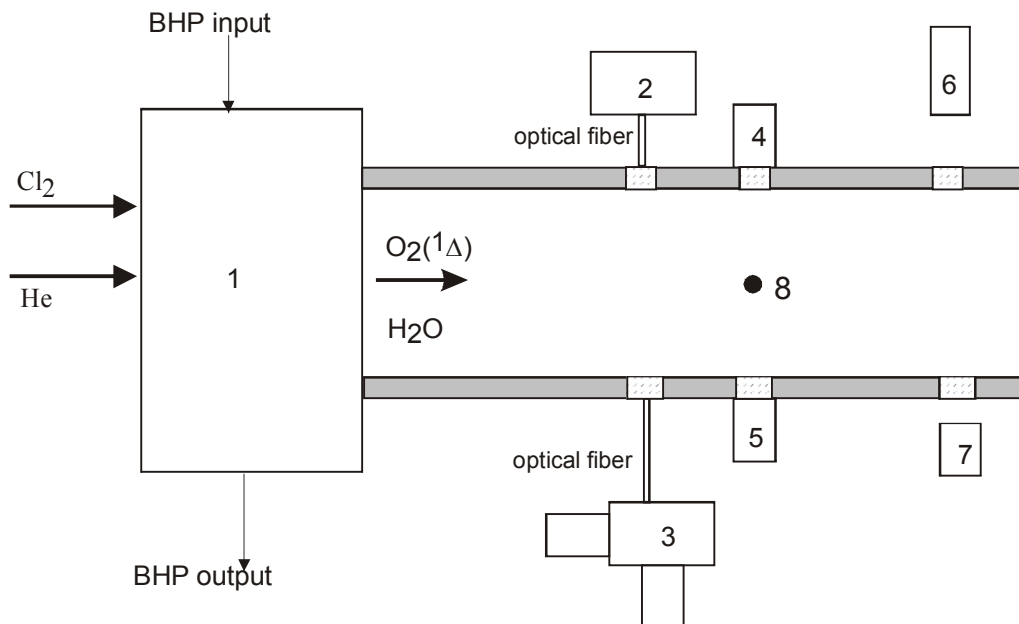
Fig. 35. 1-CBSOG, 2- MSA AvaSpec-3648, 3-MSA M266 with two CCD cameras, 4,5-Ge and Si detectors, 6- N$_2$ laser (337nm), 7 –detector of 337 nm, 8-thermocople.

Relative spectral sensitivity of M266 with Hamamatsu S5931-1024S) and Hamamatsu G9212-512S was calibrated by tungsten lamp. AvaSpec-3648 spectral sensitivity was also calibrated by tungsten lamp. A detection of light emitted by oxygen was performed at the same spectra analyzer condition as in the spectral calibration procedure. The comparison of partially resolved rotational structure of 762 nm band and synthetic spectra was also used for the estimation of the gas temperature T_g. For the synthesis of 762 band structure we have used HITRAN data base [34] and experimentally measured instrument function of AvaSpec-3648. This measurement of T_g have been applied for diagnostics of CBSOG-2,3. Knowing total number of counts of CCD camera in each spectral band the concentrations of $O_2(^1\Delta)$ and H_2O was possible to obtain.

A water vapor and $O_2(^1\Delta)$ concentrations were calculated from the formulas

$$N_W = \frac{f_{634}}{f_{762}}\left(\frac{A_\Sigma k_{38}}{k_{39}k_{36}}\right) \text{ or } N_W = \frac{f_{703}}{f_{762}}\left(\frac{A_\Sigma k_{38}}{k_{39}k_{36}}\right) \qquad \textbf{(40)}$$

$$N_\Delta = \frac{f_{634}}{f_{1268}}\frac{A_\Delta}{k_{36}} \qquad \text{ or } N_\Delta = \frac{f_{703}}{f_{1268}}\frac{A_\Delta}{k_{37}} \qquad \textbf{(41)}$$

where f_i is the integral in i band $f_i = \int \frac{F_i(\lambda)}{S(\lambda)}d\lambda$, that proportional to the total number of emitted photons in band i.

The examples of spectra are presented in Fig. 36, Fig. 37.
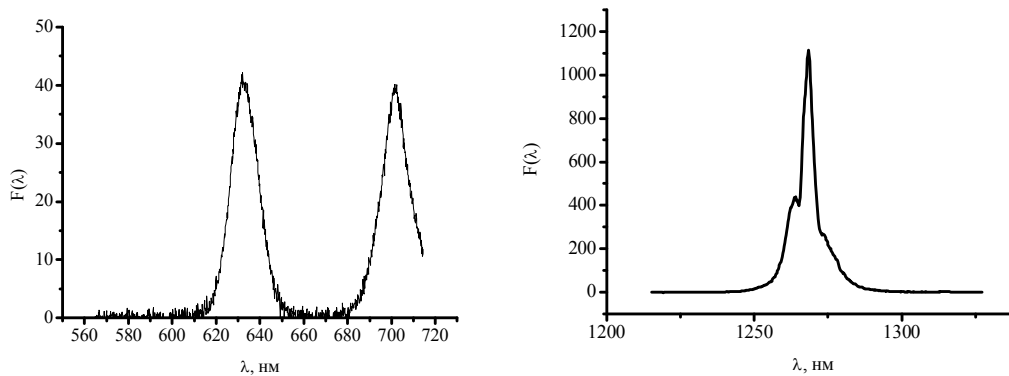
Hamamatsu S5931-1024S (dimole emission)   Hamamatsu G9212-512S ($O_2(^1\Delta)$ emission)

Fig. 36. Spectra obtained by MSA M266.
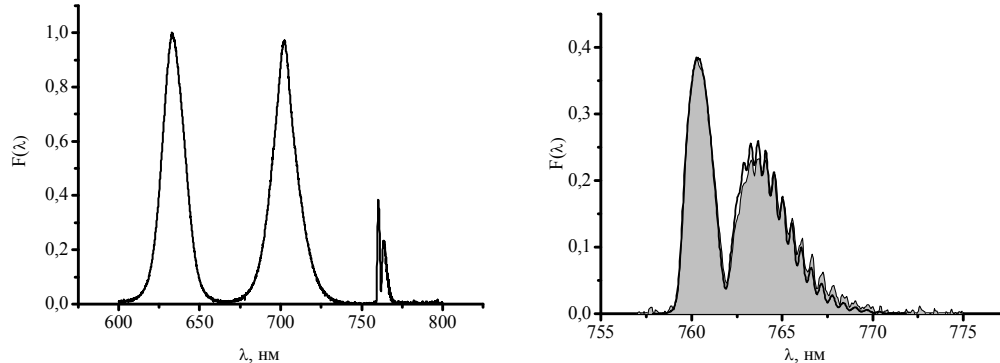
Fig. 37. Spectra obtained by MSA AvaSpec-3648. The left is enlarging spectra of 762nm band from right picture. A shadow is experimental spectrum, line is sanitized spectrum with rotational temperature $O_2(^1\Sigma)$ 340K

From formulas (40) and (41) the concentrations of $O_2(^1\Delta)$ and water vapor have been calculated for several CBSOG runs. Then the absolute calibration (coefficient C_2) of the Ge detector and silicon detector (coefficient C_1) for the on-line detection of $O_2(^1\Delta)$ and H_2O concentration have been made. All data described in 1st annual report for CBSOG-1 were recalculated using new calibration of Ge and Si photodetectors. The residual Cl_2 concentration N_c and partial pressure $P_c=N_cRT_g$ were measured by absorption emission at $\lambda=337$ nm. Sensitivity of chlorine detection was $\sim$ of 0.1 torr. The list of measured pressures is presented in Table 10. The He molar flow rate was measured by MKS Instruments Mass Flow Meter.

Table 10. The list of measured pressures.

P_1	Plenum pressure in front of the gas nozzles
P_2	Pressure in the measuring cell
P_3	Pressure in tank with gaseous chlorine
P_4	Pressure inside CBSOG cavity

The average chlorine molar flow during CBSOG run was calculated from the formula

$$M_c = \frac{V_{CT}(P_{3i} - P_{3f})}{RT_a t_{run}}$$

where P_{3i} is the initial pressure in chlorine tank, P_{3f} is the final pressure, t_{run} is the duration of CBSOG test ($t_{run}=4 \div 8$ s), $V_{CT} = 156$L is the volume of the tank with gaseous chlorine, T_a –the ambient temperature.

The chlorine utilization was calculated as

$$U = 1 - \frac{P_c}{\left(\dfrac{M_c}{M_c + M_{He}}(P_2 - P_W)\right)}$$

The $O_2(^1\Delta)$ yield is calculated from

$$Y = \frac{C_2 I_{1.27}}{\left(\dfrac{M_c}{M_c + M_{He}}(P_2 - P_W)\right)U}$$

Water vapor fraction is defined as the ratio of water vapor partial pressure to the sum of oxygen and chlorine pressures and is given by

$$\eta_w = \frac{P_w(M_c + M_{He})}{M_c(P_2 - P_W)}$$

Water vapor partial pressure in the CBSOG cavity was calculated from

$$P_{W4} = P_W P_4 / P_2.$$

The photo and video cameras were used for the observation of the BHP column near drain holes, where gas has been separated from liquid phase. The photo camera exposition time was $\sim 2 \times 10^{-5}$s. The frequency repetition of frames from video is 25Hz. Using these pictures it was easy to measure the height of the "gas-free" BHP column height H.

5. Parametric study of CBSOG-1.

When BHP starts to feed CBSOG the BHP column height grows in time, chlorine utilization increases and after several seconds the height H (**Fig. 38**-39) and sensor outputs (thermocouple, pressure gages, photodetectors) aproache to the steady state values (example of oscillogramms in Fig. 40-43). All results presented below obtained only for steady state conditions of sensors and height H.
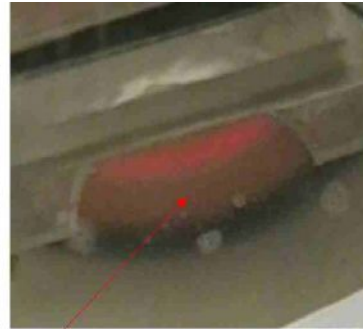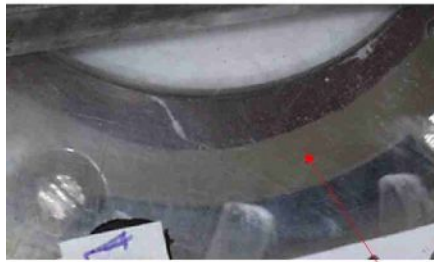
Fig. 38. Picture from photo camera.   Fig. 39. The frame from the video.
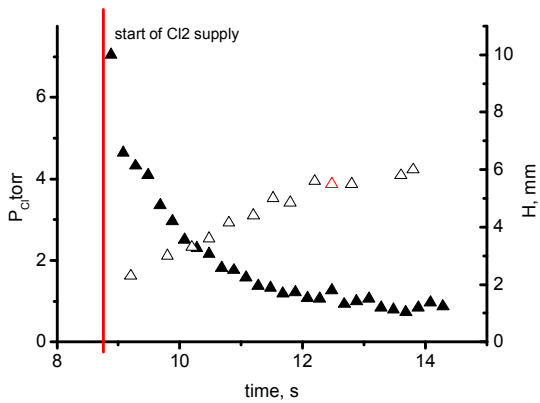
Fig. 40. Residual chlorine(▲) and BHP(Δ) column height H. Fig.   41. Outputs $I_{1.27}$(▲), $I_{0.76}$(Δ.)
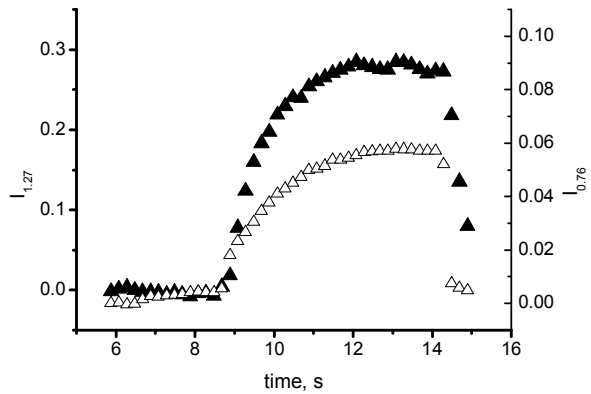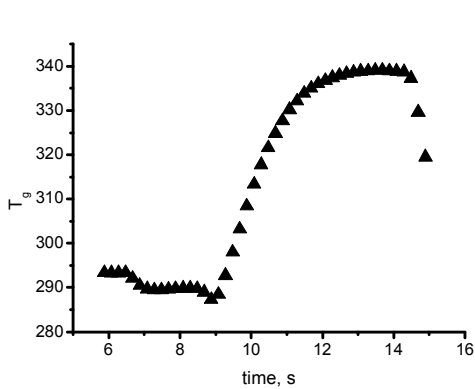
Fig. 42. Gas temperature T_g.   Fig. 43. Pressures P_1(▲), P_2(Δ)
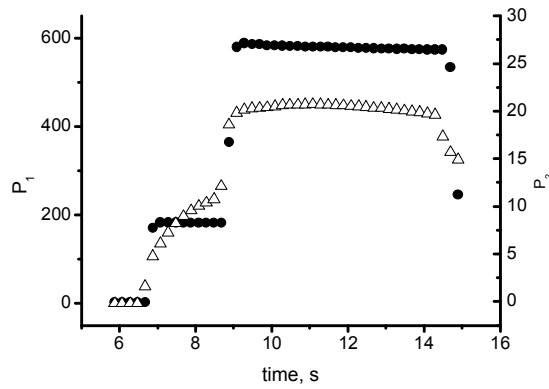
5.1.   Dependence of U, Y and η_w on the chlorine molar flow rate and BHP column height.

The increase of M_c results in increase of initial chlorine pressure in bubbles and heat release. In these tests the steady state BHP column height H was varied by changing of BHP volumetric rate V_l. The dependence of chlorine utilization on H for two different chlorine molar flow rates are presented in Fig. 44.
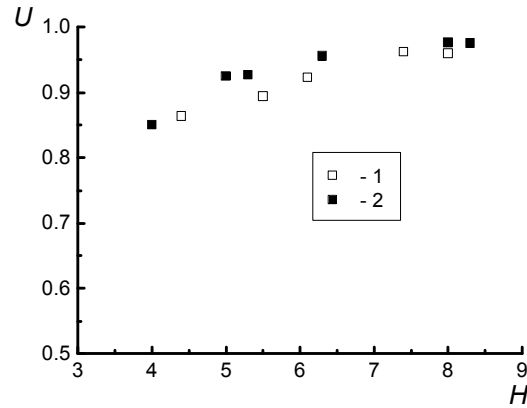
Fig. 44. CBSOG-1f. Dependence of chlorine utilization on H and chlorine molar flow rate. n=46 s^{-1}, N_H=7.5 mole/liter, N_B=6 mole/liter, M_{He}=95 mmole/s, T_{li}=257K: 1- M_C=37 mmole/s; 2 – M_C=56 mmole/s.
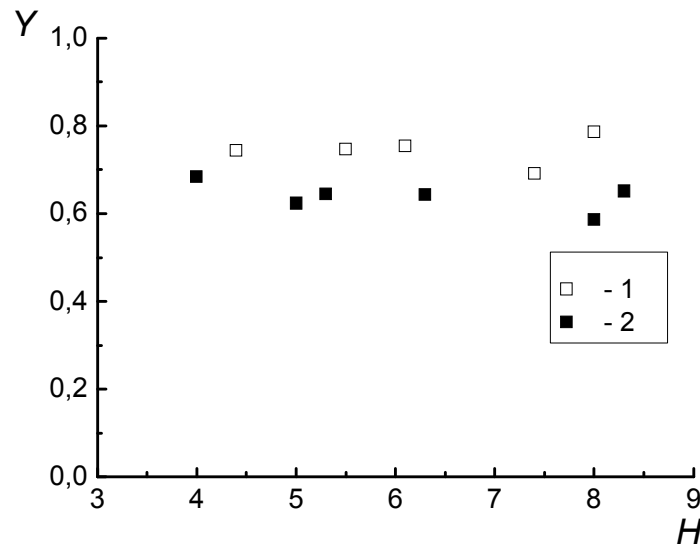
Fig. 45. CBSOG-1f. O$_2$($^1\Delta$) нield as function of H and chlorine molar flow rate. n=46 s^{-1}, N_H=7.5 mole/liter, N_B=6 mole/liter, M_{He}=95 mmole/s, T_l=257K : 1- M_C=37 mmole/s; 2 – M_C=56 mmole/s.

The dependence of U and Y on chlorine molar flow rate at H≈const is presented in *Fig. 46*.
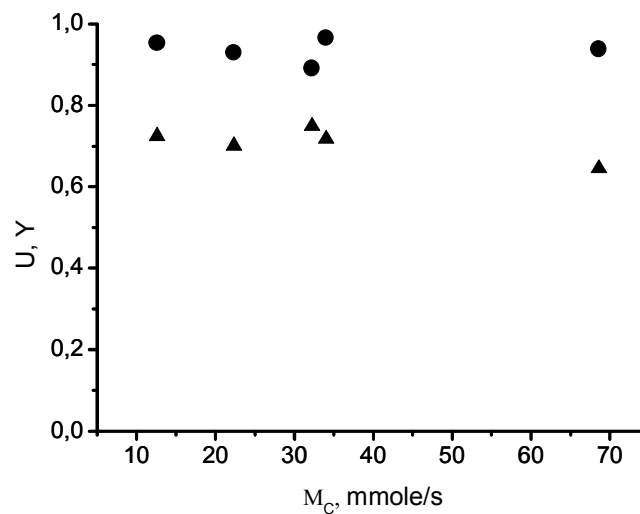
Fig. 46. CBSOG-1h. U($\bullet$) and Y($\blacktriangle$) on chlorine molar flow rate. N_H=7.5 mole/liter, N_B=6 mole/liter, M_{He}=95 mmole/s , H=5÷6 mm, n=46 s^{-1}, T_{li}=257K.

The results of this series demonstrate independence of utilization on M_c. It means that kinetics of chlorine absorption close to the first-order reaction approximation [36]. $O_2(^1\Delta)$ yield slowly depends on H and lower for higher M_c.

5.2.   Dependence of water vapor fraction on chlorine molar flow rate.

In these tests the pressure P_2 was approximately proportional to the chlorine molar flow rate M_c. The increase of P_2 results in increase of P_4 and this forces slightly to increase BHP volumetric rate V_1 to save the BHP column height H=5-6mm and chlorine utilization.(Fig. 47). In spite of decreasing of water vapor fraction the absolute water vapor pressure increases with increase of chlorine molar flow rate (Fig.48).
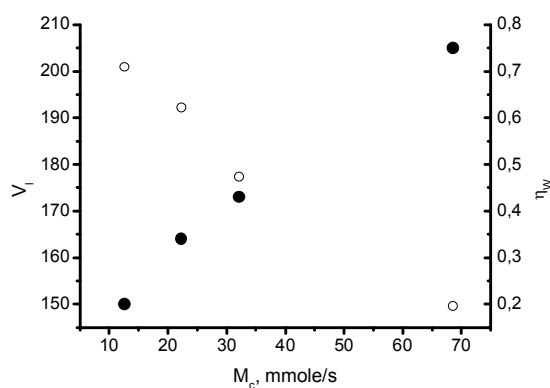
Fig. 47. The BHP volumetric rate ($\bullet$) and water vapor fraction ($\circ$).

Fig. 48. Partial water vapor P_{w4} in CBSOG cavity.

(CBSOG-1h. N_H=7.5 mole/liter, N_B=6 mole/liter, M_{He}=95 mmole/s , H=5÷6 mm, n=46 s^{-1}, T_{li}=257K.)

The increase of P_{w4} is due to increase of the heat release in the chemical reaction of chlorine with BHP. The increase of V_1 (with increase of M_c and P_4) doesn't compensates this heat release.

5.3.   Dependence of U and Y on the BHP molarity and temperature.

The BHP freezing point and point of KCl salt crystallization depend on the solution molarity. It is important to check CBSOG output parameters on BHP molarity and temperature. The result of measurements of U, Y for two diferent BHP molarities are presented in Fig.49.
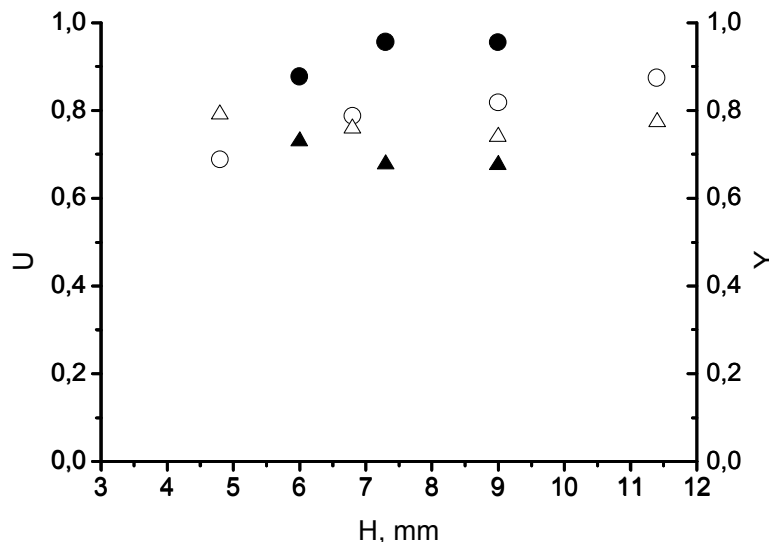
Fig. 49. Utilization U($\bigcirc$-M_B=2M, N_B=11M, $\bullet$-M_B=6.5M, N_H=7.5M) and yield Y ($\triangle$-M_B=2M, N_B=11M, $\blacktriangle$-M_B=6.5M, N_H=7.5M) on BHP column height H and BHP molarity.
(CBSOG-1h, M_c=55 mmole/s, M_{He}=95 mmole/s, n=45c^{-1}, T_I=258K).

The chlorine utilization is lower but yield is slightly higher for lower KOH concentration. It is possible to increase BHP temperature at lower KOH molarity to keep the mass transfer rate for chlorine absorption (Fig. 50). It was found that yield Y doesn't depend on N_H in these series of tests. The increase of BHP temperature results in increase of the water vapor fraction.
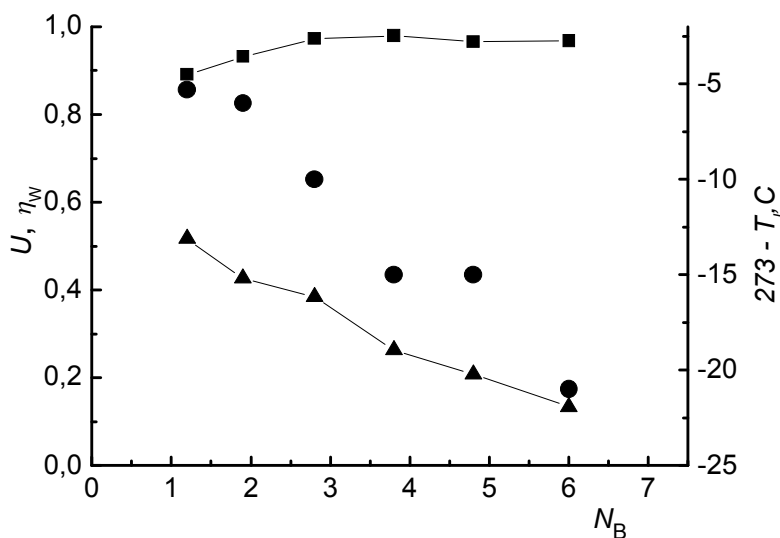
Fig. 50. Utilization ($\blacksquare$), water vapor fraction ($\blacktriangle$) and initial BHP temperature (right axis $\bullet$). CBSOG-1b, n=27 s^{-1}, H=7÷8mm, M_C=37 mmole/s, M_{He}=95 mmole/s.

The water vapor fraction can be decreased by increasing the pressure over BHP column by decreasing the area S_g (Fig. 51). The CBSOG-1a has in 5.6 times bigger area S_g in the internal perforated cylinder than in CBSOG-1b. Hence the gas pressure over sparged layer is higher in the case of CBSOG-1b. The water vapor partial pressure over BHP column equals approximately to the saturated P_{sw}. The last value is determined by T_l, V_l and heat release in reaction. P_{sw} approximately are equaled for CBSOG-1a and CBSOG-1b. At constant rotation frequency n and constant area of the drain holes the increase of H is due to increase of BHP volumetric rate V_l. Therefore with increase of H the output BHP temprature decreases and decreases water vapor fraction η_w.
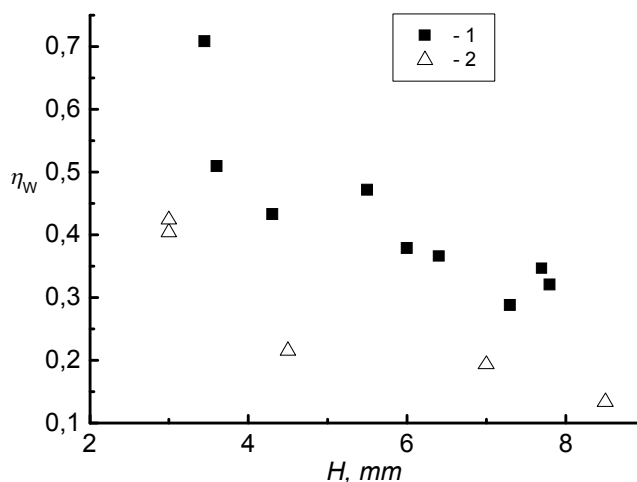
Fig. 51. Water vapor fraction on H for different S_g. (n=27 s^{-1}, M_C=37 mmole/s, M_{He}=95 mmole/s, N_H=7.5M, N_B=6 M, T_l=253K: 1-CBSOG-1a; 2-CBSOG-1b.

5.4.   Dependence of U and Y on BHP column height H.

The value H is the gas free BHP column height. In the bubbling layer the real height of "gas-liquid" column can differ from H due to gas content in sparger layer. Nevertheless H is the most important parameter of the any bubble apparatus. The dependence of utilization on H is shown in Fig. 52. In contrast to modeling (Fig.11, 12) the utilization substantially depends on KOH molarity. It is quite easy to explain. In calculations (Fig.11, 12) we didn't take into account heating of solution. But the increase of the BHP temperature results in decrease of the BHP viscosity and enhancement of the diffusivity coefficients of chlorine molecules and HO_2^- ions in BHP.
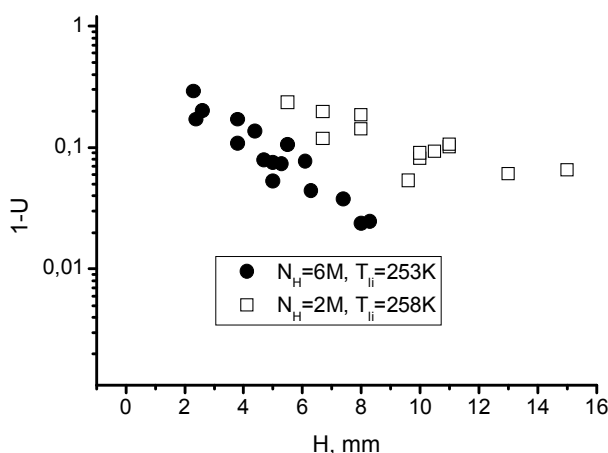
Fig. 52. The dependence of U on H in a wide range of M_c=34÷70 mmole/s for all CBSOG-1 from a) to f) modifications with d_n=0.3 mm. n=46s^{-1}.

So the key to increase of U is the increase of H and N_H. The yield strongly depends on the gas volumetric rate and oxygen partial pressure in the bulk duct. So yield strongly depends on S_g and M_c. For example in CBSOG-1a S_g in 5.6 time bigger than for CBSOG-1b. Hence the $O_2(^1\Delta)$ losses in bubbling layer should be less for CBSOG-1a. (Fig. 53).
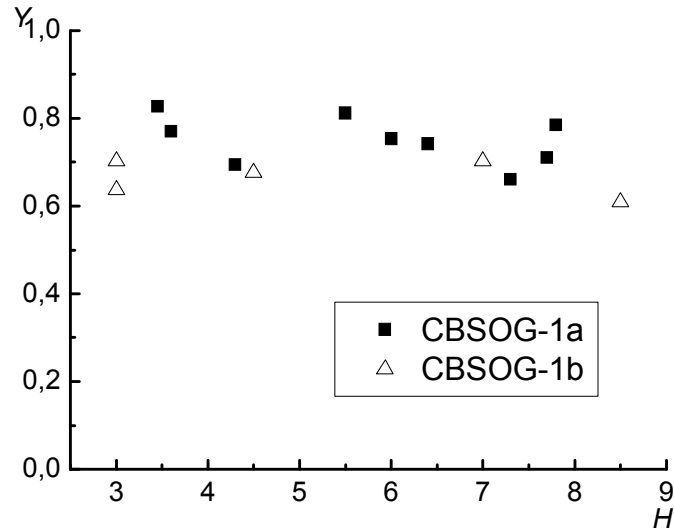
Fig. 53. $O_2(^1\Delta)$ yield as function of H. (n=27 s^{-1}, M_C=37 mmole/s, M_{He}=95 mmole/s, N_H=7.5 M, N_B=6M, T_I= 253K).

5.5.   Influence of the BHP volumetric rate.

In CBSOG the BHP volumetric rate influences on BHP column height, efficiency of the consumption of chemicals in BHP in the single pass through CBSOG, BHP output temperature. A relative consumption of chemicals in the single pass is defined by parameter $\eta_{BHP} =2UM_c/(V_lN_B)$. Parameter η_{BHP} increases with the decrease of BHP volumetric rate. Consumption of chemicals in the single pass through CBSOG and output BHP temperature are higher at higher η_{BHP}. On the one hand a higher consumption of chemicals results in lower basic concentration N_B in the effluent BHP. On the other hand a higher consumption of BHP results in higher temperature of the effluent BHP and as result higher diffusivity of chemicals in the solution. So the rate of chlorine absorption and chlorine utilization will depend on the competition of these two effects. The results of measurements of chlorine utilization on BHP column height H at different consumption parameter ηBHP is presented in Fig. 54. It seen that there is not dependence of chlorine utilization on η_{BHP} or volumetric rate V_l.
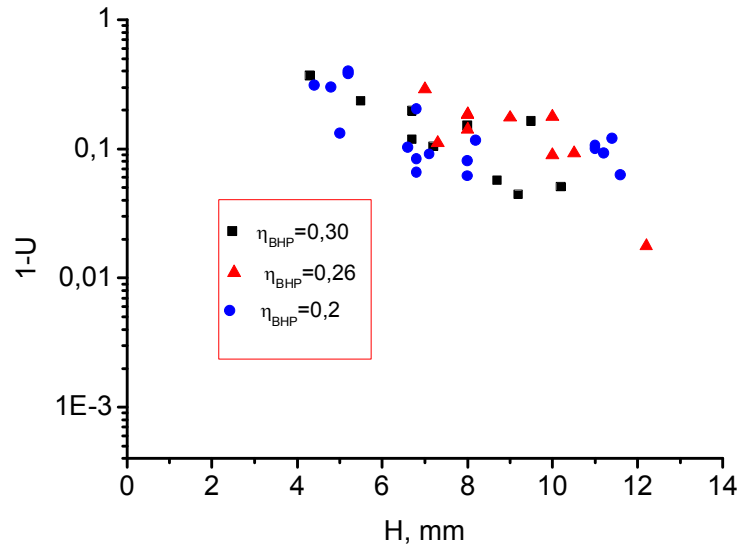
Fig. 54. The dependence of chlorine utilization on BHP column height and parameter $\eta_{BHP} = 2UM_c/(V_l N_B)$. $M_{He} = 90$ mmole/s, $M_c = 30 \div 70$ mmole/s, $V_l = 70 \div 210$ cm^3/s, $N_B = 2 \div 6.5$ mole/liter. Summary of experiments with CBSOG-1a-1h at rotation frequency n = 30s^{-1} and n = 46s^{-1}.

Any dependence of $O_2(^1\Delta)$ yield on V_l has not been detected in these tests.

With the decrease of BHP volumetric rate V_1 the output BHP temperature increases. A water vapor partial pressure at the exit of the CBSOG depends on initial BHP temperature t_{li} and final BHP t_{lf}. The BHP temperature rise depends on the ratio UM_c/V_1 (the first annual report, formula (25)). The dependence of the partial water vapor pressure P_{W4} at the exit CBSOG (inside perforated cylinder) is presented in Fig. 55.
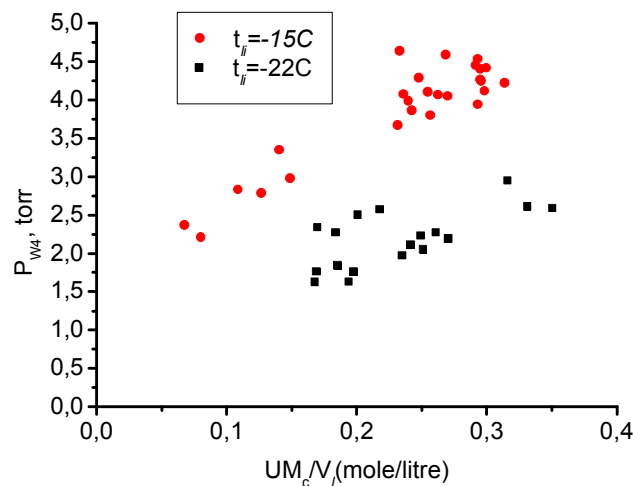
Fig. 55 The dependence of water vapor pressure inside CBSOG cavity on BHP volumetric rate. $M_{He} = 90$ mmole/s, $M_c = 30 \div 70$ mmole/s, $V_l = 70 \div 210$ cm^3/s. Summary of experiments with CBSOG-1a-1h at rotation frequency n = 30s^{-1} and n = 46s^{-1}.

The output water vapor pressure is higher for higher ratio UM_c/V_1 and higher initial BHP temperature t_{li}.

5.6. Influence of chlorine dilution with helium.

The experiments have been performed with CBSOG-1a. A simulation of CBSOG operation demonstrated the next result: the increase of dilution of chlorine with helium results in the decrease of the initial chlorine pressure in bubbles, increase of the bubble size and the decrease of the bubble frequency formation. As a result of these effects the chlorine utilization should decrease with the increase of helium dilution. The experimental dependence of the chlorine utilization on the helium dilution is shown in Fig. 56.
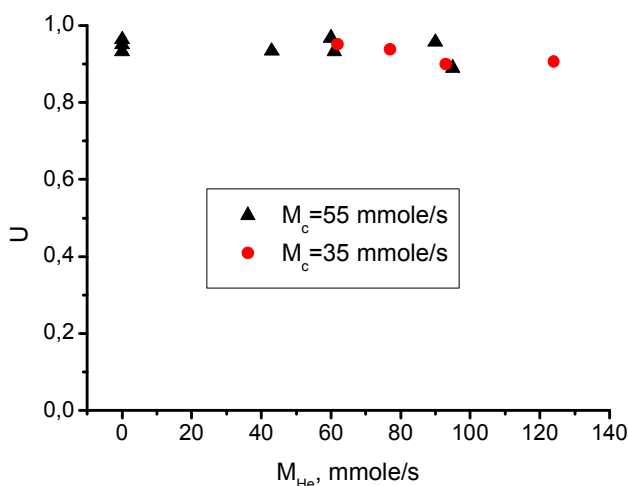
Fig. 56. Dependence of the chlorine utilization on the dilution of chlorine with helium. V_l=180 cm^3/s, H=7 mm, N_B=6 mole/liter. Rotation frequency n =30s^{-1} and n = 46s^{-1}.

The increase of chlorine dilution with helium resulted in bigger generated bubbles, larger bubble velocity and lower initial partial chlorine pressure in bubbles. As a result the $O_2(^1\Delta)$ yield has to increase with increase of helium dilution. The experiment verified this qualitative conclusion (Fig. 57).
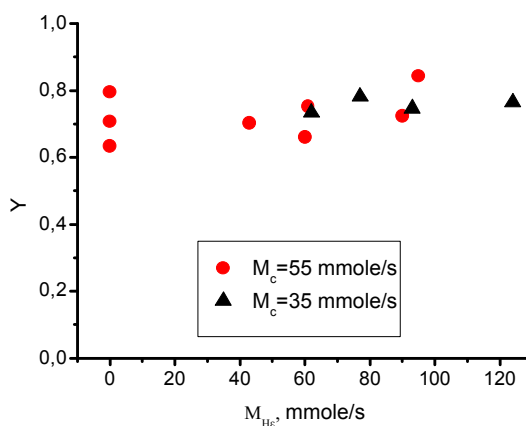
Fig. 57. Dependence of Y on the helium dilution. V_l=180 cm^3/s, H=7 mm, N_B=6 mole/liter. Rotation frequency n =30s^{-1} and n = 46s^{-1}.

The water partial pressure P_{W4} inside CBSOG depends on initial and final BHP temperature only and in the first approximation doesn't depend on helium molar flow rate (Fig. 58). It is necessary to mark that a slit throat was installed downstream from the measuring chamber to emulate the nozzle bank throat. Water vapor fraction relative to the sum of the residual chlorine and oxygen pressures in the measuring cell is

$$\eta_W = \frac{P_W(M_c + M_{He})}{M_c(P_2 - P_W)}$$

When throat is installed downstream measuring chamber the increase of the helium molar flow rate results in the decrease of the sum of residual chlorine and oxygen pressure inside CBSOG. As a result the water vapor fraction in the measuring chamber increases with the increase of chlorine dilution with helium (Fig. 59).
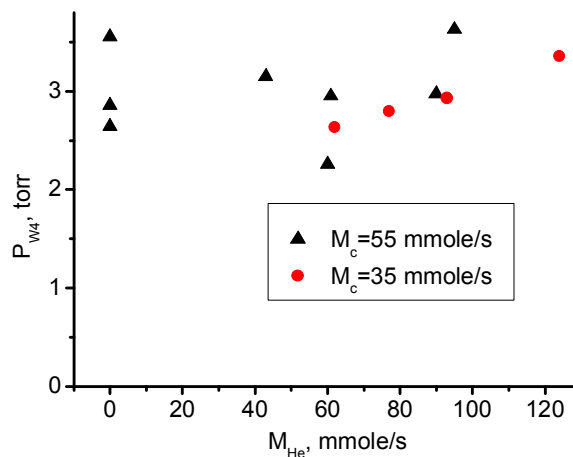
Fig. 58. The water vapor partial pressure inside CBSOG as a function of the helium molar flow rate. V_i=180 cm^3/s, H=7 mm, N_B=6 mole/liter. Rotation frequency n =30s^{-1} and n = 46s^{-1}.
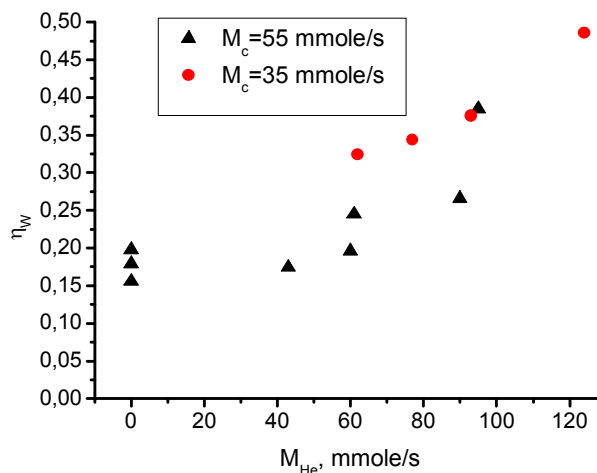
Fig. 59. The water vapor fraction at the exit of CBSOG as a function of the helium molar flow rate. V_i=180cm^3/s, H=7 mm, N_B=6 mole/liter. Rotation frequency n =30s^{-1} and n = 46s^{-1}.

5.7.   Influence of the centrifugal acceleration.

CBSOG-1 operated up to the maximum rotation frequency n=46s^{-1} or centrifugal acceleration G=3.78×10^{3}m/s^2 (386g). Variation of the centrifugal acceleration changes many hydrodynamics parameters of CBSOG. The increase of G results in final bubble size decrease, decrease of the time

of the bubble growth and increase of the bubble velocity. The increase of G is accomplished with increasing of the initial chlorine pressure in bubbles. Numerical simulations showed that utilization would be higher but $O_2(^1\Delta)$ yield would be less for higher G. But experiments showed that utilization and yield quite slowly depend on G, as it seen from Fig. 60, Fig. 61.
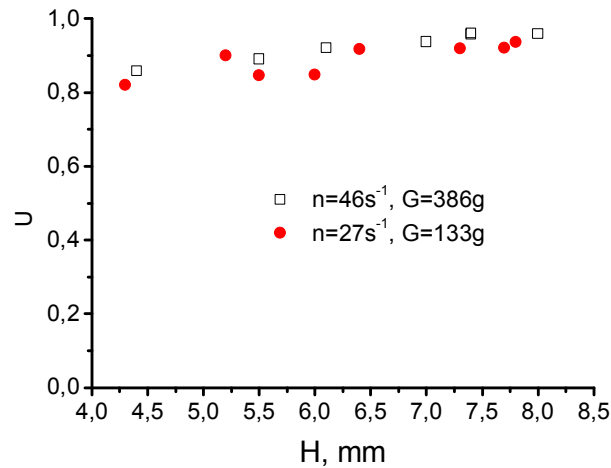
Fig. 60. Dependence of chlorine utilization on H and G. M_{He}=90 mmole/s, M_c=35 mmole/s, V_l=180 cm^3/s, N_B=6 mole/liter.
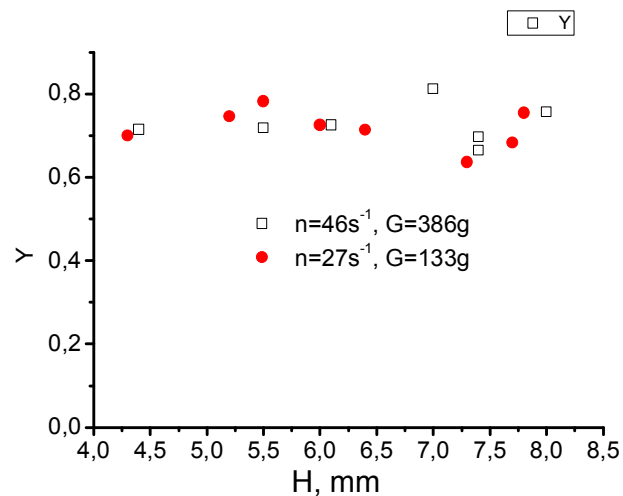
Fig. 61. Dependence Y on H and G. M_{He}=90 mmole/s, M_c=35 mmole/s, V_l=180 cm^3/s, N_B=6 mole/liter.

Water vapor. As it was expected no any dependence of water vapor fraction on the centrifugal acceleration has been detected.

5.8. Influence of the number of nozzles per cm^2 of the bubbler surface and diameter of nozzle.

In the CBSOG a number of the gas nozzles N_n per 1cm^2 of the bubbler influences on the specific productivity of the CBSOG or how mmole/cm^2/s of the oxygen flux can be generated. The increase of N_n can lead to the coalescence of the generated bubbles and results in increasing of the superficial gas velocity U_{sf} over BHP column. In this section it is more convenient to present results as a function of chlorine molar loading per 1 cm^2 of the bubbler i.e. as a function of j_c(mmole/cm^2/s)=$m_c N_n$.
Parameters of the bubblers used to study influence of N_n and d_n on the CBSOG output are presented in Table 11.

Table 11. Designing parameters of CBSOG-1.

Parameter	Parameters of bubblers for CBSOG-1 modifications				
	a-d	e-f	g	h	i**
N	561	561	165	165	55
D, mm	93	93	93	93	93
d_n, mm	0.3	0.3	0.55	0.55	0.95
N_n, cm^{-2} a, mm	3.43 , 5.4	11.1 3	3.78 5.4	7.71 3.6	5.16 4.4
S_b, cm^2	164	50.5	43.6	21.4	10.6

The chlorine utilization as a function of chlorine flux is presented in.Fig.62, Fig.63.

| a) | b) |
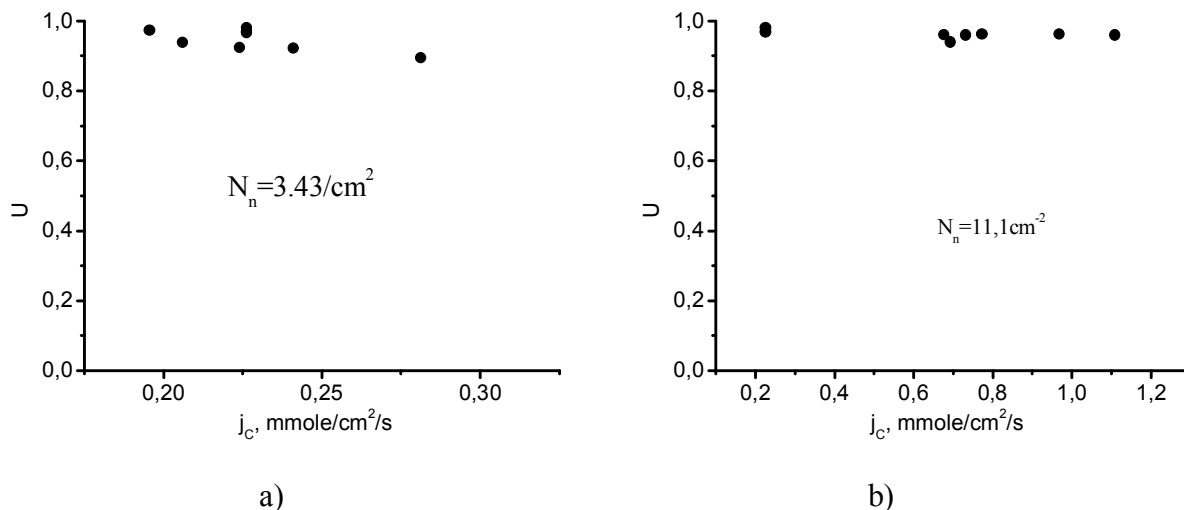
Fig.62. Chlorine utilization as a function of chlorine flux for two different nozzle densities N_n. a) N_n=3.43 cm^{-2} (CBSOG-1, a-d versions), b) N_n=11.1 cm^{-2} (CBSOG-1, e-f versions). H=8mm, N_H=7.5M, N_B=6M, M_{He}=90 mmole/s, $P_g \approx P_4$=33±3 torr. Rotation frequency n =30s^{-1} and n = 46s^{-1}.

At j_c=1 mmole/s and P_g=33 torr a superficial gas velocity reaches of U_{sf}=5.53 m/s

a)   b)
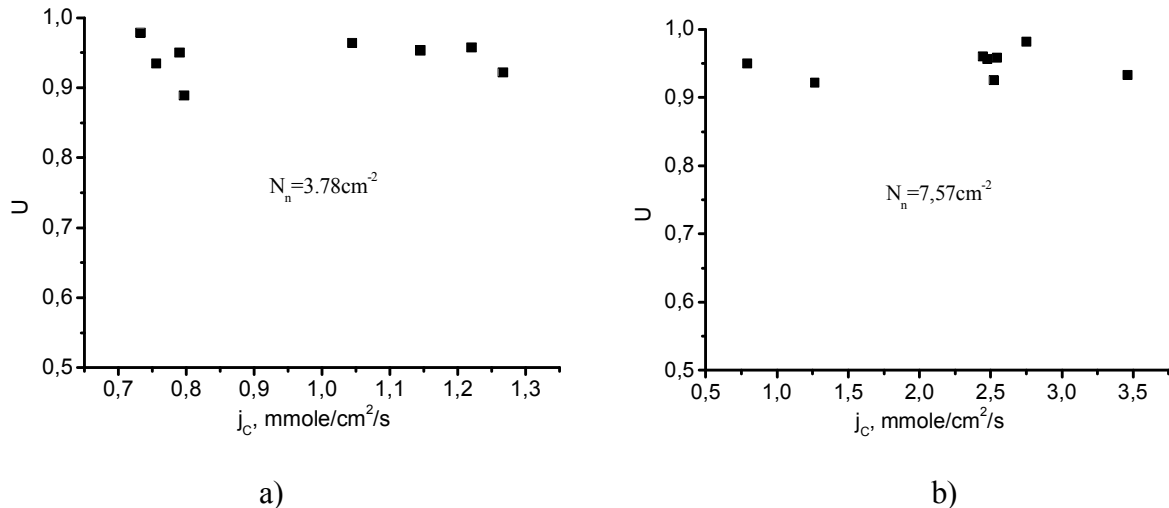
Fig.63. Chlorine utilization as a function of chlorine flux for two different nozzle densities N_n. a) N_n=3.78 cm^{-2} (CBSOG-1, g versions), b) N_n=7.57 cm^{-2} (CBSOG-1, h versions). H=8mm, N_H=7.5M, N_B=6M, M_{He}=90 mmole/s, $P_g{\approx}P_4$=33±3 torr. Rotation frequency n =30s^{-1} and n = 46s^{-1}.

At j_c=3.5 mmole/ cm^2/s and P_g=33 torr the gas velocity reaches of U_{sf}=20 m/s. It is seen that U slowly depends on j_c (for d_n=0.3mm up to N_n =11.1 cm^{-2} and for d_n=0.55mm up to N_n=7.57 cm$^{-2)}$. The chlorine utilization in the range of chlorine loading 0.2÷3.5 mmole/cm^2/s is near or higher than 90% when h=8mm, N_H=7.5M, N_B=6M, M_{He}=90 mmole/s.

The $O_2(^1\Delta)$ yield as a function of chlorine flux is presented in Fig.64, Fig.65. These tests have been performed at identical gas transport time from bubbler surface to the measuring chamber.

a)   b)
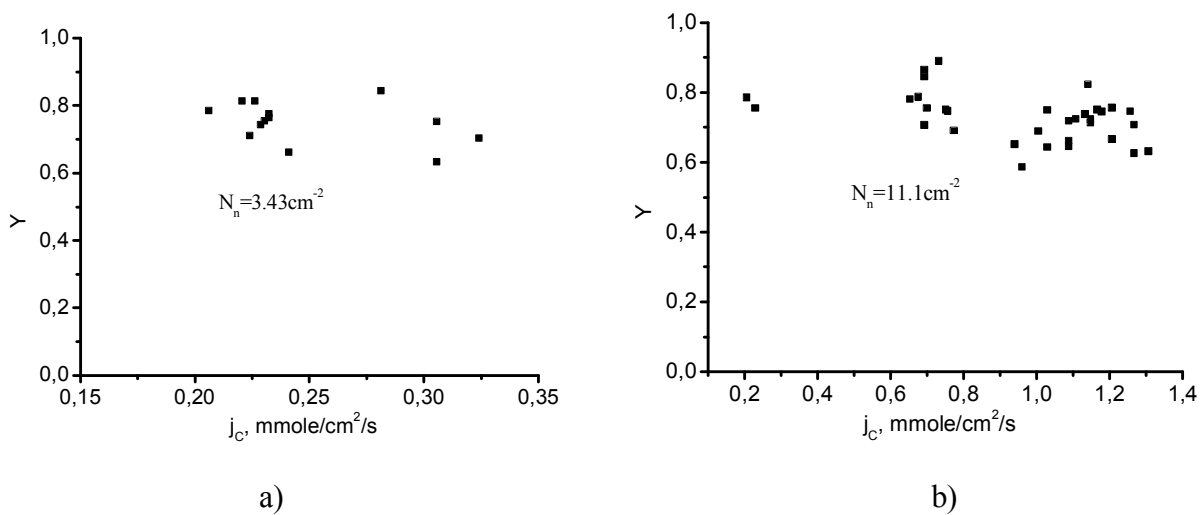
Fig.64. $O_2(^1\Delta)$ yield as a function of chlorine flux for two different nozzle densities N_n. a) N_n=3.43 cm^{-2} , d_n=0.3mm (CBSOG-1, a version), b) N_n=11.1 cm^{-2}, d_n=0.3 mm (CBSOG-1, e-f versions). H=5÷8mm, N_H=7.5M, N_B=6M, M_{He}=90 mmole/s. Rotation frequency n =30s^{-1} and n = 46s^{-1}.

a)   b)
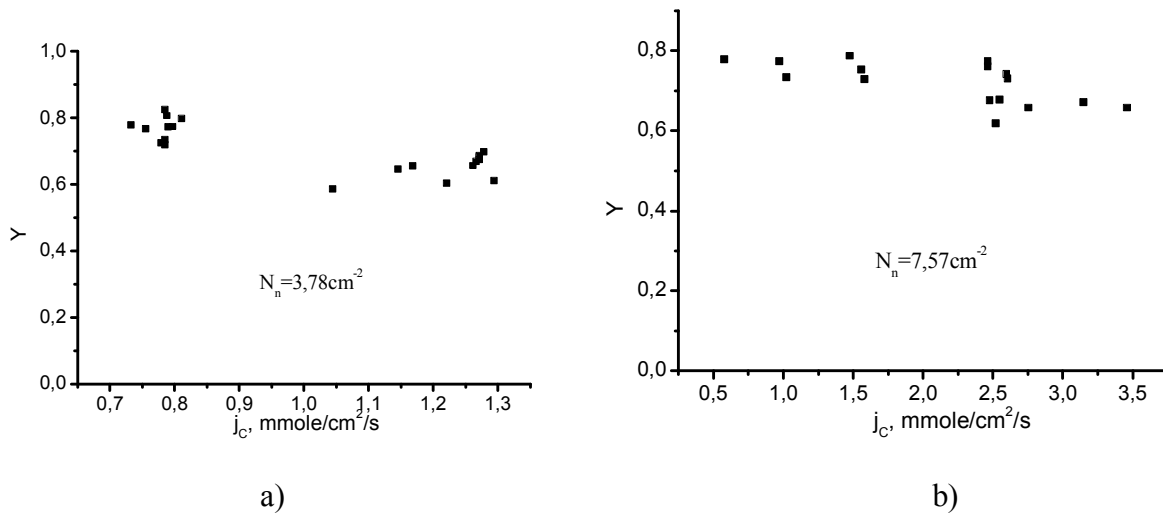
Fig.65. $O_2(^1\Delta)$ yield as a function of chlorine flux for two different nozzle densities N_n. a) N_n=3.78 cm^{-2}, d_n=0.55mm (CBSOG-1, g versions), b) N_n=7.57 cm^{-2}, d_n=0.55mm (CBSOG-1,h versions). H=5÷8mm, N_H=7.5M, N_B=6M, M_{He}=90 mmole/s. Rotation frequency n =30s^{-1} and n = 46s^{-1}.

Water vapor fraction as a function of chlorine flux j_c is presented in Fig.66. We select only tests with near equivalent BHP initial temperature, ratio UM_c/Q_{BHP} and oxygen pressure over BHP column. We selected tests with next near equivalent parameters UM_c/Q_{BHP}= 0,22 mole/litre, t_{li}= -18C°, $P_g\approx P_4$=36 torr. The data presented in Fig.68 have been obtained from tests of different modifications of CBSOG-1. For example the highest j_c have been achieved for CBSOG-1i having lowest working bubbler area S_b=10.6cm^2 and nozzles 0.95 mm of diameter (see also Fig.69).
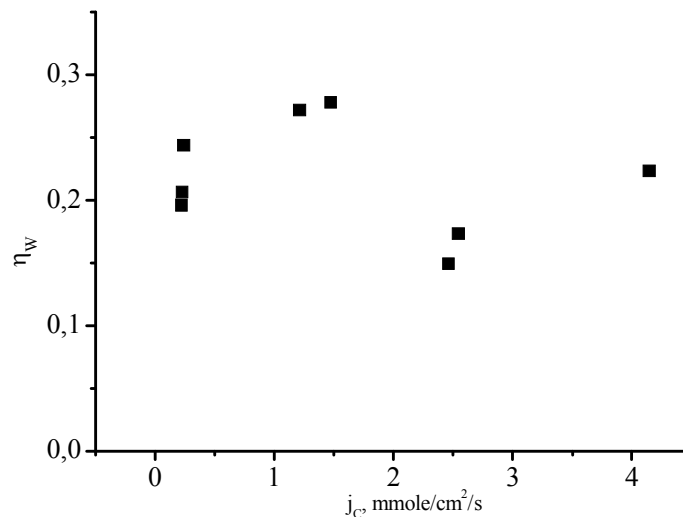
Fig.66. The water vapor fraction as a function of chlorine flux.

No substantial effect of j_c on η_w has been found.
It was expected that the increase of d_n results in increasing of the bubble detachment size and decreasing chlorine utilization at the identical BHP column height H. But from the practical point of view the bigger d_n is more preferable. At large d_n the clogging of the nozzles by salt or KOH particles is less probable. In the case of bigger d_n higher oxygen flux j_o from bubbler surface can be generated.

The tests had been performed for three different gas nozzle diameters d_n (0.3, 0.55 and 0.95mm). Chlorine+helium plenum pressure P_1 was in the range 450÷550 torr depending on liquid hydrostatic pressure P_l and pressure P_4. So, it is more convenient to present chlorine utilization and $O_2(^1\Delta)$ yield as a function of chlorine molar flow rate through the single nozzle (**Fig.67**-**Fig.69**).
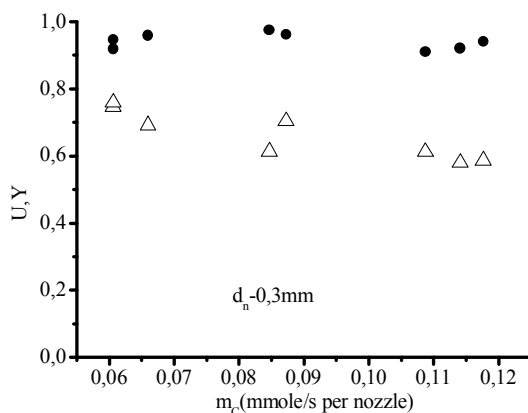
Fig.67. U – (♦) and Y- (Δ) as a function of chlorine molar flow rate through the nozzle m_C. H=8÷10 mm, d_n=0.3mm. Rotation frequency n =30s^{-1} and n = 46s^{-1}.
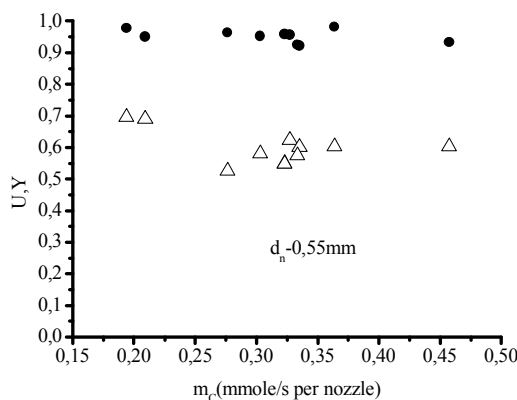
Fig.68. U- (♦) and Y- (Δ) as a function of chlorine molar flow rate through the nozzle m_C. H=8÷10 mm, d_n=0.55mm. Rotation frequency n =30s^{-1} and n = 46s^{-1}.
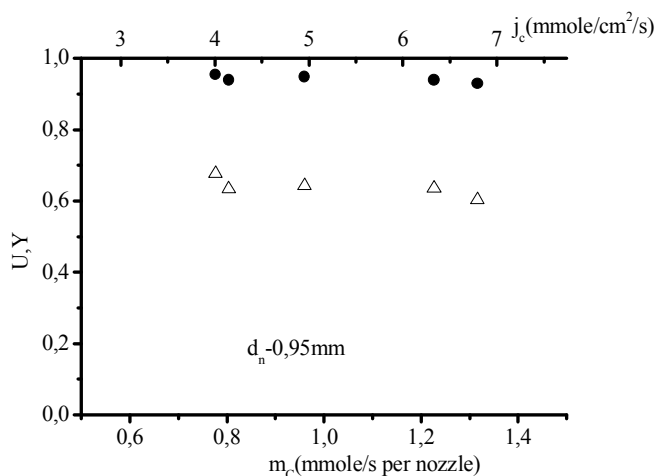
Fig.69. U- (●) and Y- (Δ) as a function of chlorine molar flow rate through the nozzle m_C. CBSOG-1i. H=8÷10 mm, d_n=0.95mm. j_c=$m_C N_n$. Rotation frequency n =30s^{-1} and n = 46s^{-1}.

It is seen that chlorine utilization is near the same for nozzles with d_n=0.3÷0.95mm when h=8÷10 mm. It was quite unexpected result. $O_2(^1\Delta)$ yield is lower for higher m_c due to stronger $O_2(^1\Delta)$ quenching at high pressures. But for the same m_c $O_2(^1\Delta)$ yield doesn't depend on the nozzle diameter d_n. A highest chlorine loading (~7 mmole/cm^2/s) and oxygen flux (~6.3 mmole/cm^2/s) without substantial drop of Y and U have been achieved for CBSOG-1,i with the biggest nozzle diameter d_n=0.95 mm.

5.9. Droplet fraction at the exit of CBSOG-1.

The aerosol carry over strongly depends on the gas superficial velocity U_{sf} and centrifugal acceleration. In all SBSOG runs (approximately 150 runs for CBSOG-1)) the operation of CBSOG was stable or without catastrophic BHP carry-over. Even at high superficial gas velocity U_{sf}=20 m/s the traces of droplets were not observed visually. We installed 3 layers of mesh in bulk duct between CBSOG and measuring chamber. This mesh has cell size 10x10 μm^2 and filament diameter 10μm. If droplets have size bigger that 10μm we believe that all of them were trapped by this mesh. In one of the experimental days 10 runs of CBSOG (5 second duration, 34 mmole/s of Cl_2+95 mmole/s of He) were performed at the superficial gas velocity over bubbling layer U_{sf}=21 m/s. Then we removed this mesh and put it into glass vessel containing 100 ml of distilled water. We tried to detect traces of KOH in this vessel by acid-base titration method. It was found that less than 2×10^{-5} mole of KOH was deposited on this mesh. The initial KOH concentration in BHP was 4mole/litre. It means that maximum 5×10^{-6} liter of BHP was deposited on this mesh. The total mass of gas passed through CBSOG was 73 grams. So the maximum aerosol mass fraction was $f_d<10^{-4}$. Probably rotating perforated cylinder serves like an efficient separator. It was reasonably to suppose that residual chlorine reacts with trapped KOH and KCl particles formed on the mesh. Therefore we have made several new experiments to detect KCl particles on this mesh. We have put mesh into distilled water and then measured specific electric conductivity of this solution. The measurements of specific electric conductivity of this solution showed that total KCl trapped by this mesh was less that 10^{-4} mole after 10 runs of CBSOG. The concentration of K in BHP was 2÷6 mole/l, BHP mass density was 1.3 g/cm^3. In these experiments the total mass of the gas (including helium) passed through CBSOG during one day was 150 g. Thus, a mass fraction of the big size droplets was less than 4.5×10^{-4}.

5.10. Preliminary conclusions from tests of CBSOG-1.

A first design of CBSOG was based on the theoretical estimations of hydrodynamic and gasdynamic of the bubble formation and motion in liquid being under condition of high centrifugal acceleration. All estimations were performed for the bubbling mode of the gas dispersion [1-6]. The expected bubble velocity is of 200÷600 cm/s for the bubbles of 2÷5 mm in diameter at centrifugal acceleration (200÷600)g. The size of the bubble decreases with increase of the centrifugal acceleration and height of the liquid column. The bubble generation from the single cylindrical nozzle in condition of a high centrifugal acceleration has been observed. At low centrifugal acceleration of ~10^3 m/s^2 and height of the liquid column of ~10 mm the gas jetting is observed. At higher centrifugal acceleration of ~4×10^3 m/s^2 the gas bubbling was observed and the bubble shape close to the sphere. For large nozzle diameter (~1 mm) and liquid layer height of ~10 mm the size of the bubble is compared with the height of the liquid column. For the nozzle of 0.3mm in diameter and the centrifugal acceleration ~400g the diameter of the generated bubbles was of ~3mm, velocity of ~500 cm/s. For this case the estimated size of the bubble is in a good agreement with observed but observed velocity is higher than estimated. A simplified model of the chlorine absorption and $O_2(^1\Delta)$ generation has been applied for the estimation of chlorine utilization and

$O_2(^1\Delta)$ yiled. Approximately 90% of chlorine utilization can be achieved for BHP column height of ~10 mm in a wide range of the centrifugal acceleration and nozzle diameter $d_n<0.5$mm. The $O_2(^1\Delta)$ yield decreases with increase of the centrifugal acceleration. The chlorine utilization was calculated for the low molarity of the BHP([KOH]=2M) and for high molarity of the BHP ([KOH]=6.5M). It was shown that the utilization for both BHP is almost equivalent. It is due to higher diffusivity of ions in BHP in the case of low KOH concentration. To achieve "good" utilization and $O_2(^1\Delta)$ yield at 100 torr of the oxygen pressure the diameter of the generated bubbles should be less than 2 mm and centrifugal acceleration should be ~500g.

A simplified thermal model of CBSOG has been applied for the estimation of the output BHP temperature and water vapor fraction. The water vapor pressure at the exit of CBSOG is substantially less that saturated water vapor pressure at the output BHP temperature. The water vapor fraction is less than 10% at BHP-1 (KOH=2M, H_2O_2=11M) consumption 50%, ratio M_c/V_l=0.6 mole/liter and active gas (chlorine, oxygen) pressure more than 40 torr. The water vapor fraction is less than 10% at BHP-2 (KOH=6.5M, H_2O_2=7.5M) consumption 30%, ratio M_c/V_l=1 mole/liter and active gas (chlorine, oxygen) pressure more than 30 torr.

The mechanisms of the droplet generation have been analyzed. The droplets can be generated as a result of the bubble film rapture and destruction of jet, created by surface tension effect after film destruction. Estimations showed that the size of the film droplet is less 1μm and their mass fraction is less 1% at high centrifugal acceleration. The big jet droplets are expected can not be generated at high centrifugal acceleration and bubble size more than 170μm. At condition of a high centrifugal acceleration the gas pressure inside bursting bubble may be substantially higher than pressure over the liquid. It is expected in this case that the droplets with big size to be generated during rapture of the thick film of the bubble dome. For the estimation of the efficiency of droplet separation the trajectory has been calculate for the droplet leaving BHP column. In a wide range of CBSOG working parameters an efficient separation of droplets with size more than 20μm is expected for D>10cm and moderate superficial gas velocity of ~20 m/s.

These estimations have been as the basis for the first designing of CBSOG. The preliminary estimation of the optimal parameters of the first CBSOG design parameters to achieve U>90%, Y>60% and highest molar oxygen flux at total chlorine of 50 mmole/s have been obtained. A first version of CBSOG have been designed and manufactured. It is was planned to operate at next conditions: bubbler diameter 93 mm, rotation frequency less than 50c^{-1}, liquid layer height is less than 10 mm, distance between of ∅0.3mm nozzles is more than 2.5 mm, gas pressure over BHP is less than 100 torr. For the selected CBSOG parameters the droplets with size more than 20 μm will be totally separated.

The next results of the experimental study of CBSOG have been obtained. The chlorine utilization higher than 90% has been achieved at BHP column height higher than 6 mm and centrifugal acceleration of 1.34×10^4 m/s^2. The utilization is higher than predicted from theoretical estimation based on the known physical-chemical data. U>50% is achieved when H≈3 mm (Fig52). Hence a substantial part of chlorine is absorbed at the stage of the bubble growth as was predicted theoretically. The chlorine utilization doesn't depend on chlorine molar flow rate in the range M_c=10÷70 mmole/s (Fig46). Chlorine utilization more strongly depends on KOH molarity for the same initial BHP temperature (Fig.52). The increase of initial temperature of BHP with lower molarity can increase chlorine utilization. High chlorine utilization can be achieved with BHP-1 and BHP-2 for H≈7÷8 mm if one will use BHP-1 at higher temperature than BHP-2. In any case at KOH=2M the utilization higher than 90% can be achieved for H>10 mm without substantial losses of $O_2(^1\Delta)$ yield.

It was found that Y doesn't depend on BHP column height H in the range H<10 mm (Fig.45, 46). It means that gas-liquid contact time is a very small and $O_2(^1\Delta)$ losses in the bubbling layer at high centrifugal acceleration is negligible. $O_2(^1\Delta)$ yield was in the range 50÷80% depending on the

transport losses in bubbling column, inside CBSOG cavity and transport duct. The decrease of Y with increase of M_c is mainly due to $O_2(^1\Delta)$ transport losses in the bulk duct between CBSOG and measuring chamber (Fig 46). $O_2(^1\Delta)$ yield is higher for the larger dilution of chlorine with helium because of the lower transport losses. The variation of the centrifugal acceleration in the range 138g-386g didn't effect on the Y and U. It is the mostly unexpected result from the tests of CBSOG-1 (Fig.60,61).

It was found that water vapor fraction strongly depends on BHP temperature and gas volumetric rate over BHP bubbling surface (or on S_g). This fact strongly evidences that aerosol mass fraction from CBSOG is too small. It was undertaken to detect aerosol by trapping of particles by small scale mesh installed into gas flow. But chemical titration and electro conductive method showed that mass fraction of aerosol is less than 5×10^{-4}.

6.　CBSOG-2,3 with radial oxygen flow outlet and minimal transport losses.

6.1.　The design of the CBSOG-2, 3.

CBSOG-1 has ~500 ml of the gas transport volume including CBSOG cavity and intermediate duct. As a result of CBSOG-1 can operate efficiently only with oxygen pressure P_{4O} near 10 torr. As follows from tests of CBSOG-1 an efficient operation is possible at chlorine loading of 3÷7 mmole/cm²/s without substantial droplet carry over. Therefore the size of CBSOG bubbler surface can be made substantially less to produce oxygen molar flow rate 30÷50 mmole/s, simultaneously gas transport time can be made much less also. So, in this case we can increase output oxygen pressure conserving $O_2(^1\Delta)$ yield. Hence, the mane goal of designing and development of CBSOG-2,3 is to increase output pressure without losses of $O_2(^1\Delta)$ and to increase the specific oxygen molar flow rate per unit of the SOG volume.

In principle the design of CBSOG-2 has not substantially differ from CBSOG-1. But some improvements have been made. The bubbler has diameter of 60 mm and height of 45mm. Gas transport volume from BHP surface to the diagnostic chamber was reduced to 170 cm³ and gas transport volume inside rotating bubbler was reduced to 110 cm³. A basic sketch of CBSOG-2 is presented in Fig.70. The BHP feed bubbler through the pipe 3. This improvements simplified rotary motion feedthrough. An additional temperature sensor was installed near the drain hole 5 to measure the output BHP temperature.
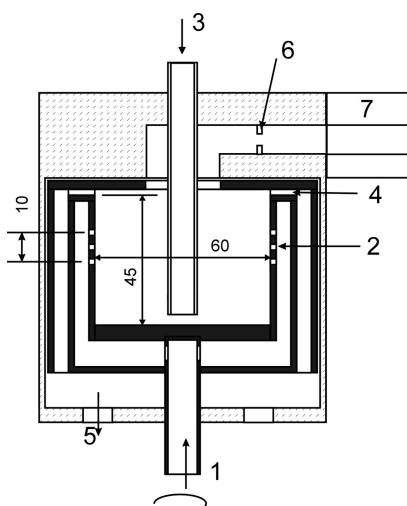
Fig.70. Basic sketch of CBSOG-2. 1- gas inlet, 2- bubbler, 3-BHP inlet, 4, 5-BHP drain holes, 6- slit throat, 7- measuring chamber. All dimensions are given in mm.

The some assembly drawings of CBSOG-2 are shown in Fig.71, Fig.72. In the lower part of CBOG-2,3 the BHP drained from the bubbler is removed to the catch tank by liquid centrifugal pump which rotates on the same driving shaft as bubbler.

Fig.71. General view of CBSOG-2

Fig.72. Rotary bubbler of CBSOG-2,3.

Photos of the main parts of SBCOG-2 are presented in Fig.73,Fig.74 and Fig.75.

Fig.73. CBSOG-2 insides are presented in the right picture

The CBSOG-3 has almost the same design. But some additional improvements in the design of CBSOG have been made. In CBSOG-1,2 the BHP column height H depends on the centrifugal acceleration G, the BHP volumetric rate V_1 and the cross section area of the drain holes S_1. It was a great art to provide desirable H. Therefore in the CBSOG-3 design a special barrier (6) and siphon (7) were induced into construction to support fixed BHP layer height H independently on the bubbler rotation frequency and the BHP volumetric rate (Fig.74). The siphon (7) is also assigned to prevent gas penetration into BHP drain system. The orifice (10) is assigned to support high pressure inside SOG cavity. Rotating separator (11) is assigned to separate droplets. The cross section of slits in the separator is assigned to support high pressure over BHP bubble layer. The working pressure over BHP layer depends on the ratio of areas between orifice (10) and all separator slits. When BHP layer height is of H=6mm then volume of the cavity inside SOG is 77 cm^3. But part of the cavity volume is occupied by separator. Hence volume of the cavity free for the gas is near of 50cm^3. Also in CBSOG-3 bubblers has slit nozzles for the chlorine injection into BHP column. It was necessary to test the difference of CBSOG output characteristics and optimal working parameters with slit nozzle relative cylindrical nozzles. The manufacturing of bubbler with slits nozzles is much simpler and chipper that with cylindrical nozzles.
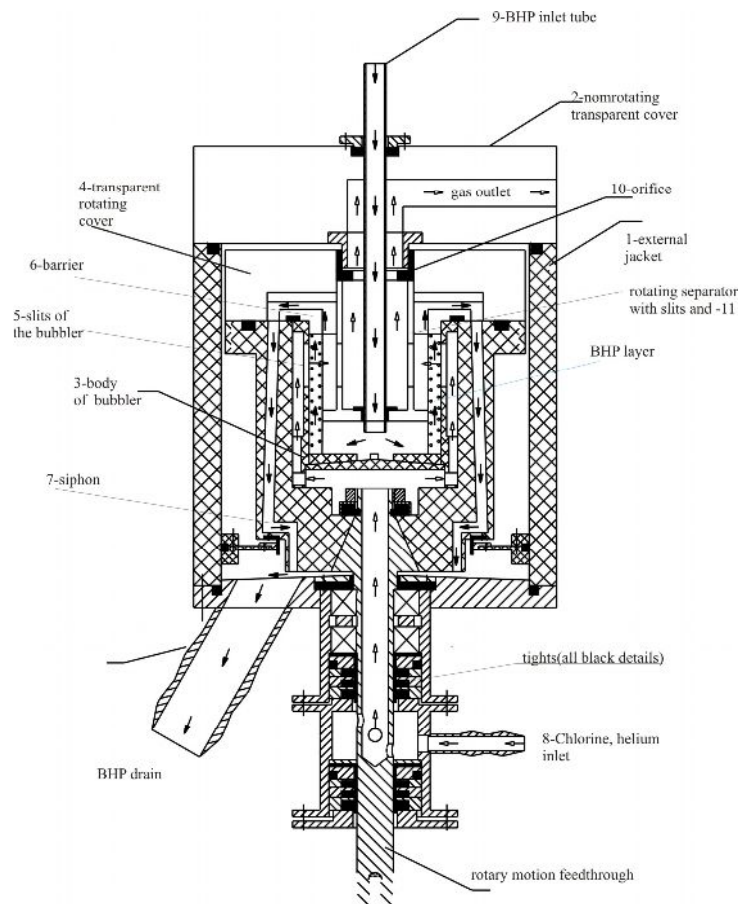
Fig. 74 Design of CBSOG-3.

Several bubblers have been used in CBSOG-2,3. A one of them was like bubbler-h for CBSOG-1 and has 165 cylindrical nozzles of 0.55mm in diameter (Fig 75) (total nozzles area S_g=0.39cm^2). 165 nozzles are arranged in three rows spaced at distance a=3.4 mm. So the density of nozzles is 8.65 per 1 cm^2. In contrast to bubbler-h for CBSOG-1 these cylindrical nozzle nozzles were directed on the angle 30° to the bubbler surface. All other bubblers have bubbler with slits nozzle for the gas injection (Fig.76). The walls of these nozzles also were directed on the angle 30° to the bubbler surface. The angular injection of the gas into BHP column induces additional rotation of the liquid layer and decreases normal gas momentum.

Fig.75 Rotary bubbler for CBSOG-2 with 165 cylindrical nozzles.
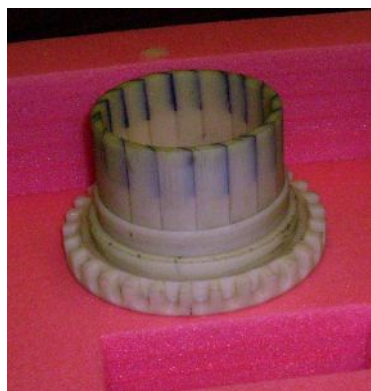
a)

b)

c)

d)

e)

Fig.76. Rotary bubblers for CBSOG-3 with the narrow slit nozzles.

The parameters of the slit bubblers are presented in the next Table (α is the angle between slit axis and bubbler surface).

	number of slits	height of slits mm	width of slits mm	Total geometrical area of slits, cm^2	α, °
a	18	12	0.2	0.42	20
b	52	8	0.2	0.83	20
c	92	8	0.2	1.47	20
d	140	8	0.2	2.24	20
e	52	14	<0.1	0.73	10
f	15	20	0.1	0.3	10

6.2.   Observation of the bubbling column in "cold" tests.

The visual observation of the bubbling layer in CBSOG-2 was performed. A 60% red-tinted glycerin-water solution was used for better visualization. Air of 160 mmole/s was injected into this solution. The pressure P_1=100 torr. The structure of the bubbling layer is shown in Fig.77.

n=60s^{-1} n=80s^{-1} n=100s^{-1}
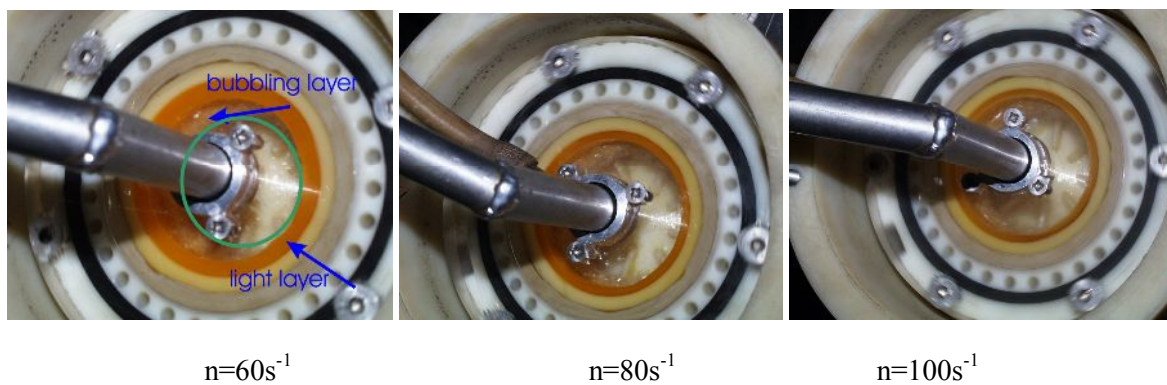
Fig.77. Structure of the bubbling layer in the CBSOG-2.

The bright orange is the bubble free layer or "light" layer and its height is approximately H=5 mm. A foggy-orange layer is a bubbling layer. The increase of rotation frequency n results in decrease of the bubbling layer height. The height of the bubbling layer is approximately 5 mm higher than the height H of the bubble-free layer. A green circle $\varnothing\approx$40 mm in the first picture marks the liquid free space in the CBSOG cavity.
        A small spherical plastic flocet on the filament was fixed to the bubbler surface. Glycerin-water solution with volumetric rate of ~100 ml/s passed through bubbler. In the first experiment the gas nozzles were closed to avoid liquid leakage. The experiment was performed at atmospheric pressure inside CBSOG. The frequency of the bubble rotation n=60s^{-1}. It is seen from Fig.78 that the filament is on the angle to the bubbler surface (because the real filament is a quite difficult for resolution, a black line indicates filament position). This observation demonstrates that the angular velocity of the bubbler surface is higher than the angular velocity of the liquid. Hence there are radial gradient in angular velocity inside liquid. It means that there are not enough liquid dwelt time in CBSOG or liquid viscosity is not enough to provide equality of angular velocity of the liquid and the bubbler.
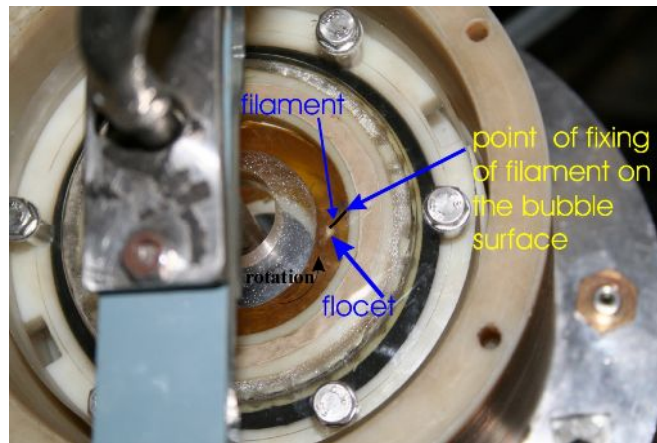
Fig.78. Demonstration of distinction in angular velocity of the bubbler and liquid layer.

Then the air flow of 140mmole/s was injected through the gas nozzles. It is clear from Fig.79 that in this case the filament is perpendicular to the bubbler surface. It means that injection of gas on the angle to the surface induces additional rotation of liquid layer. In this particular case the liquid layer has the same angular velocity as the bubbler. The additional angular velocity n_{ad} of the BHP layer induced by gas injection on the angle 30° to the bubbler surface is possible to estimate from the law of momentum conservation

$$n_{ad} = \frac{2U_g(M_c + M_{He})\mu\cos(30^O)}{2\pi DV_\ell\rho_\ell}$$

For M_c=60 mmole/s, M_{He}=90 mmole/s, μ=29 g/mole, U_g=300 m/s, D=6 cm, V_l=100 cm³/s, ρ_l=1.3 g/cm³ one obtains additional angular rotation $n_{ad}\approx50s^{-1}$. This estimation was obtained when we neglected by viscous friction of BHP layer. Nevertheless it is clear that gas momentum can induce essential additional rotation of BHP layer.
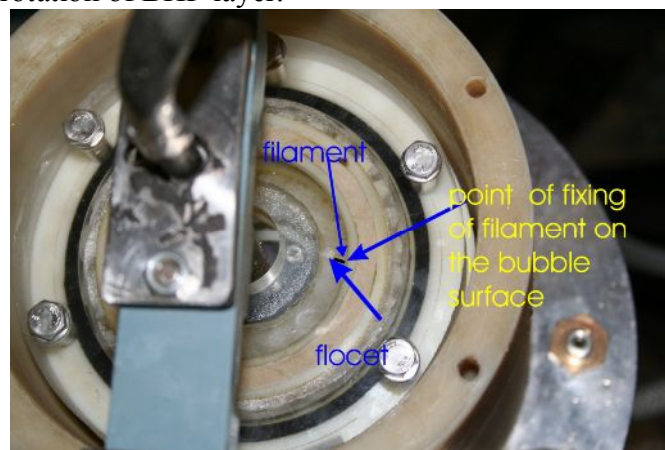
Fig.79. Gas injection at the angle to the bubbler surface induces additional liquid rotation and reduces difference between angular velocity of the bubbler and the liquid layer.

7. Parametric study of CBSOG-2.

A some parametric experiments with CBSOG-2,3 like with CBSOG-1 have been performed.

7.1.   Influence of BHP volumetric rate and BHP layer height.

The measurements were made for the chlorine molar flow rate of 60 mmole/s and He of 90 mmole/s through CBSOG, BHP molarity N_B=4.2 M, N_H=9M, initial BHP temperature t_{li} =-13C°.Conditions of CBSOG operation: P_1=560÷600 torr which depends on n and H; P_4=100 torr, P_2=20 torr, The results of measurements of U and Y are presented in Fig.80,Fig.81.
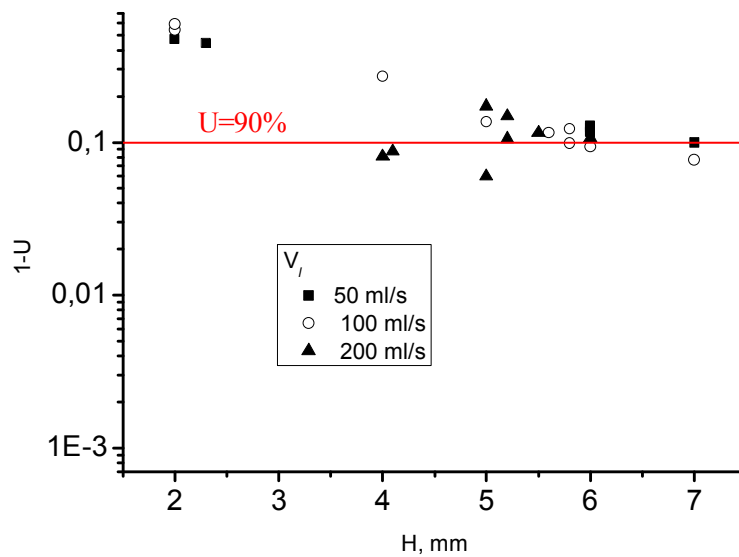
Fig.80. Chlorine utilization as a function of BHP column height H and solution volumetric rate. M_C=60 mmole/s, M_{He}=90mmole/s, P_1=100 torr. Rotation frequency range n =50÷80s[-1].
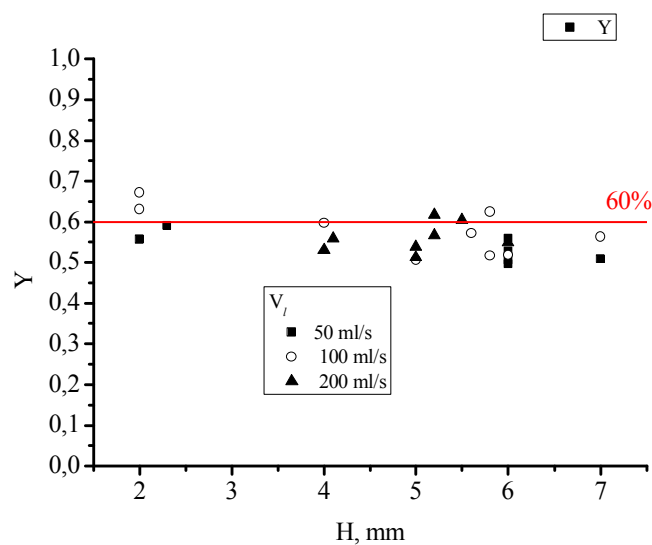
Fig.81. $O_2(^1\Delta)$ yield as a function of H and V_l. M_C=60 mmole/s, M_{He}=90mmole/s, P_1=100 torr. Rotation frequency range n =50÷80s[-1].

It is seen that U substantially increases with the increase of H but Y depends on H weakly in range H=2÷7 mm. Both values Y and U depend on BHP volumetric rate V_l weakly.

The output BHP temperature t_{lf} depends on V_l, M_C, U and t_{li}. The water vapor pressure P_{W4} at the exit of CBSOG, should be equal to the average logarithmic value

$$P_{W4a\,var\,Log} = \frac{P_{wsf} - P_{wsi}}{\ln\left(\dfrac{P_{wsf}}{P_{wsi}}\right)}$$

Where P_{wsi} and P_{wsf} are the water vapor saturated pressures at BHP temperatures t_{li} and t_{lf} accordingly.

The experimental dependence of P_{W4} as a function of t_{lf} is presented in Fig.82. A value t_{lf} was varied by changing of ratio V_l/M_C.
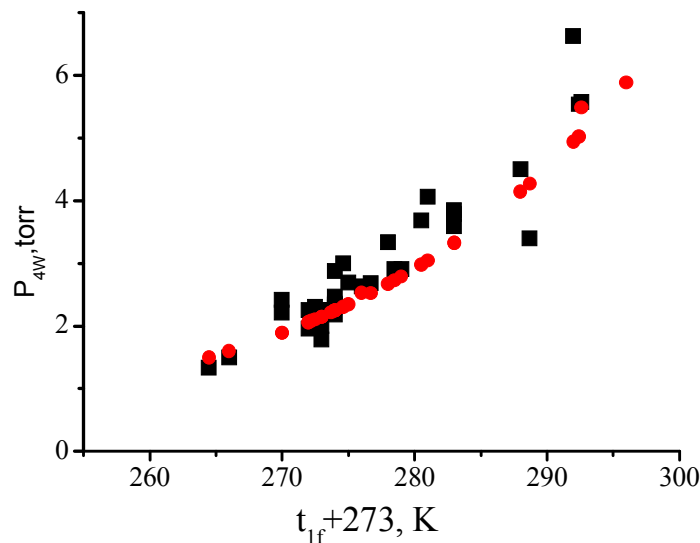
Fig.82. Water vapor pressure at the exit of CBSOG as a functions of BHP output temperature (■). Initial BHP temperature was equal to t_{li}=-13C. The average logarithmic pressure (●).

A water vapor pressure at the exit of CBSOG is slightly more than the average logarithmic value. It seems to us that it is due to higher temperature of the upper layer of the bubbling column than average output BHP temperature t_{lf}. But good news that water vapor pressure P_{4w} is substantially less than saturated water vapor pressure for t_{lf}.

The dependence of water vapor fraction η_W on the parameter UM_C/V_1 is presented in Fig.83. Sometimes water vapor fraction much higher than expected. Possibly it is due to penetration of the BHP bubbling column inside internal perforated cylinder. At ratio UM_C/V_1=1 mole/litre the water vapor fraction is near to 20%.
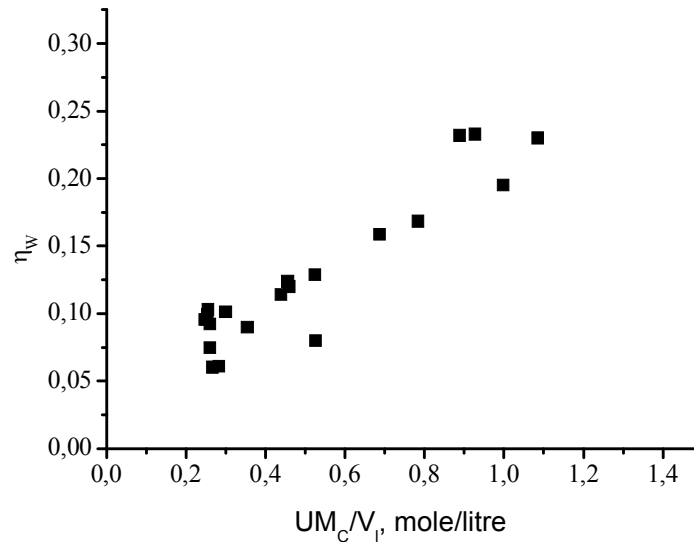
Fig.83. Water vapor fraction η_W as a function of parameter UM_C/V_1. M_C=60 mmole/s, M_{He}=90mmole/s, P_1=100 torr.

7.2.   Influence of the BHP molarity and temperature.

For these experiments the next BHP have been prepared.

Table 12. BHP compositions and initial temperatures.

[KOH], mole/l	[H_2O_2] mole/l	t_{li}, ˚C	BHP (freezing point, ˚C)
6.5	8	-19÷-21	-30
5	6,1	-19÷-20	-22
4.2	5,1	-14	-16
2.9	3,6	-10	-12
2.3	2,8	-5÷-8	-8

BHP volumetric rate V_l was near 120 cm^3/c in these tests. Chlorine molar flow rate was ≈50 mmole/s, He molar flow rate was ≈ 90 mmole/s. The pressure in the working zone of CBSOG was near 100 torr. The height of the BHP column H was equal to 6.5 mm.
The dependence of the chlorine utilization, $O_2(^1\Delta)$ yield and water vapor fraction for those BHP compositions are shown in Fig.84-Fig.86.
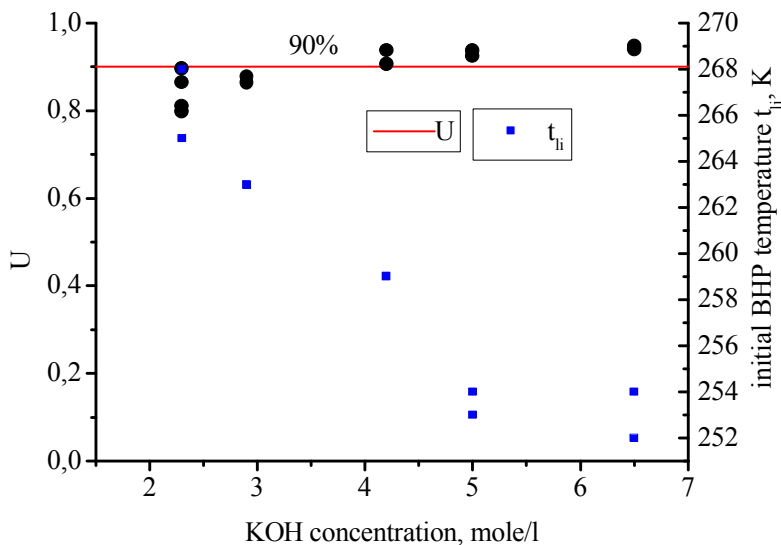
Fig.84. Dependence of the chlorine utilization for different BHP compositions and temperatures. $n=60s^{-1}$, $M_C=60$ mmole/s, $M_{He}=90$mmole/s, $P_1=100$ torr.
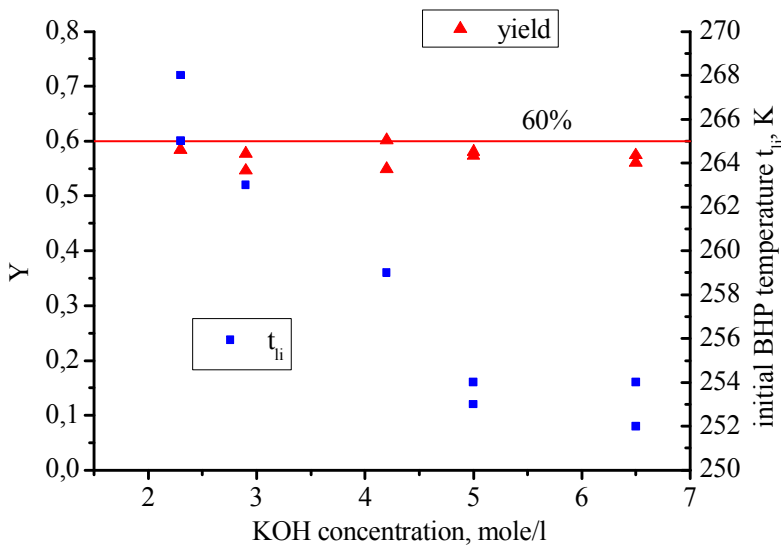
Fig.85. Dependence of the $O_2(^1\Delta)$ yield for different BHP compositions and temperatures. $n=60s^{-1}$. $M_C=60$ mmole/s, $M_{He}=90$mmole/s, $P_1=100$ torr.
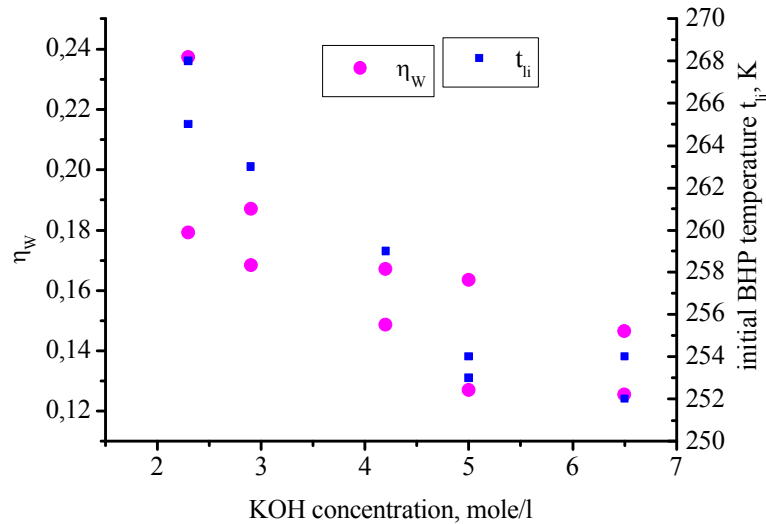
Fig.86. Dependence of the water vapor fraction for different BHP compositions and temperatures. $n=60s^{-1}$. $M_C=60$ mmole/s, $M_{He}=90$mmole/s, $P_1=100$ torr.

An absolute water vapor partial pressure P_W in the measuring chamber as a function of the initial BHP temperature is shown in Fig.87.
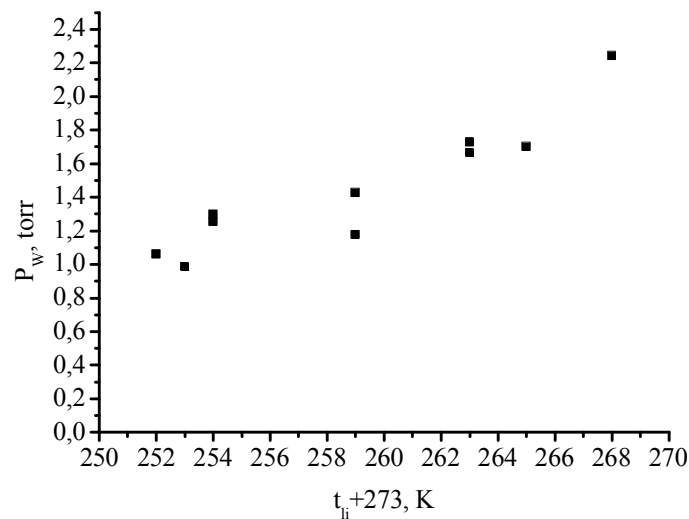
Fig.87. Partial water vapor pressure P_{4W4} as a function of initial BHP temperature t_{li}. $n=60s^{-1}$.

7.3.   Influence of centrifugal acceleration.

The value of n (number of revolution per second) was varied to change the centrifugal acceleration. The BHP volumetric rate and cross section of the BHP drain holes were chosen to support desirable BHP column height H. The results of measurements of utilization and $O_2(^1\Delta)$ yield are presented in Fig. 88, Fig. 89. The dependence of the chlorine utilization on H can be expressed by approximate formula $U = 1 - \exp(-0.41H)$, where H has dimension in mm. A weak dependence of utilization on G can be explained in next manner. The increase of G results in decrease of the bubbler radius and simultaneously the bubble velocity increases. Hence the ratio $3H/(d_b U_b)$ is approximately doesn't

depend on G. Here $3/d_b$ is a gas-liquid contact surface, H/U_b is dwelt time of the bubble in the BHP column.
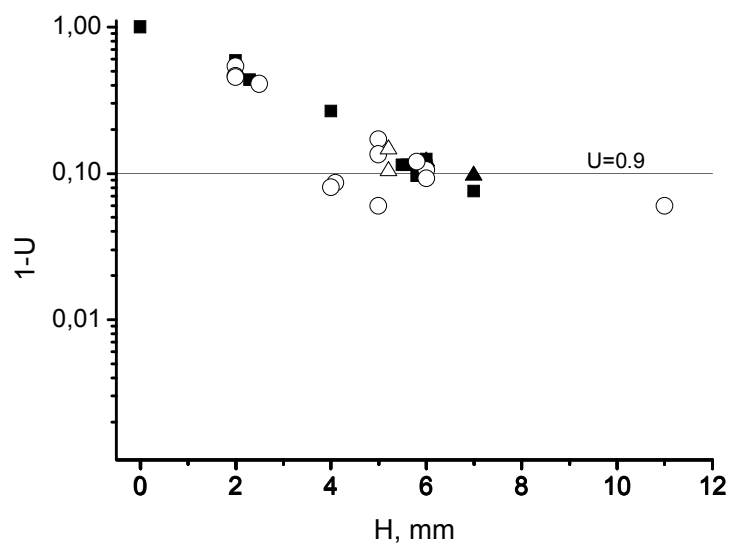
Fig. 88. Efficiency of chlorine utilization as a function of H for different centrifugal accelerations. M_C=60 mmole/s, M_{He}=90mmole/s, P_1=100 torr. n(G) :▲- 45÷49 s^{-1} (244g÷290g), ■- 60÷64 s^{-1} (435g÷495g), ○67÷73s^{-1} (542g÷644g), △-75÷80 s^{-1} (680g÷773g);
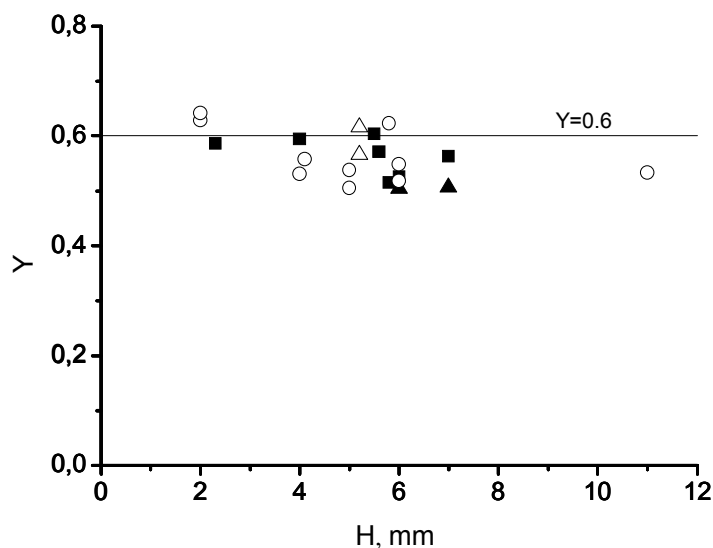
Fig. 89. $O_2(^1\Delta)$ yield as a function of H for different centrifugal accelerations. M_C=60 mmole/s, M_{He}=90mmole/s, P_1=100 torr.n(G) :▲- 45÷49 s^{-1} (244g÷290g), ■- 60÷64 s^{-1} (435g÷495g), ○67÷ 73s^{-1} (542g÷644g), △-75÷80 s^{-1} (680g÷773g);

Weak dependence of the $O_2(^1\Delta)$ yield on G can be explained in the next manner. The increase of G results in growth of pressure P inside the bubble. But simultaneously the dwelt time H/U_b of the bubble in BHP decreases. Hence approximately the "pi-tau" parameter PH/U_b doesn't depend on G.

7.4.   Droplet fraction at the exit of CBSOG-2.

A droplet mass fraction was determined similar as for CBSOG-1. A mass droplet fraction was not exceed 2×10^{-4} of total gas mass passed through CBSOG-2 in all tests.

8.   Parametric study of CBSOG-3.

Measured water vapor fraction 20% is too large at ratio $M_c/V_l = 1$ mole/liter because of the output oxygen pressure at the exit of CBSOG is only 40 torr. It is necessary to increase the output oxygen pressure up to 100 torr to achieve $\eta_W < 10\%$ and simultaneously to save high $O_2(^1\Delta)$ yield and chlorine utilization. To decrease BHP column height H for reducing $O_2(^1\Delta)$ losses at high pressure in the bubbling layer.

2. To decrease the gas transport volume considerably and to reduce $O_2(^1\Delta)$ transport losses.

3. To keep the high chlorine utilization at low column height H<6 mm.

For these goals we plan to use in CBSOG-3 having the bubbler with the narrow slit nozzles of width less than 0.2mm but with higher total working area. The SOG-3 is intended to produce of 50 mmole/s of oxygen flow with high $O_2(^1\Delta)$ yield. The next goal is to produce oxygen at highest pressure. We hope that in this case the water vapor fraction (relative to the oxygen) can be reduced to less than 10% at ratio (chlorine molar flow rate/ BHP volumetric rate) close to 1 mole/liter. It was expected that using slit gas nozzles would reduce bubble size and high chlorine utilization would be achieved at BHP column height H less than 6 mm. So we hope to minimize $O_2(^1\Delta)$ losses in the BHP column at high pressures over BHP layer. Also in several tests we plan to minimize $O_2(^1\Delta)$ transport losses from BHP surface to the diagnostic cell. For this purpose we minimized the transport time of the gas at high pressure. The volume of duct with gas of high pressure is only volume of the cavity inside CBSOG-3 between BHP surface and orifice (10)) in **Fig. 74**.

a) ***Results of tests of CBSOG with slit bubbler (a).*** This bubbler has 18 slits 0.22mm in width and 8mm in length. Tests have been performed for the next conditions: M_c=35 mmole/s, helium molar flow rate of 43 mmole/s, initial BHP temperature of -10C, frequency of the bubbler rotation of $40 \div 60s^{-1}$, alkaline molarity N_B=4 mole/liter and BHP volumetric rate of 50 ml/s. The working pressure inside CBSOG was 55 torr and transport volume was of 120 cm^3.

The results of measurements of chlorine utilization and $O_2(^1\Delta)$ yield are presented in **Fig. 90**.
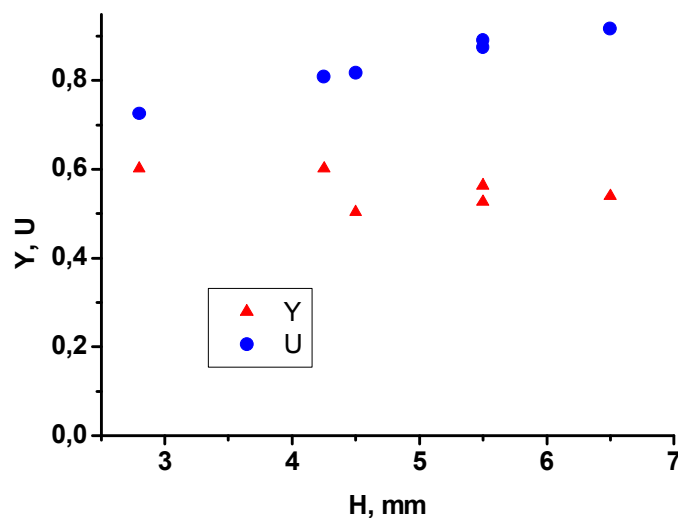
Fig. 90. Chlorine utilization and $O_2(^1\Delta)$ yield for CBSOG-3 with bubbler type of "a".

It is seen that **we have failed** to achieve high chlorine utilization at small BHP column height H≈3÷4 mm even for chlorine molar flow rate of 35 mmole/s.

b) ***Results of tests of CBSOG with slit bubbler (b).*** The slit bubbler "b" has in 4 time larger cross section area of slits than bubbler "a". But chlorine molar flow rate was increased up to 60 mmole/s. Helium molar flow rate of 90 mmole/s, initial BHP temperature of -10C, frequency of the bubbler rotation of 40÷60s^{-1}, alkaline molarity of N_B=4mole/liter, BHP volumetric rate of (70÷80)ml/s. The working pressure inside CBSOG was changed from 40 to 240 torr by varying the area of the output slit (10, **Fig. 74**) at the exit of CBSOG . Nevertheless it seen from **Fig. 91** than U depends mainly on H. For CBSOG with bubbler "b" we didn't achieve high chlorine utilization also when H≈3÷4 mm (**Fig. 91**).
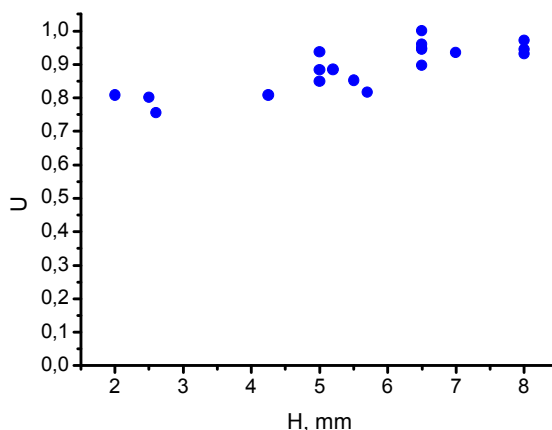
Fig. 91.Chlorine utilization in CBSOG with bubbler "b".

The $O_2(^1\Delta)$ yield was near 60% for total pressure of 100 torr inside CBSOG as for CBSOG-2 with bubbler having 165 cylindrical nozzles of 0.5 mm in diameter. The dependencies of U, Y on BHP volumetric rate for CBSOG having barrier(**Fig. 74**) height of 8 mm are presented in **Fig. 92**. The bubbler rotation frequency was varied from 40 to 65 s^{-1}.
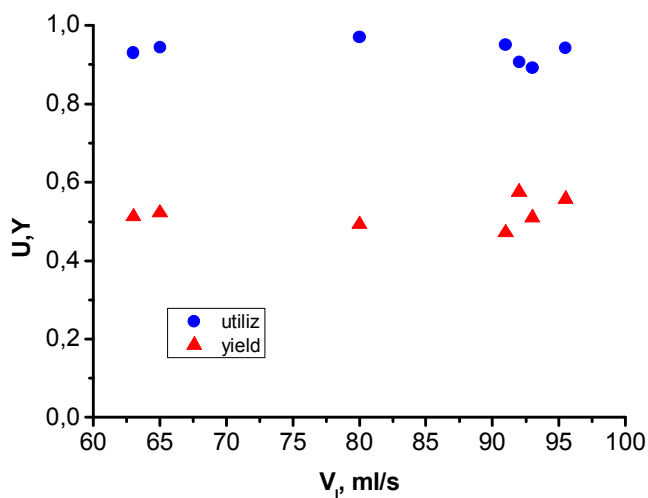
Fig. 92. Chlorine utilization and $O_2(^1\Delta)$ yield as a function of BHP volumetric rate for bubbler with the height of the barier-6 of 8 mm.

It is seen that U and Y don't depend on V_1 and n because the height H of the BHP column was fixed by barier-6 and was equaled to 8 mm.

c) ***Results of CBSOG tests with slit bubbler (c).***

It was assumed that the increase of the number of the narrow slits would result in generation of smaller bubbles due to the smaller gas velocity in nozzles for the same chlorine and helium molar flow rate. The BHP layer height H can be made less to achieve good chlorine utilization and higher $O_2(^1\Delta)$ yield at high pressure. The results of measurements of utilization and $O_2(^1\Delta)$ yield at "standard" conditions ($M_c \approx 60$ mmole/s, helium molar flow rate of 90 mmole/s, pressure inside CBSOG of $P_4 \approx 100$ torr) are presented in **Fig. 93**.
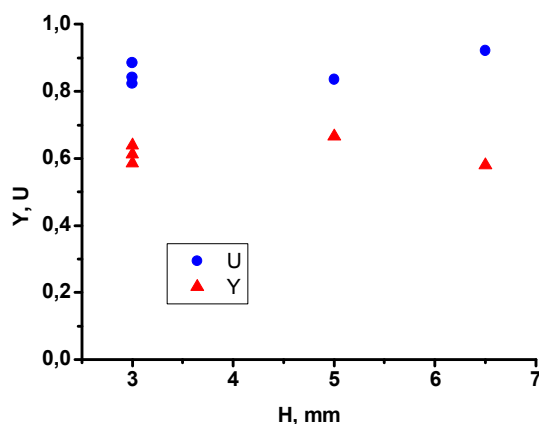
Fig. 93. Chlorine utilization and $O_2(^1\Delta)$ yield as a function of BHP column height H. BHP volumetric rate was near of 80 ml/s. N_B= 4M.

A three points for H=3 mm were obtained at different rotation frequency of the bubbler: 68s^{-1} and 80s^{-1} (**Fig. 93**). A frequency of 80s^{-1} corresponds to linear velocity 15m/s of the bubbler surface. It is seen that at BHP column height near 3 mm the chlorine utilization ~85÷90% can be achieved. Simultaneously $O_2(^1\Delta)$ yield was near 60%. Then the working pressure P_4 inside CBSOG-3 was increased up to 180 torr. The $O_2(^1\Delta)$ yield reduced to 48% at H=4 mm, but chlorine utilization was still less than 90% (**Fig. 94**).
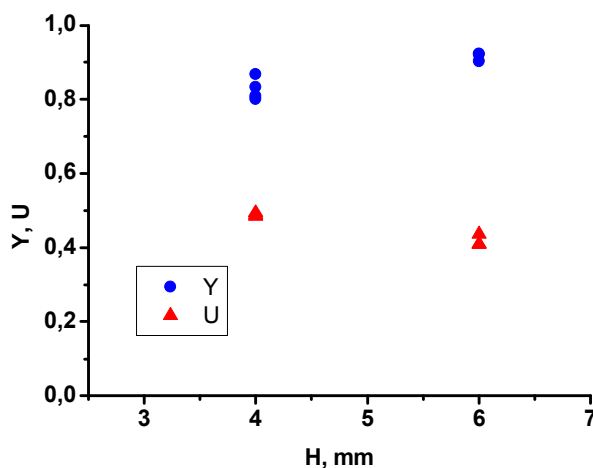
Fig. 94. Chlorine utilization and $O_2(^1\Delta)$ yield as a function of BHP column height H. BHP volumetric rate was near 100 ml/s. N_B= 4M.. CBSOG working pressure P_4=180 torr, Partial oxygen pressure P_{4O}=72torr ($M_{Cl}:M_{He}$ = 1:1.5).

d) ***Results of tests of CBSOG with slit bubbler (d).***

Then the number of the narrow slit nozzles was increased to 140 (bubbler d) with aim to raise utilization higher than 90% and keep $O_2(^1\Delta)$ yield. The height of the barrier (6) was 4 mm and bubbler rotation frequency was $60s^{-1}$ in all tests. So the height of the BHP column was near 4 mm. The results of measurements of utilization and $O_2(^1\Delta)$ yield at "standard" conditions ($M_c \approx 60$ mmole/s, Helium molar flow rate 90 mmole/s, pressure inside CBSOG $P_4 \approx 100$ torr) are presented in **Fig. 95**.
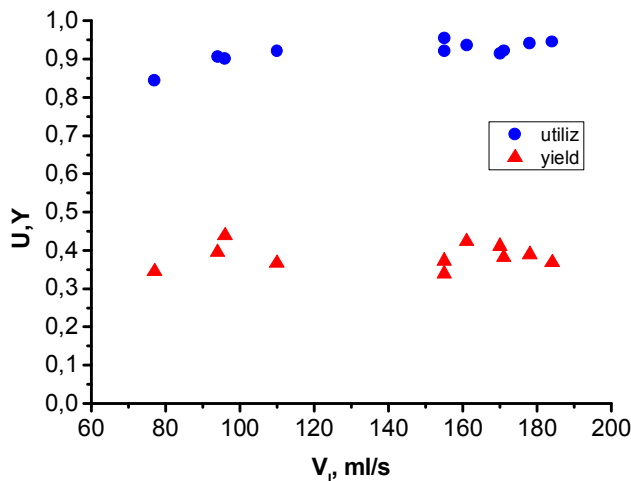
Fig. 95. $O_2(^1\Delta)$ yield and chlorine utilization as a function of BHP volumetric rate.

It is seen that the $O_2(^1\Delta)$ yield is independent on BHP volumetric rate. Chlorine utilization slightly increases with increase of BHP volumetric rate.

As it was expected the chlorine utilization and $O_2(^1\Delta)$ yield weakly depend on BHP temperature (**Fig. 96**). Experiments have been performed with bubbler (d) at next conditions: M_c=50mmole/s, M_{He}=90mmole/s, H=6.5 mm, KOH molarity N_B=6.5M, n=60s^{-1}, BHP volumetric rate of 120 ml/s. It was found that at low initial temperature (~253K) and high alkaline concentration (N_B=6.5M) particles of salt KCl were generated and deposited on the surface of the bubbler. Then this deposit clogged the narrow slit nozzles. At higher temperatures (~263K) particles of salt KCl were not observed on the surface of the bubbler.
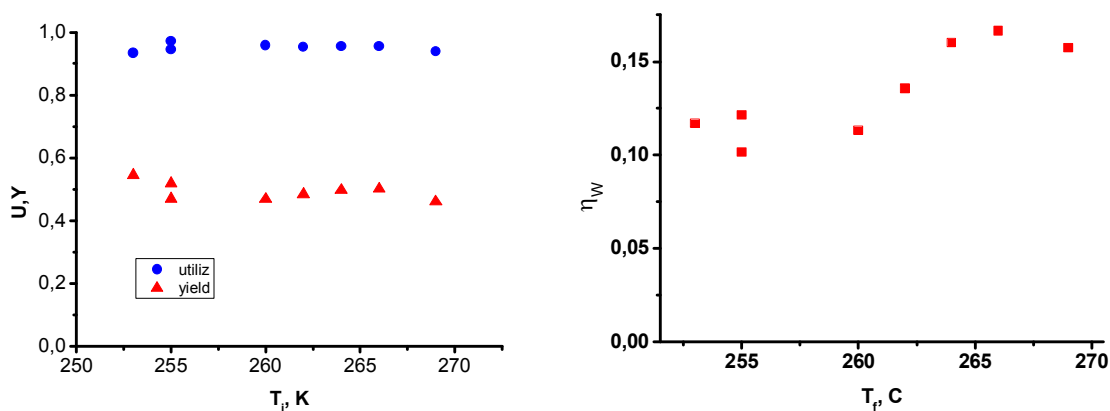
Fig. 96. $O_2(^1\Delta)$ yield, chlorine utilization and water vapor fraction as a function of initial BHP temperature. Working pressure P_4 inside CBSOG was 120 torr.

The influence of BHP molarity on $O_2(^1\Delta)$ yield and chlorine utilization is shown in next Table :

KOH molarity	Cl$_2$ utilization	$O_2(^1\Delta)$ yield
6	0,96	0,50
6	0,96	0,54
4	0,80	0,51
4	0,85	0,49
4	0,82	0,49
4	0,84	0,53

These tests were performed at the next conditions: M_c=50 mmole/s, M_{He}=90 mmole/s, SOG working pressure P_4=150 torr, t_i=-14C.Water vapor fraction as a function of output BHP temperature is presented in Fig. 97. These tests were performed with CBSOG-c at next conditions: M_c=50mmole/s, M_{He}=90mmole/s, SOG working pressure P_4=120 torr, initial BHP temperature t_i was equal to -13C.
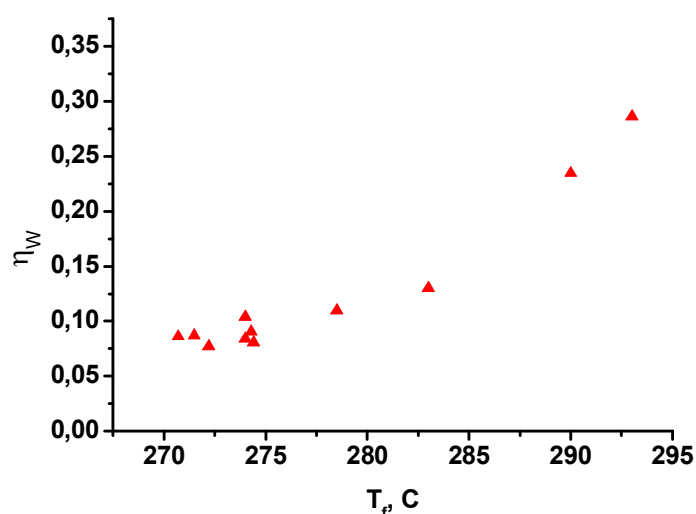
Fig. 97. Water vapor fraction as a function of output BHP temperature.

In SOG-1 and SOG-2 cylindrical nozzles for gas injection in rotary bubbler were used. Tests showed weak dependence of chlorine utilization and $O_2(^1\Delta)$ yield with variation of rotation frequency or centrifugal acceleration. It was expected that in the case of slit nozzles (having substantially bigger cross section) the increase of centrifugal acceleration would result in generation of small bubbles and higher chlorine utilization at the same BHP column height. Therefore it was assumed to reduce BHP column height, reduce gas-liquid contact time and to obtain good chlorine utilization, $O_2(^1\Delta)$ yield at higher pressure over BHP column.

The tests of CBSOG-3 have been performed with rotary bubbler of type "c". This rotary bubbler has 92 slits 8 mm of length and 0.2mm of width. Conditions of tests:

Chlorine molar flow rate ~55 mmole/s
Helium molar flow rate 90 mmole/s
BHP volumetric rate 90÷100 cm^3/s
BHP temperature -13C
BHP molarity N_B=4.3 M, N_H=9M
Pressure over BHP column P_4=100 torr

The results of these tests are presented in **Ошибка! Неверная ссылка закладки.**.
Table 13

n(s^{-1}) rotation frequency, G centrifugal acceletation	h(mm), the BHP column height	U, chlorine utilization	Y, O$_2$($^1\Delta$) yield
68 (558g)	3	0,88	0,61
68(558g)	3	0,82	0,58
80(773g)	3	0,87	0,68
80(773g)	3	0,84	0,64
80(773g)	3	0,85	0,66

It is seen that chlorine utilization doesn't depend on centrifugal acceleration G. In the limit of O$_2$($^1\Delta$) yield detection accuracy (±0.10) its value also doesn't depend on G.

9.   COIL powered by CBSOG.

COIL powered by CBSOG-1. The demonstration of the efficient COIL operation is the universal and overall method of testing of the efficency of chemical SOG. The universal test of the first version of CBSOG-1 have been performed with aid of the ejector COIL described in [**39**] and bubbler of type 1a. The scheme of ejector COIL powered by CBSOG is presented in **Fig. 98**.
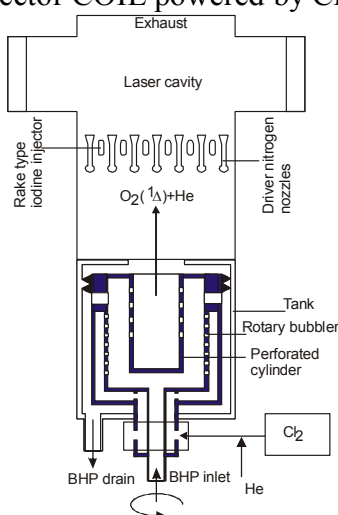
Fig. 98. The principle scheme of ejector COIL powered by CBSOG.

CBSOG-1a has 561 chlorine nozzles 0.3 mm in diameter (Table 8). The tests have been performed for the conditions listed below in the Table 14.

Table 14. Operational parameters of COIL and CBSOG-1a.

BHP molarity	N$_H$=7.5M; N$_B$=6.8M, t$_i$=-20C
angular velocity of rotary bubbler	27 revolutions per second
BHP volumetric rate	varied in range 160÷190cm^3/s
chlorine flow rate	37 mmole/s
primary helium flow rate	95 mmole/s
secondary nitrogen flow rate	20 mmole/s
molecular iodine flow rate	0.9 mmole/s
driver nitrogen flow rate	100 mmole/s
molecular iodine molar flow rate	0.8 mmole/s
pressure upstream of bubbler, P$_1$	410 torr
pressure over BHP layer, P$_4$	36 torr
Partial oxygen pressure over BHP layer. P$_{O4}$	~10 torr
plenum pressure	24 torr
stagnation pressure of the driver nitrogen	310 torr
Total mirror transmission	1.7%

Before stating COIL tests the chlorine utilization as a function of H was measured again (**Fig. 99**). In these tests and COIL tests the BHP column height was varied by changing of the BHP volumetric rate. Fo example at V_I=180 cm³/s the BHP column height was equaled to 8 mm.
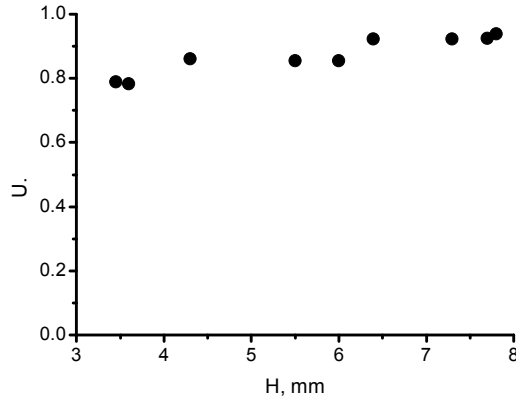
Fig. 99. Utilization versus H. CBSOG-1a. (n=27 s⁻¹, M_C=37 mmole/s, M_{He}=95 mmole/s, N_H=7.5 M, N_B=6M, T_I= 253K). The dependence of COIL chemical efficiency as a function of BHP column height is presented in **Fig. 100**.
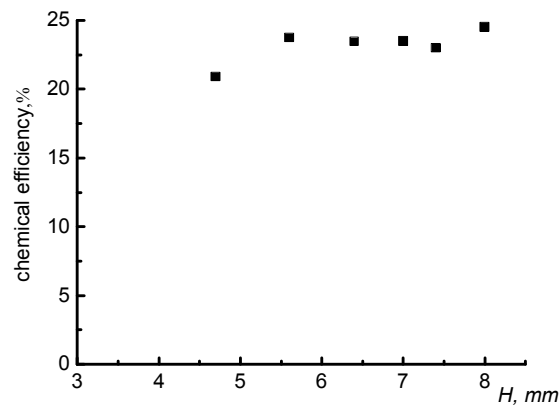
Fig. 100. COIL chemical efficiency versus BHP column height H.

It is seen that COIL chemical efficiency increases as BHP column height increases from 4.5mm to 8 mm. These first tests of COIL powered by CBSOG demonstrate that CBSOG is an efficient source of energy. The increase of power with increase of H additionally proof that $O_2(^1\Delta)$ yield almost constant for CBSOG-1 up to H=8 mm and droplet fraction is a very small at the exit of CBSOG.

The COIL tests also have been performed with CBSOG-1e having higher density of chlorine nozzles than CBSOG-1a. The tests have been performed at the conditions listed in **Ошибка! Неверная ссылка закладки.**. A total output power of 1264 W has been obtained that corresponds to 24,6 % of the total chemical efficiency. In this test the specific chlorine loading was j_c=1.13 mmole/cm^2/s and specific power was 25.3W/cm^2 of the bubbler surface area

Table 15. Operational parameters of COIL and CBSOG-1e.

angular velocity of rotary bubbler	46 s^{-1}
BHP volumetric rate	208 cm^3/s
BHP molarity	N_B=6.5 M, N_H=7,5M, t_i=-20C
chlorine flow rate	56.5 mmole/s
helium flow rate	90 mmole/s
driver nitrogen flow rate	250 mmole/s
secondary nitrogen flow rate	60 mmole/s
molecular iodine flow rate	1 mmole/s c
BHP column height, H	~6 mm
pressure upstream of bubbler, P_1	538 torr
Plenum pressure	26 мм.рт.ст.
laser cavity wall pressure	8.9 мм рт.ст.
Total mirror transmission	3%

Also COIL was tested with CBSOG-1i having only 10.6 cm^2 of bubbler working area. The output power of 1000W has been achieved for M_c=50 mmole/s. The specific power of 94W per 1 cm^2 of the bubbler surface has been attained.

COIL powered by CBSOG-2. The laser experiments have been performed with ejector nozzle bank as was described earlier. The throat orifice was installed at the exit of CBSOG-2 to decrease high pressure in transport volume as shown in Fig. 101. A special siphon system for BHP drain was design to support constant H=6mm at different values of V_1 as shown in Fig. 101. Chlorine utilization was U=90% and $O_2(^1\Delta)$ yield was in the range 50÷ 60% at this column height. The ejector nozzle bank cross section area and value gas flow rates control the pressure downstream orifice 6. The output power was measured by two Ophir laser power meters from both mirrors.
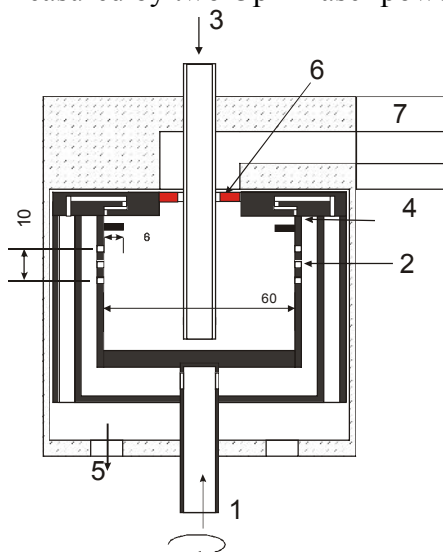
Fig. 101. 1- gas inlet, 2- bubbler, 3-BHP inlet, 4 -siphon system, 5-BHP drain holes, 6- throat orifice, 7- gas transport duct. All dimensions are given in mm.

. The operational parameters of COIL and CBSOG-2 are shown in
Table 16.
Table 16. Operational parameters of COIL powered by CBSOG-2 .

Chlorine molar flow rate	50 mmole/s
BHP volumetric rate	V_l=80 cm^3/s.
Primary helium molar flow rate	85 mmole/s
Secondary helium molar flow rate	60 mmole/s
Driver N_2 molar flow rate	260mmole/s
Iodine molar flow rate	0.8 mmole/s
Gain length	5 cm
Distance between exit plane of NB and optical axis	4.5 cm
Total Mirror transmission T_1+T_2	3%
"Light" BHP column height, H	6 mm
Plenum pressure	25 torr
Revolutions per second of the bubbler, n	60 s^{-1}
BHP composition N_B, N_H and temperature	4 M, 9M, t_i=-13C
Initial BHP temperature	-13C
Total pressure in CBSOG (over BHP layer), P_4	100 torr
Partial oxygen pressure in CBSOG (over BHP layer), P_{4O}	35 torr

A typical oscillogram of the output power is shown in Fig. 102. A maximum power corresponds to
chemical efficiency 22%.
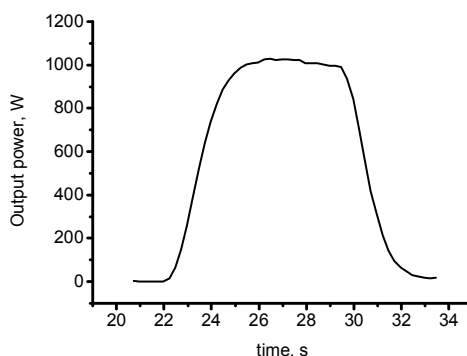
Fig. 102. An oscillogram of the output power of COIL powered by CBSOG-2.

COIL powered by CBSOG-3. The universal test of CBSOG-3 by demonstration of COIL
operation was performed only with bubbler-c (picture of the bubbler-c is presented in **Fig.76**).
Operational parameters of COIL and CBSOG-3c are listed in **Table 17.**
Table 17. Operational parameters of COIL and CBSOG-3c

Chlorine molar flow rate	45.9 mmole/s
BHP volumetric rate	V_l=270 cm^3/s.
Primary helium molar flow rate	80 mmole/s
Secondary helium molar flow rate	60 mmole/s
Driver nitrogen molar flow rate	260 mmole/s
Iodine molar flow rate	0.8 mmole/s
Gain length	5 cm
Distance between exit plane of NB and optical axis	4.5 cm
Mirror transmission T_1+T_2	3%
"Light" BHP column height, H	6 mm
Plenum pressure	25 torr
Revolutions per second of the bubbler, n	60 s^{-1}
BHP composition N_B, N_H, initial BHP temperature	4 M, 9M, t_i=-13C
Initial BHP temperature	-13C
Total pressure in CBSOG (over BHP layer), P_4	84 torr

Partial oxygen pressure in CBSOG (over BHP layer), P_{4O}	31 torr
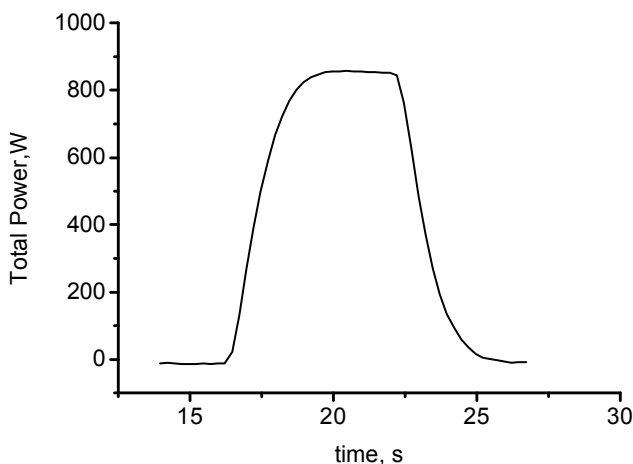
Fig. 103. An oscillogram of the output power of COIL powered by CBSOG-3c.

A typical oscillogram of the output power is shown in **Fig. 103**. A maximum power corresponds to chemical efficiency 21.5%. It seen that at the same operational conditions COIL powered by CBSOG-3c demonstrated almost the same efficiency as with CBSOG-2. But BHP volumetric rate in this test was higher than in test with CBSOG-2.

Optimization of BHP volumetric rate. So it was quite important to check how COIL efficiency depends on the ratio M_c/V_1. We have performed these tests when COIL was powered by CBSOG-2. The operational parameters are listed in
Table 16. Only BHP volumetric rate V_1 has been changed. A chemical efficiency as a function of BHP volumetric rate is shown in Fig. 104. A specific energy ε is defined as the ratio of the output power to the BHP volumetric rate.
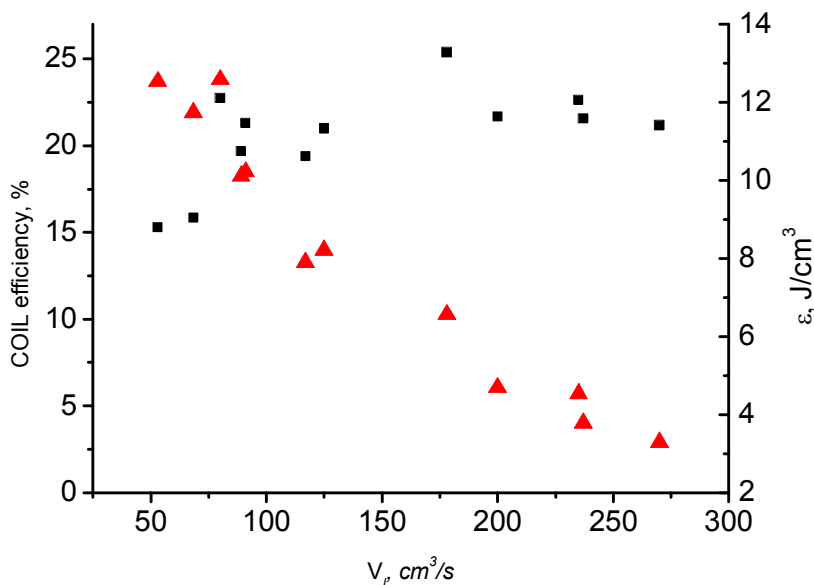
Fig. 104. COIL chemical efficiency (■) and specific energy (▲) as functions of BHP volumetric rate.

Specific energy ε of 12 J/cm^3 at chemical efficiency near 22% and ratio M_c/V_1=0.68 mole/liter has been attained. At ratio M_c/V_1=0.68 mole/liter a water vapor fraction relative to the oxygen was near

15% and output BHP temperature was equaled to 293K (+20C). The efficiency of depletion of HO_2^- ions reached ~40% in the single pass of BHP through CBSOG.

10. Conclusion and discussion.

The chlorine utilization, $O_2(^1\Delta)$ yield and water vapor fraction at the exit of CBSOG have been measured in a wide range of the working parameters. The next facts have been obtained from the investigation of CBSOG-1, CBSOG-2, CBSOG-3 in the range of tested working parameters.

<u>Chlorine utilization.</u>

1. Chlorine utilization depends weakly on the centrifugal acceleration in the range of G=133÷770g.
2. Chlorine utilization depends weakly on the configurations of the gas nozzle at bubbler surface. Chlorine utilization is almost the same for cylindrical nozzles of diameter in the range of 0.3÷0.95 mm and tested slit nozzles.
3. Chlorine utilization depends weakly on the number of chlorine cylindrical nozzles or slit nozzles per 1 cm^2 of the bubbler area.
4. Chlorine utilization decreases weakly with the increase of chlorine molar flow rate through the nozzle and chlorine loading per 1 cm^2 of the bubbler area up to 5 mmole/cm^2/s but not so dramatically.
5. Chlorine utilization increases with the increase of alkaline concentration in BHP in the range N_B=2 M to N_B=6.5M.
6. Chlorine utilization decreases weakly with the increase of chlorine dilution by helium but not so dramatically.
7. Injection of the gas on the angle 30° to the bubbler surface didn't change chlorine utilization in comparison with normal injection at the same BHP column height H.
8. The primary factor, influencing on the chlorine utilization, is the height of the BHP column. In the range of the tested parameters the chlorine utilization as a function of the BHP column height can be expressed by formula: $U \approx 1 - \exp(-0.41H)$, where H has dimension in mm. This formula is valid for alkaline concentration N_B=4÷6.5 M and for nozzle configuration tested in CBSOG-1,2,3. To achieve 90% of chlorine utilization the BHP column height must be more than 6 mm. For alkaline concentration N_B=2M the BHP column height has to be more 8 mm to achieve U>90%.
9. A substantial part of chlorine (~80%) is absorbed at the BHP column height H=3÷4mm.

These experimental facts force us to make the next conclusions. The chlorine utilization is equal **to U =1-exp(-βs×t$_c$).** β is the mass transfer rate in first order reaction approximation, **s** is the specific gas-liquid contact surface, **t$_c$** is the gas-liquid contact time. The rate of the renewal of the liquid-gas contact surface is a very fast and depletion of HO_2^- at the BHP surface is negligible. In the range of investigated configurations of chlorine nozzles, geometry of nozzles (cylindrical or slit), centrifugal acceleration, specific chlorine loading per the product **s×t$_c$** should be approximately constant for the given height H of the BHP column. The independence of **s** on the configuration and geometry of nozzles is in contradiction with our preliminary estimations. But preliminary estimations of **r$_b$** and **s** were made for single nozzle, relatively small gas flow rate through this nozzle and big distance between nozzles. But our SOGs operated at high density of cylindrical nozzles per 1cm^2 or relatively high cross section area of the slit nozzles per 1 cm^2 and high specific gas loading. It seems that in these cases the size of generated "bubbles" doesn't depend on nozzle configuration. In this case the gas "cushion" is formed near bubbler surface. This cushion is quite unstable and destroys into the bubbles. The size of the bubbles rather depends on the physical properties of the BHP and centrifugal acceleration. The bubbles size reduction continues until they become stable against momentum head of the liquid. It occurs when tension pressure $2\sigma_\ell/r_b$ equals to the pressure $c_b\rho_\ell U_b^2/2/\pi r_b^2$ of the liquid momentum head. On the other hand liquid momentum

head $c_b \rho_\ell U_b^2/2$ should be equals to the buoyancy force $\dfrac{4\pi r_b^3}{3} G\rho_\ell$. So the stable size of the bubble is proportional to the capillary size:

$$r_b \sim L_c = \sqrt{\sigma_\ell /(\rho_\ell G)} ,$$

where σ_ℓ is surface tension, G is the centrifugal acceleration, ρ_ℓ is liquid density. So $s \sim \sqrt{(\rho_\ell G)/\sigma_\ell}$. At high G a turbulent motion of the bubble is expected and a drag coefficient for the bubble motion c_b is independent on its velocity. Hence bubble velocity $U_b \sim \sqrt{r_b G}$, gas-liquid contact time $t_c = H^*/U_b \sim H^*/\sqrt{r_b G} \sim H^*/G^{0.25}$, where H* is the real height of the BHP bubbling column. The product $s \times t_c$ is proportional to $H^*/U_b \sqrt{(\rho_\ell G)/\sigma_\ell} \sim H^* \times G^{0.25}$ and

$$\ln(1-U) \sim (-H^* \times G^{0.25})$$

The value of real BHP column height H* differs from BHP column height H near drain orifices. H*=H/(1-ϕ), where ϕ is the gas content in the bubbling layer. H* decrease and ϕ increases with the increase of G because the gas pressure inside bubbling layer increases with G. Hence a weak dependence of the chlorine utilization as a function of G is expected. In our tests G was varied from 133g to 770g. Hence the product $s \times t_c$ was varied in 1.55 times. For example, if chlorine utilization $U_1=0.87$ at $G_1=133g$ then U_2 is lower than $1-(1-U_1)^{(G_2/G_1)^{0.25}} = 95\%$ is expected at G=770g. If $U_1=95\%$ at $G_1=133g$ then U_2 lower than 99% is expected at $G_2=770g$.

It seems us that the real physics of bubble generation, motion and mass transfer at high G is much more complex but these simplest speculations showed that changing of G weakly influences on chlorine utilization.

$O_2(^1\Delta)$ yield.

1. $O_2(^1\Delta)$ yield depends weakly on the centrifugal acceleration in the range of G=133÷770g.

2. $O_2(^1\Delta)$ yield depends weakly on the tested configurations of gas nozzles at bubbler surface.

3. $O_2(^1\Delta)$ yield depends weakly on the geometry size of gas nozzles at bubbler surface

4. $O_2(^1\Delta)$ yield monotonically decreases with the increase of the chlorine molar flow rate through the nozzle. The increase of M_c didn't result in increase of O_2+Cl_2 pressure in the gas fragments in the bubbling layer because this pressure is due to hydrostatic pressure of the BHP column. So in the first approximation the increase of M_c didn't result in rise of $O_2(^1\Delta)$ losses in the bubbling layer. In the next approximation the increase of M_c raises the gas pressure over BHP column and in the bubbling layer. Hence the reduction of $O_2(^1\Delta)$ yield is due to the rise of $O_2(^1\Delta)$ transport losses in bubbling layer and in the free volume inside rotating bubbler.

5. $O_2(^1\Delta)$ yield monotonically increases with the increase of helium dilution. This fact is explained by lower partial chlorine and $O_2(^1\Delta)$ pressure in the bubbles, lower partial $O_2(^1\Delta)$ pressure and lower dwelt time in the transport duct.

6. $O_2(^1\Delta)$ yield doesn't depends on alkaline concentration in BHP from $N_B=2$ M to $N_B=6.5M$. This fact also support conclusion about negligible depletion of the chemical near BHP surface.

7. $O_2(^1\Delta)$ yield monotonically decreases with the increase of H. But the increase of H in CBSOG-2,3 resulted in substantial reduction of the gas transport volume in CBSOG. For example, at H=6 mm the gas transport volume in CBSOG-2,3 reduces by 46 cm^3 from initial volume of 170 cm^3 without BHP column. Hence drop of $O_2(^1\Delta)$ yield with the increase of H is due to enhancement of $O_2(^1\Delta)$ losses in the bubbling layer.

8. $O_2(^1\Delta)$ yield as high as 60% can be ensured at the column height H=6÷8 mm in the range of tested parameters.

Why $O_2(^1\Delta)$ weakly depends on centrifugal acceleration? The $O_2(^1\Delta)$ quenches mainly in pooling reaction and $O_2(^1\Delta)$ yield at the exit of bubbling column is defined by $P_c t_c$ parameter approximately

as $Y = \dfrac{Y_0}{1 + Y_0 K P_c t_c}$, P_c is average chlorine+oxygen partial pressure in a floating up bubble, K is the constant. As a bubble size doesn't depend on nozzle configuration then the bubbles size is proportional to $r_b \sim L_c = \sqrt{\sigma_\ell /(\rho_\ell G)}$, the velocity proportional to $\sqrt{r_b G} \sim G^{0.25}$, gas-liquid contact time proportional to $\mathbf{G^{-0.25}}$. The pressure inside bubble is equal to the sum of gas pressure over BHP column and liquid column pressure: $P = P_g + \rho_\ell GH$. An average partial pressure of $Cl_2 + O_2$ in a floating up bubble is $M_c(P_g + 0.5\rho_\ell GH)/(M_c + M_{He})$. The tests of CBSOGs-2,3 were performed when P_g=100 torr, M≈55 mmole/s, M_{He}=90 mmole/s and G varied from 244g to 776g. So the average partial oxygen-chlorine pressure inside bubble increases from 73 torr to 150 torr, or in 2 times but the gas-liquid contact time t_c decreases in 1.36 times for H=8 mm. Hence the maximum increase of $P_c t_c$ parameter is in 1.5 times. But if for Y_0=0.8 and G=224g $O_2(^1\Delta)$ yield is equal to 70% then for G=776g the expected $O_2(^1\Delta)$ yield ~65%. The difference 5% is in the accuracy limit of $O_2(^1\Delta)$ yield measurements. It is seen also that the increase of M_{He} resulted in increase of $O_2(^1\Delta)$ yield for the same H and G.

The main conclusion. Chlorine utilization ~90% and $O_2(^1\Delta)$ yield Y>60% are achieved at H≈6÷8mm and independent on nozzle configuration and centrifugal acceleration.

Water vapor fraction.
1. A water vapor partial pressure at the exit of CBSOG depends only on initial temperature of BHP and ratio $M_c U/V_l$.
2. An absolute water vapor pressure is substantially less than saturated water vapor pressure at the output BHP temperature and slightly higher than average logarithmic water vapor pressure

$(P_{wsf} - P_{wsi})/\ln\left(\dfrac{P_{wsf}}{P_{wsi}}\right)$ where P_{wsi} and P_{wsf} are the water vapor saturated pressures for BHP

temperatures t_{li} and t_{lf} accordingly.

 Hydrodynamic stability and droplet fraction.
1. In all tests CBSOG worked stable and without catastrophic carry-over of BHP.
2. Droplets at the exit of CBSOG were not observed visually in the interval of t_{run}<5 s from the start of operation.
3. A mass fraction of droplets was not exceed 2×10^{-4} relative to the mass of the gas passed through CBSOG.

COIL powered by CBSOG.

COIL powered by CBSOG demonstrated moderate chemical efficiency of ~25% at high ratio M_c/N_l=0.68 mole/litre and power level of ~1000W. The efficiency of depletion of HO_2^- ions reached ~40% in the single pass of BHP through CBSOG. The extracted energy of 12.5 J from 1 cm^3 of BHP volume has been attained in the single pass of BHP through CBSOG. A specific productivity of ~ 0.4(mole/s) per 1 litre of CBSOG volume has been attained that substantially higher than for jet-SOG, UDSOG, μSOG. Also specific power of ~10^4W per 1 Litre of the CBSOG volume has been demonstrated. All these characteristics have been obtained for 5 cm gain length COIL and mirror transmission of ~3%.

11. Specification

Capital letters

$A = m_H/m_c$	the ratio of the dilution of chlorine by helium
C_l	specific heat capacity of the BHP
D	diameter of the rotary bubbler
D_c	Chlorine diffusion coefficient in BHP
D_o	Oxygen diffusion coefficient in BHP
D_H	HO_2^- diffusion coefficient in BHP
$F = 1 - \pi d_n^2 N_n / 4$	relative bubbler free area
$F_n = 1 - F$	Relative bubbler area occupied by gas nozzles
$G = (2\pi m)^2 D / 2$	centrifugal acceleration
H_c	chlorine Henry constant
H	the height of the BHP column at low gas content or "light" height
$I_{1.27}$	output from Ge-detector measuring $O_2(^1\Delta)$ spontaneous emission
$I_{0.762}$	output from Si-detector measuring $O_2(^1\Sigma)$ spontaneous emission
K -	Rate constant of reaction $Cl_2 + HO_2^- \rightarrow O_2(^1\Delta) + 2Cl^- + H^+$
L	the length of the bubbler along the BHP stream
M_c	the total chlorine molar flow rate through SOG
M_{He}	the total helium molar flow rate through SOG
N_B	KOH molarity in BHP , mole/liter
N_H	Initial H_2O_2 molarity, mole/liter
N_n	density of nozzles on the bubbler surface ($1/cm^2$)
N_w	water vapor concentration in measuring chamber
N_c	chlorine concentration in the measuring chamber
P_1	plenum pressure in front of gas chlorine nozzles
P_2	pressure in the measuring chamber
P_3, P_{3i}, P_{3f}	pressure in chlorine tank, initial before CBSOG start, final pressures (after CBSOG run)
P_4	pressure in the cavity of CBSOG
P_g	back pressure or pressure over BHP column
$P_l = \rho_l GH(1-H/D)$	hydrostatic pressure of the liquid at the bubbler surface
P_{sw}-	saturated vapor pressure over BHP
P_w	water vapor partial pressure in the measuring chamber
P_{w4}	water vapor partial pressure inside perforated cylinder
P_{O4}	oxygen partial pressure inside CBSOG cavity
P_c	chlorine partial pressure in the measuring chamber
Q_r	the heat release in process $Cl_2 + 2HO_2^- \rightarrow O_2(^1\Delta) + 2Cl^- + H_2O_2$, J/mole
Q_Δ	the heat release in process $O_2(^1\Delta) \rightarrow O_2(^3\Sigma)$, J/mole
Q_w	specific heat of water evaporation, J/mole
$\vec{R}_d$	Coordinate of the droplet
R -	universal gas constant
R_c	radius of the gas collector
$Re_b = 2rU_b/\nu$	Reynolds number for bubble
$Re_g = \dfrac{\rho_\ell U_g d_n}{\eta_\ell}$	Reynolds number for gas in the nozzle
$Re_w = 2U_l r_b/\nu$	Reynolds number for liquid velocity relative bubbler surface

$Re_d = 2 | \bar{v}_d - \bar{v}_g | d_d / v_g$ Reynolds number for the droplet

S_b	Efficient area of the bubbler occupied by gas nozzles
S_g	The total area of holes in the perforated cylinder
S_l	The area of the BHP drain holes
T_l, T_{li}, T_{lf}	BHP temperature in K, input temperature, output temperature
T_g	gas temperature in the measuring chamber
U	chlorine utilization
U_b	rising bubble velocity near the nozzle
U_d	initial droplet velocity
U_g -	gas velocity at the outlet of the chlorine nozzles
$U_s = (kRT/\mu)^{0.5}$	sonic velocity in chlorine-helium mixture
U_l	liquid cross velocity or velocity of liquid relative bubbler surface
U_{sf}	superficial gas velocity over liquid surface (average radial gas velocity over BHP)
V_l	volumetric BHP discharge, l/s
Y_d	detachment $O_2(^1\Delta)$ yield
Y	$O_2(^1\Delta)$ yield at the exit from BHP column

Small letters

a	the distance between gas nozzles
c_b	drag coefficient for bubble motion
c_d	drag coefficient for the droplet motion
d_n -	diameter of the gas nozzles
$d_b = 2r_b$	diameter of the bubble
d_d	diameter of the droplet
f_d	BHP droplet mass fraction in the gas from SOG
f	frequency of the bubble generation from the gas nozzle
g	980 cm/s^2 earth gravity acceleration
$j_c = m_c N_n$	chlorine flux through BHP column
j_o	oxygen flux over BHP column
k	specific heat ratio for chlorine-helium mixture
l_n	the length of the gas nozzle
m_c	chlorine molar flow rate per nozzle
m_H	Helium molar flow rate per nozzle
$m = m_H + m_c$	total molar flow rate through the nozzle
n -	Revolutions per second (RPS) of the BHP column relative to the axis of rotation
n_d	number of generated droplets
r_d	droplet radius
r_b	detachment bubble radius
t_l-	BHP temperature in C°
t_{li}-	initial BHP temperature in C°
t_{lf}-	output BHP temperature in C°
t_{run}	duration of CBSOG run
$\bar{v}_d$	current droplet velocity

Greek letter

ε	COIL power divided by BHP volumetric rate
$\beta = \sqrt{K N_H D_c} / H_c$	mass transfer rate in first order reaction approximation, cm/s
ρ_l	BHP density

ρ_g	gas density at the nozzle outlet
ρ_{g1}	gas density in the light scattering region
η_l	BHP viscosity
η_g	viscosity of the $Cl_2:O_2:He$ mixture
η_W	water vapor fraction relative to the oxygen+residual chlorine in measuring cell
$\eta_{BHP}=2UM_c/N_B/V_1$	efficiency of BHP consumption in the single burn dawn
μ	molecular weight of the chlorine-helium mixture
σ_l	liquid surface tension
μ_1	molecular weight of the $Cl_2:O_2:He$ mixture
ν	Kinematical viscosity of the BHP
$\nu_g \approx 100/P_g$	kinematic viscosity of gas in the region over BHP, cm^2/s, P_g(torr)
τ	time of the bubble growth
τ_Δ	Lifetime of $O_2(^1\Delta)$ in the BHP

12. References

1. A.I. Safonov, V.S. Krylov, *The study of bubble motion in rotating liquid layer*, Theoretical Foundation of Chemical Engineering 6 (No1), 51-67 (1972) (in Russian).

2. A.I. Safonov, V.S.Krylov, *Some rules of gas issue into a rotating layer of liquid*, Theoretical Foundation of Chemical Engineering 6 (No 2), 214-217 (1972) (in Russian).

3. A.I.Safonov, V.S.Krylov, *The movement of single bubble in rotating liquid layer*, Theoretical Foundation of Chemical Engineering, 7 (No 2), 267-269 (1973) (in Russian).

4. A.I. Safonov, V.S. Krylov, P.A. Gorshenin, *A mechanism of gas dispersion in rotating layer of liquid*, Theoretical Foundation of Chemical Engineering 7 (No3), 448-451 (1973) (in Russian).

5. A.I. Safonov, V.S. Krylov, K.V. Gomonova, *A dynamics of gas dispersion in rotating layer of liquid*, Theoretical Foundation of Chemical Engineering 12 (No 6), 914-916 (1978) (in Russian).

6. A.I. Safonov, V.S. Krylov, K.V. Gomonova, *Features of hydrodynamics rotating sparger layer with cross flow*, Theoretical Foundation of Chemical Engineering 12 (No 3), 454-455 (1978) (in Russian).

7. V.N. Azazov , M.V.Zagidullin , V.D.Nikolaev, N.I.Ufimtzev , "Kinetics of absorption of Cl_2 by H_2O_2-H_2O-KOH and H_2O-KOH solutions", *Russ. Journ.Phys.Chem*. pp. 1850-1854 , 1998.

8. A.I. Safonov, E.P. Reva,V.S. Krylov, K.V. Gomonova, *Mass transfer in the initial region of sparger layer,* Theoretical Foundation of Chemical Engineering 10 (No 4), 495-500 (1976) (in Russian).

9. A.R.Dorokhov, O.Yu.Kileeva. Heat exchange with horizontal cylinders in a centrifugal-bubbling bed. Journal of Engineering Physics and Thermophysics, Vol.74, N.3, pp. 800-805 (2001)

10. C.Ramshaw, R.H.Mallinson. Mass transfer process. US Patent 4283255.

11. C.Ramshaw, R.H.Mallinson.Mass transfer apparatus and process. US Patent 4400275.

12. A.O.Kuzmin et al. Vortex centrifugal bubbling reactor. Chemical Engineering Journal, v.107, N.1-3, pp. 55-62 (2005)

13. J.W.Wem, R.J.P.Brierley. Centrifugal gas-liquid contact apparatus. US Patent 4692283.

14. A.O.Kuzmin, M.Kh.Pravdina, A.I.Yavorsky, V.N.Parmon. Vortex centrifugal bubbling reactor. Chemical Engineering journal

15. Emanuel G., "High-Pressure, Gravity-Independent, Singlet Oxygen Generator, Laser Nozzle, and Iodine Injection System for the Chemical Oxygen-Iodine Laser," *High-power Laser Ablation Conference V,* Taos, NM, 2003, *Proc. SPIE, ed. C. R. Phipps,* Vol. 5448, pp. 233-241.

16. G.Emanuel USA Patent Application Publication 0050979.

17. Kutateladze S.S., Nakoryakov V.S. Heat-mass transfer and waves in gas-liquid systems. "Nauka", 1984 (in Russian)

18. Payne G.J., Prince R.G.H. The transition from jetting to bubbling at submerged orifice. Transaction of the Instituttion of chemical engineering, v.53, 209-223 (1975)

19. Hofhuis P.A.M., Zuiderweg F.J. Sieve plates: Dispersion density and flow regimes. Institute of chemical engineers symposium series, v.56, 2.2/1-2.2/26 (1979)

20. W.E.McDermott et all. Operating experience with a high throughput jet generator. AIAApaper 97-2385/ 1997/

21. J.M.Boulton-stone, J.R.Blake. Gas bubble bursting at a free surface. J.Fluid.Mech. v.254, pp.437-466 (1993).

22. S.S.Kutateladze, M.A.Styrikovich. The hydrodynamics of gas-liquid systems. Moscow, Energy, 1976 (in Russian)

23. Koch M.K. et al. Radionuclide re-entrainment at bubbling water pool surface. J.Aerosol science, V.31, N.9, pp.1015-1028, (2000)

24. N.Reinke et al. Aerosol generation by bubble collapse at ocean surface. Water, Air and soil pollution: Focus 1, 333-340 (2001)

25. Ovsiannikov L.V. About rising of the bubble. In book "Some problems of mathematics and mechanics", 1970

26. G.B.Wallis. One-dimensional two-phase flow. McGraw-Hill book company.

27. A.I.Safonov, V.S.Krilov. The problems of design and development of mass-transfer apparatus with rotating bubbling kayer. Journal of Applied Chemistry, V.50, N.10, 2288-2295 (1977)

28. Naus H., Ubachs W. // Applied Optics. 1999. V. 38, P. 3423.

29 .Tiedje, DeMille S., MacArtur, Brooks R.L. // Can.J.of Physics. 2001. V. 79, P. 773

30. Cheah S, Lee Y., Ogilvie J.F. // J.Quan.Spectr.Rad.Trans. 2000. V. 64. P. 467.

31. Newman S.M., Lane I.C., Orr-Ewing A. J., Newnham D.A., Ballard J. // J.Chem. Phys. 1999. V. 110, P. 10749.

32. Aviles R.G., Muller D.F., Houston P.L. // Appl.Phys.Lett. 1980. V. 37. P. 358.

33. Lilenfeld H.V., Carr P.A.G., Hovis F.E. // J.Chem.Phys. 1984. V. 81. P. 5730.

34. L.S. Rothman, D. Jacquemart, A. Barbe et.al. *J.Quant.Spec.Rad.Trans*. 96, 139-204 (2005)

35. R.B.Bird, W.E.Stewart, E.N.Lightfoot. Transport phenomena, Wiley&Sons, 1965).

36. P. V. Dankwerst, *Gas-liquid reactions*, "Chimia", Moscow, 1973.

37. 11. Endo M., Nagatomo S., Takeda S., Zagidullin M. V., Nikolaev V. D, Fujii H., Wani F, Sugitomo D., Sunako D., Nanri K., and Fujioka T. High-efficiency operation of chemical oxygen-iodine laser using nitrogen as buffer gas. IEEE J.Quantum Electronics. 1998. Vol. 34, №. 3. Pp. 393-398

38 Rittenhouse T. L., Phipps S. P., and Helms C. A. Performance of a high-efficiency 5-cm gain length supersonic chemical oxygen-iodine laser. IEEE J. Quantum Electronics. 1998. Vol. 35, №. 6. Pp. 857-866

39. M.V. Zagidullin, Valery D.Nikolaev, Michael I.Svistun, Nikolai A.Khvatov, Gordon D.Hager˙. Characteristics of the gain medium for an ejector COIL with supersonic nozzles for the driver buffer gas. *Applied Physics A,* 81, 311-315 (2005)

13. Attachment 1. List of published papers and reports with abstracts.

1. **M.V.Zagidullin, V.D.Nikolaev, M.I.Svistun, N.A.Khvatov, "Results of testing a centrifugal bubble singlet-oxygen generator", Journal of Engineering Physics and Thermophysics, 2007, vol.80, №.3, pp.555-562.** The results of parametric tests of a centrifugal bubble singlet-oxygen generator based on the reaction of chlorine with an alkaline hydrogen peroxide solution have been given. The utilization of chlorine grows with bubble-layer height, whereas the relative content of $O_2(^1\Delta)$ remains constant. Growth in centrifugal acceleration leads to a more efficient utilization of chlorine. A specific oxygen output of more than 1 mmole·cm^{-2}·sec^{-1} from the bubble layer for a degree of chlorine utilization of 95% and a singlet-oxygen yield of more than 50% has been attained. It has been shown that a centrifugal bubble singlet-oxygen generator is an efficient energy source for an oxygen-iodine laser.

2. **M. V. Zagidullin, V. D. Nikolaev, M. I. Svistun, N. A. Khvatov, and E. V. Fomin. Diagnostics of an $O_2(^1A)$ Generator Using Multichannel Recording of Oxygen Emission Spectra.** *Optics and Spectroscopy, 2008, Vol. 105, No. 2, pp. 202-207.*

The concentrations of water vapor and $O_2(^1\Delta)$, as well as the temperature in the gas flow at the exit of a singlet oxygen generator are determined using multichannel recording of the singlet oxygen emission spectrum in the bands at 634, 703, 762, and 1268 nm. The water vapor concentration is found from the intensity ratio of the 762-nm band, which corresponds to the $O_2(^1\Sigma)$ —$O_2(^3\Sigma)$ transition of the oxygen molecule, and the dimole emission band at 634 nm. From the ratio of the integrated intensities of the bands at 634 and 1268 nm, the $O_2(^1\Delta)$ concentration is determined and it is shown that the content of $O_2(^1\Delta)$ at the exit from the gas generator is about 52%. The temperature of the gas flow, determined by the rotational structure of the oxygen emission spectrum in the band at 762 nm, is about 300 K under the nominal conditions of the gas generator operation. The ratio of the photon fluxes in the 703 and 634nm bands of the $O_2(^1\Delta)$ dimole emission is equal to 1.06. The temperature dependence of the dimole emission bandwidths is determined, which can be used for estimating the gas temperature at the exit of the $O_2(^1\Delta)$ generator.

3. **M. V. Zagidullin, V. D. Nikolaev, M. I. Svistun, N. A. Khvatov. Centrifugal bubble $O_2(^1\Delta)$ gas generator with a total pressure of 100 Torr.** Quantum Electronics 38(8) 794-800 (2008)

A centrifugal bubbling singlet-oxygen gas generator is developed in which chlorine with helium are injected into the rotating layer of the alkali solution of hydrogen peroxide through cylindrical nozzles directed at an angle of 30° to the bubbler surface. The concentrations of water vapour and $O_2(^1\Delta)$ and the gas temperature were determined by using the multichannel recording of the emission bands of oxygen at 634, 703, 762, and 1268 nm. For the chlorine and helium flow rates of 60 and 90 mmol s^{-1}, respectively, the specific chlorine load of 3.2 mmol cm^{-2}, a total pressure of 100 Torr in the working region of the gas generator and the oxygen partial pressure of 36 Torr, the chlorine utilisation was 90% and the content of $O_2(^1\Delta)$ was ~60%. For the ratio of the flow rates of chlorine and the alkali solution of hydrogen peroxide equal to 1 mol/L the water vapor content was ~25 %. The chemical efficiency of the oxygen-iodine laser with this gas generator achieved 23% for the specific power of 12.7 W cm per 1 cm^3/ s per pass of the solution through the gas generator.

14. Attachment 2. List of presentations at conferences and meetings with abstract

1. Performance of high pressure COIL with centrifugal bubble singlet oxygen generator.M.V.Zagidullin, V.D.Nikolaev, M.I.Svistun, N.A.Khvatov. Presented at International Symposium GCL/HPL, Gmunden, Austria, September 2006.

The singlet oxygen in the centrifugal bubble singlet oxygen generator (CBSOG) is produced via bubbling of chlorine containing gas through the basic hydrogen peroxide (BHP) column being under a high centrifugal acceleration. It is the gravity independent SOG with high potential characteristics. At condition of a high centrifugal acceleration (higher 10^3 m/s^2) rather bubbling regime than jetting regime of the gas dispersion occurs up to the sonic velocity of gas in the feeding nozzles. The visual observation of the bubbling at high centrifugal acceleration verified this conclusion. The generation of small bubbles with high rise velocity provide optimal conditions for the high chlorine utilization and the producing of oxygen with high $O_2(^1\Delta)$ yield. The bubbling regime and centrifugal acceleration provide no BHP carry-over and minimal aerosol fraction in the oxygen flow. A simplified model of chlorine absorption and $O_2(^1\Delta)$ producing has been developed. For most regimes a substantial part of chlorine reacts with BHP at the stage of the bubble growth. The optimal height of the BHP column was estimated 8÷10 mm. The results of modeling served as a basis for the first design of the CBSOG. The efficiencies of singlet oxygen production, chlorine utilization, BHP consumption were studied in a wide range of CBSOG operating parameters. In tests CBSOG was supplied by 30÷60 mmole/s of chlorine molar flow rate and 60÷240 mmole/s of helium molar flow rate. CBSOG operated when BHP column was been under centrifugal acceleration up to 4×10^3m/s^2. The main factor for high chlorine utilization was the height of the BHP column. The efficiency of chlorine utilization and $O_2(^1\Delta)$ yield slowly depended on BHP molarity and gas loading per nozzle. The CBSOG produced oxygen flux from the bubbler surface more than 1 mmole/cm^2/s at the chlorine utilization more than 90% and $O_2(^1\Delta)$ yield higher than 60%. The chemical efficiency of 25% has been obtained in 5 cm gain length supersonic ejector COIL powered by CBSOG. None zero power was observed up to the mirror transmission 11%. The efficiency of COIL didn't depend on dilution of oxygen flow with helium up to 1:4. The specific laser power more than 6 kW per 1 L/s of BHP volumetric rate has been obtained.

2. Perspective methods for the generation of COIL gain medium. M.V.Zagidullin, V.D.Nikolaev, M.I.Svistun, N.A.Khvatov. Presented at International conference "Laser Optics-2006", St.Petersburg, june, 2006.

A singlet oxygen generator (SOG) and gain flow generation system are the main parts of the chemical oxygen-iodine laser (COIL). It is necessary to provide a high reaction specific surface in SOG and a short refreshment time of the basic hydrogen peroxide (BHP) surface for the generation of a high pressure oxygen flow with high $O_2(^1\Delta)$ yield. The heat management and recirculation of high BHP flow is complicated by a low temperature range of homogeneous state of BHP and salt formation. A high pressure bubble type SOG with centrifugal BHP layer is the most proper for this goal. The singlet oxygen in centrifugal bubble singlet oxygen generator (CBSOG) is produced via bubbling of chlorine containing gas through BHP column being under high centrifugal acceleration. It is the gravity independent SOG with high potential characteristics. Estimations showed that at condition of high centrifugal acceleration (higher 10^3 m/s^2) rather bubbling regime than jetting regime of the gas dispersion occurs up to the sonic velocity of gas in the feeding nozzles. The visual observation of the bubbling at high centrifugal acceleration verified this conclusion. The generation of the small bubbles with high rise velocity provide optimal conditions for the high chlorine utilization and the producing of oxygen with high $O_2(^1\Delta)$ yield. The bubbling regime of a gas dispersion and centrifugal acceleration provide no BHP carry-over and minimal aerosol fraction in the oxygen flow. The BHP volume flow rate through the SOG can be made as small as possible to achieve high BHP chemical consumption without decreasing of chlorine utilization and $O_2(^1\Delta)$

yield. A simplified model of chlorine absorption and $O_2(^1\Delta)$ producing has been developed. For most regimes a substantial part ~50% of chlorine reacts with BHP at the stage of the bubble growth. The optimal height of the BHP column was estimated 8÷10 mm. The results of modeling served as a basis for the first design of the CBSOG. The efficiencies of singlet oxygen production, chlorine utilization, BHP consumption were studied in a wide range of CBSOG operating parameters. In tests CBSOG was supplied by 30÷56 mmole/s of chlorine molar flow rate and 60÷240 mmole/s of helium molar flow rate. CBSOG operated when BHP column was been under centrifugal acceleration up to 4×10^3m/s^2. The main factor for high chlorine utilization was the height of the BHP column. The efficiency of chlorine utilization and $O_2(^1\Delta)$ yield slowly depended on BHP molarity and gas loading per nozzle. The CBSOG produced oxygen flux from the bubbler surface more than 1 mmole/cm^2/s at chlorine utilization more than 90% and $O_2(^1\Delta)$ yield higher 60%. The ejector nozzle bank generates supersonic gain flow with temperature lower 200°K and potential recovered pressure of the order of 100 torr. The output power more than 1 kW at chemical efficiency 25% has been obtained in 5 cm gain length ejector COIL powered by CBSOG. None zero power was observed up to the mirror transmission 11%. The efficiency of COIL didn't depend on BHP molarity and dilution of oxygen flow with helium up to 1:4. The specific laser power more than 6 kW per 1 L/s of BHP volumetric rate has been obtained. But the experiments showed that the small signal gain drop in 2÷3 times at distances ~10 cm from the nozzle bank and flow velocity level ~600 m/c. Possible mechanisms for the quenching and losses of excited iodine atoms at low gas temperatures are discussed.

3. Advanced singlet oxygen generator and nozzle bank in traditional COIL technology. M.V.Zagidullin, V.D.Nikolaev, M.I.Svistun, N.A.Khvatov. A report at the International Conference on Coherent and Nonlinear Optics (ICONO) collocated with the International Conference on Lasers, Applications, and Technologies (LAT), May 28-June 1, 2007, Minsk, Belarus.

A singlet oxygen generator (CBSOG) and gain flow generation system are the main parts of the chemical oxygen-iodine laser (COIL). It is necessary to provide a high reaction specific surface in CBSOG and a short refreshment time of the basic hydrogen peroxide (BHP) surface for the generation of a high pressure oxygen flow with high $O_2(^1\Delta)$ yield. The heat management and recirculation of high BHP flow is complicated by a low temperature range of homogeneous state of BHP and salt formation. Hence for high power COIL the CBSOG should work in a single BHP liquid pass burn down and low level of the water vapor fraction in the oxygen flow. A high pressure bubble type CBSOG with centrifugal BHP layer is the most proper for this goal. The singlet oxygen in a centrifugal bubble singlet oxygen generator (CBSOG) is produced via bubbling of chlorine containing gas through BHP column being under high centrifugal acceleration. The generation of the small bubbles with high rise velocity provides optimal conditions for the high chlorine utilization and the producing of oxygen with high $O_2(^1\Delta)$ yield. The bubbling regime of a gas dispersion and centrifugal acceleration provide no BHP carry-over and minimal aerosol fraction in the oxygen flow. The BHP volume flow rate through the CBSOG can be made as small as possible to achieve high BHP chemical consumption without decreasing of chlorine utilization and $O_2(^1\Delta)$ yield. The efficiencies of singlet oxygen production, chlorine utilization, BHP consumption were studied in a wide range of CBSOG operating parameters. In tests CBSOG was supplied by 30÷56 mmole/s of chlorine molar flow rate and 60÷240 mmole/s of helium molar flow rate. CBSOG operated when BHP column was been under centrifugal acceleration up to 8×10^3m/s^2. The CBSOG produced oxygen flux up to 5 mmole/cm^2/s from the bubbler surface at chlorine utilization more than 90% and $O_2(^1\Delta)$ yield higher 60%. Aerosol mass fraction was much less than 1% in the gas flow from CBSOG. The ejector nozzle bank generates supersonic gain flow with M≈3, temperature lower 200K and potential recovered pressure of the order of 100 torr. A chemical efficiency 25% has been obtained in 5 cm gain length ejector COIL powered by CBSOG. None zero power was observed at the mirror transmission up to 11%. It was found that small signal gain drop in 2÷3 times

at distances ~10 cm from the nozzle bank and flow velocity level ~600 m/c. Possible mechanisms for the quenching and losses of excited iodine atoms at low gas temperatures are discussed. A specific laser power more than 6 kW per 1 L/s of BHP volumetric rate and 100W per 1 cm^2 of the bubbler surface have been obtained.

4. Zagidullin M.V.,Nikolaev V.D., Svistun M.I., Khvatov N.A. CENTRIFUGAL BUBBLING GASGENERATOR OF SINGLET OXYGEN. VI Minsk International Heat Mass Transfer Forum, May 19-23, 2008
      A high pressure centrifugal bubbling gas generator of singlet oxygen of a high pressure has been developed on the basis of reaction of chlorine with basic hydrogen peroxide solution.. An oxygen flow up to 3,2 mmole/s per 1 cm^2 of the bubbling column at pressure of ~40 torr has been generated. Singlet oxygen yield higher then 50% and chlorine utilization higher than 90% have been obtained. A mass fraction of entrain solution was not exceed 10^{-4}. Gas generator was employed in oxygen-iodine laser. At chemical efficiency 23% of the laser the specific power was 12.7 W per 1 ml/s of solution for chlorine flow rate 48,8 mmole/s and solution volumetric rate 80 ml/s.

5. M.V. Zagidullin, V.D. Nikolaev, M.I. Svistun, N.A. Khvatov, "Supersonic COIL powered by centrifugal bubbling SOG of high pressure and efficient depletion of chemicals in one pass", International Conference "Laser Optics 2008", June 23-28, 2008, St. Petersburg
      Results of parametric study of the centrifugal bubbling singlet oxygen generator 100 torr of total pressure are presented. In this SOG chlorine-helium mixture is injected through 165 cylindrical nozzles into rotating BHP layer on the angle 30° to the bubbler surface. It provides additional rotation of BHP layer. A total working area of the bubbler was 18.8 cm^2. The tests of SOG have been performed at chlorine loading up to 3.2 mmole/cm^2/s and centrifugal acceleration up to 7.5×10^3 m/s^2. For the measurements of $O_2(^1\Delta)$ and water vapor concentration we used multichannel registration of singlet oxygen emission in 634 nm, 703 nm, 762 nm и 1268 nm bands. The dependence of singlet oxygen yield, chlorine utilization and water vapor fraction on height of the BHP layer height, centrifugal acceleration, ratio of chlorine molar flow rate to the BHP volumetric rate have been measured. The gas flow of 100 torr total pressure, partial oxygen pressure 36 torr was generated. The efficiency of chlorine utilization was higher than 90%, singlet oxygen yield was near 50%. A water vapor fraction was near 15% at ratio of the chlorine flow rate to the BHP volumetric rate 1 mole/liter. An ejector COIL 5 cm gain length powered by this generator demonstrated a specific power 12.5 W per 1cm^3/s of BHP volumetric rate at chemical efficiency 22.5%.

6. Nikolaev V.D., Svistun M.I., Khvatov M.I., Zagidullin M.V. Supersonic COIL driven by centrifugal bubbling SOG with efficient depletion of chemicals in single pass. International Symposium GCL/HPL. Lisbon, Portugal, 13-19 Sepetember, 2008.
The increase of the laser power of COIL per unit volume flow rate of the BHP passed through SOG is a quite important for decreasing of weight and size of the laser. A centrifugal bubbling SOG is the most proper for this goal. Generation of small chlorine bubbles moving with high velocity in the BHP being under high centrifugal acceleration ensures fast chlorine utilization and separation of the gas from liquid. The efficiency of chlorine utilization and $O_2(^1\Delta)$ yield are slowly depend on the ratio of chlorine molar flow rate to the BHP volumetric rate. A relative water vapor fraction can be supported at a low level by increasing of the output oxygen pressure. As a result a droplet free gas flow of a high pressure, high $O_2(^1\Delta)$ and low H_2O vapor fraction can be generated.
The centrifugal bubbling SOG consists of the rotating cylindrical bubbler of 60 mm in diameter, BHP and chlorine feeding systems. BHP flows on the rotating babbler surface as the axially moving

layer of several mm in thickness. A chlorine-helium mixture is injected into the BHP layer through the array of cylindrical nozzles located inside of the circular strip of 1 cm width on the side wall of the rotating cylinder. So, the total working area of the bubbler was 18.8 cm^2. The axis of the nozzles is on the angle of 30° to the bubbler surface. Oblique injection of the gas into BHP layer induces substantial additional rotation of the BHP layer and diminishes normal gas momentum.. The tests of SOG have been performed at the chlorine loading up to 3.2 mmole/s per 1cm^2 of the bubbler area and bubbler rotation frequency up to 80 revolutions/s. For the measurements of $O_2(^1\Delta)$ and water vapor concentration a multi channel registration of singlet oxygen emission in 634 nm, 703 nm, 762 nm и 1268 nm bands was used. The dependences of singlet oxygen yield, chlorine utilization and water vapor fraction on the height of the BHP layer, centrifugal acceleration, ratio of chlorine molar flow rate to the BHP volumetric rate were measured. A droplet free gas flow of 100 torr total pressure and partial oxygen pressure of 36 torr has been generated. The efficiency of chlorine utilization was higher than 90%, singlet oxygen yield was near 50%. A water vapor fraction was near 15% at ratio 1 mole/s of the chlorine flow rate to the 1 litre/s of the BHP volumetric rate.

An ejector COIL of 5 cm gain length was powered by this centrifugal bubbling SOG operating at 4.2×10^5 cm/s^2 centrifugal acceleration. A gas temperature of the active medium was monitored by rotational structure of oxygen $^1\Sigma \rightarrow ^3\Sigma$ transition in 762nm band. At nominal conditions the gas temperature was estimated in the range 160÷180K that corresponds to Mach number of the gas flow of 2.2. A laser power versus BHP volumetric rate was detected for total mirror transmission of 2%. The chemical efficiency was higher than 21% for the ratio of chlorine molar flow rate to the BHP volumetric rate up to 0.6 mole/liter. Hence the alkaline concentration in BHP reduced from 4M to 2.8M in single pass. The chemical efficiency 25.4% and specific power 57 W per 1 cm^2 of the bubbler area were obtained for chlorine molar flow rate of 50.8 mmole/s and BHP volumetric rate of 178 cm^3/s. 12.5 W of output laser power per 1cm^3/s of BHP volumetric rate at chemical efficiency 22.7% was obtained when COIL output power was 1kW.